POLITECNICO DI MILANO

Facoltà di Ingegneria Industriale e dell'Informazione

Dipartimento di Energia

Dipartimento di Chimica, Materiali e Ingegneria Chimica

"Giulio Natta"

FUNDAMENTAL ASSESSMENT OF GAS-TO-PARTICLE MASS TRANSFER IN MICRO-CHANNEL PACKED BED REACTORS

Relatori: Prof. Alberto CUOCI
Prof. Matteo MAESTRI

Correlatore: Dr. Tiziano MAFFEI

Tesi di Laurea in Ingegneria Chimica di:
Stefano REBUGHINI 782372

Anno Accademico 2012-2013

Abstract

In this work, gas-to-particle mass transfer phenomena in micro-channel packed bed reactors are studied in detail by the means of Computational Fluid Dynamics. Such micro-channel reactor technology is considered one of the key-factors towards the intensification and development of advanced chemical processes for energy and environment. In fact, such micro-reactors allow incorporating and coupling different properties, which are crucial in order to enhance the efficiency of the process. Thanks to the unusual geometry, micro-channel reactors have a high surface area-to-volume ratio as well as improved transport properties.

The comparisons with the CFD results demonstrate that the Sherwood number in micro-channel reactors is considerably different from those predicted by the state of the art correlations. In particular, the Wakao and Funazkri [1] and Yoshida et al.[2] correlations are found to overestimate the Sherwood number in micro-channels of a factor of two.

More specifically the analysis shows that these differences are not related to the micro-dimensions (e.g 600 μm and 300 μm sphere diameter), but to the unconventional tube-to-particle diameter ratio. These differences depend on the unusual geometry of the micro-channel reactors. In particular the deviation of the Sherwood number is related to the wall effect that creates an inhomogeneous flow distribution over the cross section. This leads to lower mass transfer properties for these unconventional devices, due to the preferential channeling of the fluid close to the wall where the porosity is higher and the contact area between fluid and particles per reactor volume is smaller. This effect is not specific of the micro-dimensions (e.g. 0.6 mm spheres diameter and 4 mm tube diameter), but also observed for "conventional" dimensions with the same tube-to-particle diameter ratio (e.g. 6 mm sphere diameter and 40 mm tube). Same behavior is found for a different a different tube-to-particle diameter ratio (e.g. 0.3 mm sphere diameter and 4 mm tube).

The CFD analysis points out that the mass transfer coefficient is higher for the channel with higher tube-to-particle diameter ratio, especially for Reynolds number higher than 40. This seems to be associated to the less importance of channeling near the wall for the highest tube-to-particle diameter ratio investigated.

The dependence on the tube-to-particle diameter ratio is observed also for the pressure drops. The pressure drops in these unconventional devices can be predicted by literature correlations, which take into account the wall the tube-to-particle diameter ratio (e.g. Eisfeld et at. [3]).

Sommario

In questo lavoro di tesi, i fenomeni di trasporto di materia tra la particella e il gas in micro-channel reactors sono studiati in modo approfondito con un'analisi di fluidodinamica computazionale (CFD). La tecnologia dei micro-channel reactors è considerata uno dei fattori chiave verso l'intensificazione e lo sviluppo di processi chimici per l'energia e l'ambiente. Questi micro-reattori possono integrare e accoppiare diverse proprietà, che sono cruciali al fine di migliorare l'efficienza del processo. Grazie alle micro-dimensioni, questi reattori hanno un rapporto area superficiale per volume tale migliorare le proprietà di trasferimento di massa e di materia.

Il confronto con i risultati CFD dimostra che il numero di Sherwood nei micro-channel reactors è diverso da quello predetto dalle correlazioni presenti in letteratura. In particolare, si osserva come le correlazioni di Wakao and Funazkri [1] and Yoshida et al.[2] sovrastimino il valore di Sherwood di un fattore due.

Quindi queste differenze dei numeri di Sherwood nei micro-channel reactors sono legate alla loro particolare geometria e all'effetto di parete che crea una distribuzione del flusso disomogenea, che a sua volta causa una riduzione delle proprietà di trasferimento di materia nel reattore. Questa diminuzione non è specifica delle micro-dimesioni (e.g. diametro sfere di 0.6 mm e diametro tubo di 4 mm), ma è osservata anche in reattori con dimensioni "convenzionali" e con lo stesso rapporto tra il diametro del tubo e della particella (e.g. diametro sfere di 6 mm e diametro tubo di 40 mm). Lo stesso fenomeno si osserva anche per micro-reattori con un diverso rapporto tra il diametro del tubo e quello della particella (e.g. diametro sfere di 0.3 mm e diametro tubo di 4 mm).

L'analisi CFD mostra che il coefficiente di scambio di materia è più alto per reattori con un più alto rapporto tra il diametro del tubo e quello della particella, specialmente per numeri di Reynolds superiori a 40. Questo effetto sembra associato alla minore importanza dei fenomeni di channeling per reattori con più alti rapporti tra il diametro del tubo e il diametro della particella.

La dipendenza dal rapporto tra il diametro del tubo e quello della particella si osserva anche per le perdite di carico. In questi dispositivi non convenzionali le perdite di carico possono essere descritte e predette solamente da correlazioni di letteratura che considerano l'effetto di parete (ad esempio Eisfeld et al. [3]), il quale è descritto dal rapporto tra il diametro del tubo e quello della particella.

Table of contents

1 Introduction

1.1 Micro-reactors technology

The chemical industry operates reactors in a few large facilities to achieve economies of scale. Often chemical intermediate are transported to smaller plants, where they will be processed, e. g., monomers may be moved to a small fibers plant where polymerization and polymer processing steps are carried out. The main problem of this large-scale chemical production is related with the safety of production and transportation. Recent reports[6] has suggest to miniaturize chemical systems for improved safety by eliminating storage and transportation of toxic and hazardous chemicals and reducing potential damage due to accidents. Moreover these micro-reactors can be integrated with sensors on-chip for early detection of runaway reactions.

Due to the micro-dimensions, micro-channel reactors have a high surface area-to-volume ratio, which can inhibit gas-phase free-radical reactions, as well as improve heat transfer for exothermic reactions. These features can be applied to hydrocarbon partial-oxidation reactions, which comprise fast reactions and short contact time used for producing oxygenates. Due to the high exothermicity of these reactions, in large-scale reactors, the temperature is difficult to control[7]. Due to the high surface area-to-volume ratio these devices can be coupled with micro-cooler in honeycomb structures to easily control the temperature. Therefore the micro-channel reactors can be considered as an integration of a honeycomb matrix and a packed bed, as shown in Figure 1.

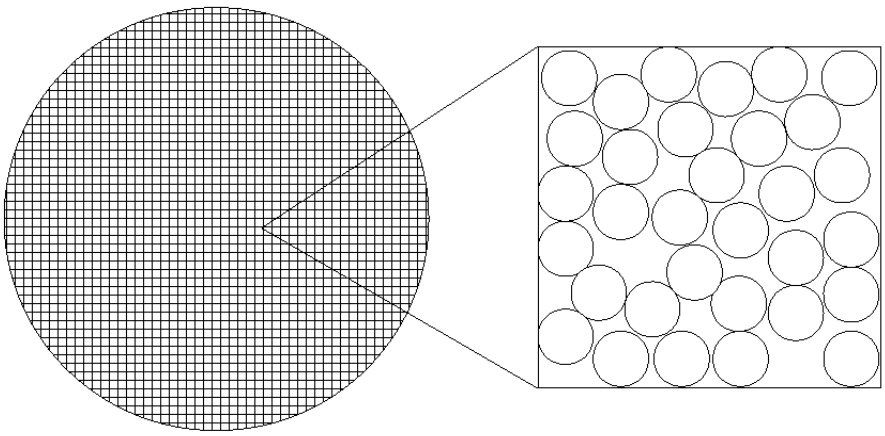

Figure 1: Micro-reactors are the coupling of honeycomb matrix and packed bed reactors

In micro-systems the properties of both co-exit. The high radial heat transfer coefficient, given by the honeycomb matrix, allows for an efficiency temperature control. Moreover the high surface-to-volume ratio of typical of packed bed, gives to a micro-channel reactor a high inter-phase mass transfer coefficient.

Srinivasan et al.[6] analyzed the oxidation of ammonia on platinum and demonstrated the feasibility of conducing chemical reactions in micro-fabricated systems. In their work the conversion and the selectivity for ammonia oxidation was studied in a prototype micro-reactor. The results can be compared with the conversion and the selectivity of a conventional reactor. Therefore the scale-up for industrial use could be achieved by operating many micro-channel reactors in parallel, as mini-chemical system.

Nevertheless, all the previous expertise developed for conventional reactor cannot be straightforwardly applied to these unconventional devices, due to their unusual geometry. This creates a huge challenge for the design and development of micro-reactor technology. The scientific and technological literature needs guidelines and procedures for the proper design of such micro-devices. Most of the works, which are presented in this chapter, are based on experimental analysis and clearly a theoretical investigation is necessary. Therefore, the understanding of the mechanisms of heat and mass transport phenomena in this new reactor concept needs to be systematically investigated and this is a requirement for a successful design and scale-up of the reactor technology at the industrial level. Therefore this work aims at a detailed theoretical study of the behavior of micro-channel reactors with a detailed analysis and simulation of fluid dynamics and heterogeneous chemistry using the code catalyticFoam [4, 5].

1.2 State of the art

In this paragraph a general overview of the mass and heat transfer phenomena is presented, with the description of Sherwood number literature correlation. At the end of the paragraph the possibility to estimated mass transfer coefficient with CFD simulations is introduced.

1.2.1 Sherwood number correlations

Simplified models are used to design and analyze all the types of catalytic reactors. The models used to describe catalytic reactors are based on mass balance, energy balance and momentum balance at the continuum level. All the balances have this form:

$$IN - OUT + PROD = ACC$$

where:

- ✓ IN : this term is the amount of considered specie introduced per unit of time.
- ✓ OUT : this describes the amount of considered specie leaving per unit of time.
- ✓ $PROD$: this is the reacting term and represents the amount of considered specie converted per unit of time.
- ✓ ACC : this term is the amount of considered specie accumulated in the reactor per unit of time.

These balances are modified and simplified with some hypothesis to represent different kind of reactors. For example if only the steady state of a continuous reactor is investigated the ACC term can be imposed equal to zero. Once the first hypotheses are applied the balance can be written in mathematical terms. The equation, that represents the chosen balance, can describe the reactor with the help of parameters, such as the mass transfer coefficient or the external heat transfer coefficient. These parameters are different for every type of reactors and they are related with the operating condition and reactor geometry. These parameters are described by experimental correlations, developed for particular type of reactor and process.

The most useful concepts employed in the development of the expressions for the rates of fluid-to-particle mass transfer phenomena in fixed packed bed is the mass transfer coefficient (K_{MAT}) defined as:

$$w = K_{MAT} a_V V \Delta C$$

where w is the rate of fluid to solid and ΔC is the concentration difference across the fluid-solid interface.

Dimensionless correlations for the mass transfer coefficient (K_{MAT}) are usually provide in terms of:

$$Sh = \frac{K_{MAT} L}{\mathfrak{D}_i}$$

where L is the characteristic length of the considered reactor and $\mathfrak{D}_i$ is the specie diffusivity.

Different correlations of Sherwood numbers were developed for packed-bed. These correlations depend on the reactor geometry, but also on the phase of the fluid processed. The Wakao and Funazkri [1] equation can be used to describe both liquid-to-particle mass transfer that gas-to-particle mass transfer. At the beginning the Wakao correlation was developed to describe only liquid-phase mass transfer.

The Sherwood number for different operating conditions, described by Reynolds and Schmidt numbers, only for liquid-phase was:

$$Sh = 2 + 0.6 * \mathrm{Re}^{0.5} * Sc^{1/3}$$

In their work Wakao and Funazkri [1] modified the parameters of this correlations. The parameters were changed by the analysis of experimental data from gas-to-particle reactors in a huge range of operating conditions. The new correlation is:

$$Sh = 2 + 1.1 * \mathrm{Re}^{0.6} * Sc^{1/3}$$

and it can be applied in a large range of Reynolds number:

$$3 < \mathrm{Re} < 10000$$

Other dimensionless correlations are based on the j-factor, instead on the Sherwood number:

$$J_m = \frac{Sh}{\mathrm{Re}\, Sc^{1/3}} :$$

This term was introduce by Colburn [8] for gas film, but it was extending to the liquid film for mass transfer between liquids and granular solids. The Reynolds number used in the j-factor is defined as:

$$\mathrm{Re} = \frac{\rho v D_{Particle}}{\mu}$$

Yoshida et al. [2] proposed these correlations to represent the Sherwood number in heterogeneous gas-solid packed bed reactor in terms of j-factor:

$$J_m = \frac{0.91}{\mathrm{Re}^{0.51}}\psi \qquad \mathrm{Re} < 50$$

$$J_m = \frac{0.61}{\mathrm{Re}^{0.41}}\psi \qquad 50 < \mathrm{Re} < 1000$$

where:

- ✓ ψ : is the shape factor and it is 1 for the spheres
- ✓ $\mathrm{Re} = \frac{GD_{Particle}}{6\mu(1-\varepsilon)}$: definition of Reynolds number that must be used in Yoshida et al. [2] correlation.

These correlations were developed considering a huge range of experimental data, thus different correlations predict different Sherwood number for the same operating conditions and fluid compositions. This effect is shown in Figure 2, where the experimental data range is described.

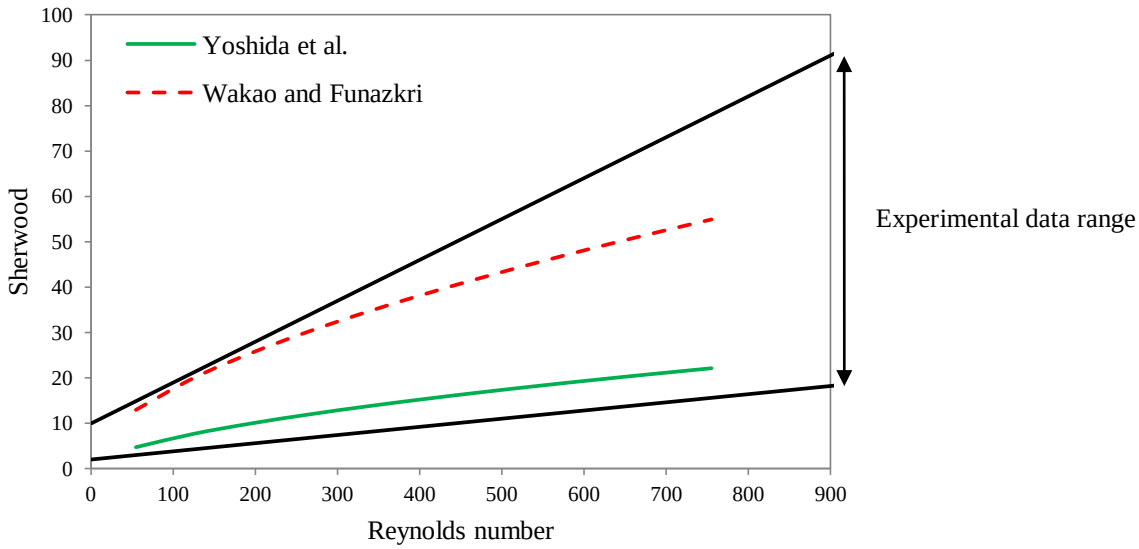

Figure 2: Comparisons between the Yoshida et al. [2] correlation and Wakao and Funazkri [1] expression.

As described by Wakao and Funazkri [1], all these correlations were developed considering the particle diameter as characteristic length of the reactor, thus the Sherwood number depends on the particle Reynolds number:

$$\mathrm{Re} = \frac{\rho v D_{Particle}}{\mu}$$

The Sherwood number, as shown by Yoshida et al.[2], depends also on the mean void fraction ε that describes the particle distribution in the channel. During the evaluation of the experimental correlations, the particle Reynolds number and the mean void fraction are considered constant in the whole reactor. Moreover the particle Reynolds number describes the flow field around a single sphere, without considering the presence of other spheres or of the confining wall of the channel. For these reasons the Sherwood number of standard correlations (e.g. Wakao and Funazkri [1] and Yoshida et al.[2]) do not take into account the different porosity and flow field near the confining wall.

Nevertheless, these correlations are successfully applied to design and modeling packed bed reactors at industrial level.

1.2.2 Heat transfer phenomena in micro-reactors

As discussed before the micro-channel reactors can be coupled with micro-heat exchanger to easily control temperature. The coupling efficiency is related with the heat transfer properties of these micro-devices. In their work, Tadepalli et al. [9], studied the catalytic hydrogenation of *o*-niroanisole in micro-reactor to compare their results with those from industries. In the pharmaceutical industry, a significant number of catalytic reactions are usually carried out in slurry semi-batch reactors. Other types of catalytic reactors, more common in other kind of industry, are the trickle-bed, fluidized-bed and conventional packed-bed configurations. Moreover the heat removal becomes important for high exothermic reactions. The non-uniform temperature distribution in the conventional reactors may develop hot spots, which have influence on the catalyst and may create undesired byproducts. Therefore a good temperature control is necessary, not only for safety, such as in partial catalytic oxidation, but also to increase the selectivity of desired compounds. The temperature is controlled through the walls of the reactors in the most common tubular reactors. Ouyang and Besser [10] demonstrate that the temperature gradient is related with the tube diameter. They studied the CO preferential oxidation in a micro-channel reactor with thin-film wall catalyst and in a laboratory packed bed reactor with conventional dimensions. The effect of the reverse water-gas-shift reaction, favor by temperature gradient, was observed. They discovered that the extremely efficient heat removal of the micro-channel reactor eliminates temperature gradients and the onset of the r-WGS reaction is prevented.

1.2.3 Mass transfer phenomena in micro-reactors

The gas-liquid-solid external mass transfer was studied by Yeong et al. [11]. In their work the nitrobenzene hydrogenation was studied in a falling film micro-structured reactor. The mass transfer coefficient was estimated to be 3-8 s^{-1} with interfacial surface are per reaction volume 9000-15000 m^2/m^3. The mass transfer coefficient for laboratory trickle-bed are 0.01-0.08 s^{-1}. Therefore, they demonstrate that the mass transfer in the micro-reactors is greatly improved over its macro-scale counterpart.

A similar results was obtained by Losey et al. [12]. In their work a micro-fabricated multiphase packed bed reactor was analyzed. First of all the pressure drops are compare with the Ergun equation[13] . They observed that the pressure drops in these unconventional devices can be compared with experimental correlations. Secondly the external mass transfer was studied. The mass transfer was evaluated to be 5-15 s^{-1}. These results show that the micro-dimensions improved the mass transfer phenomena and this effect would be expected also in gas-to-particle or liquid-to-particle packed bed.

A single-phase packed bed micro-reactor was studied by Tidona et al. [14]. In their work the liquid-to-particle mass transfer in micro packed beds of different hydraulic to particle diameter ratio and different channel geometries was studied with the copper dissolution method. In this work the experimental results are compared with the Wakao and Funazkri [1] correlation for the Sherwood numbers. Higher Sherwood numbers were measured with increasing the hydraulic to particle diameter ratio, if this value is greater than 4. For the hydraulic to particle diameter ratio smaller than 4, the effect of Sherwood number is opposite. They assumed that this different trend depends on the wall effect on channel with hydraulic to particle diameter ratio. For channel with hydraulic to particle diameter ratio smaller than 4, the packed bed cross section cannot differentiated anymore in a wall region and a center region and this increases the mass transfer, due to the homogeneous distribution of the flow in the channel.

In this work the Wakao and Funazkri [1] correlation's parameters are modified to describe the Sherwood number in micro-channel reactors with different hydraulic to particle diameter ratio (N):

$$Sh = A + B * \mathrm{Re}^{C} * Sc^{D}$$

Table 1: Modified parameters of Wakao end Funazkri for micro-channel with different hydraulic to particle diameter ratio [14]

	A	B	C	D
Wakao and Funazkri[1]	2	1.1	0.6	0.33
Different hydraulic to particle diameter ratio				
N				
4	2	1.8	0.39	0.31
6.6	2	1.6	0.40	0.33
24.4	2	1.0	0.71	0.31

1.2.4 CFD and mass transport phenomena

Computational fluid dynamics (CFD) methods have been applied to study transport phenomena in packed-bed reactors. An example of this analysis is given by Dixon et al. [15]. However, numerical investigations of mass transfer are rather limited compared to fluid dynamic studies. Kloeker et al.[16] examined the mass transfer phenomena in structured spherical arrangements for different flow rates and Romkes et al.[17] studied heat and mass transfer for very low tube-to-particle diameter ratios in rectangular packed beds. The main problem of their model is that the packed bed considered is not a random packing. Romkes et al. [17] considered Composite Structure Packing (CSP), shown in Figure 3, instead of a random packing.

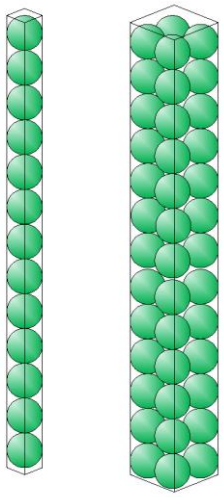

Figure 3: Concept of Composite Structured Packing [17]

The random packing is considered by Theodoros Atmakidis and Kenig [18]. In their work the mass transfer in packed bed with irregular particle arrangement was studied with a CFD model. To verify if transport phenomena can be investigated with a CFD model they reproduced two of the most common experiments to analyze transport phenomena in packed bed. The first one is the dissolution of benzoic acid particles in water, the second one is the sublimation of naphthalene particles in air. This numerical analysis can be considered as a kind of ‘‘virtual experiments’’, and their results are compared with those of real experiments. A satisfactory agreement between the numerically estimated Sherwood numbers and those obtained from the correlations is achieved. Moreover, using the CFD-based approach, it is possible to derive mass transfer correlations with higher accuracy and reliability and to deeply understand the experimental results. As described before, such approach, that connects the fluid dynamics and heterogeneous chemistry, is implemented in the OpenFOAM[19] solver called catalyticFOAM [4, 5].

1.3 Aim of the work and main results

The aim of this thesis is to use a detailed model, implemented in catalyticFOAM [4, 5], to find parameters that can be used to describe micro-channel reactor with lumped models. This work will study the external mass transfer phenomena in micro-channel packed bed reactors. Especially, the gas-to-particle mass transfer will be analyzed for these unconventional systems. First of all the results will be compared with the correlations for the Sherwood numbers developed for conventional packed-bed. The term *conventional* is describes reactor with the geometry used at industrial level

In chapter 3, the pressure drops in micro-channel reactors are investigated. The comparisons of the CFD results with the Ergun equation [13] and with the Eisfeld et al. equation [3] shows that the pressure drops in these unconventional devices are controlled by the wall effects. Therefore only literature correlations, which take into account the wall effects, introduced by the tube-to-particle diameter ratio, (e.g. the Eisfeld et al. [3] and Foumeny et al. [20]), can describe the pressure drops in micro-channel packed bed.

After the pressure drops analysis the literature correlation of Wakao and Funazkri[1] and Yoshida et al. [2] for the Sherwood number are compared with the Sherwood number estimated from the CFD simulations. These literature correlations overestimate the Sherwood number, at the considered operating conditions ($12 < \mathrm{Re} < 77$), thus they cannot be applied to describe the gas-to-particle mass transfer in these unconventional devices. This difference depends on the preferential path and the high void fraction close to the reactor walls that reduce the contact area between the flow and the catalytic surface. Due to this effect, these unconventional channels are described by a smaller Sherwood number and mass transfer coefficient. The influence of the wall effects can be investigated if the micro-channel reactors with different tube-to-particle diameter ratio are studied. Then different channel with different spheres diameter are analyzed and it is observed that the Sherwood number depends on the tube-to-particle diameter ratio. The CFD analysis shows that higher mass transfer coefficients are related to higher tube-to-particle diameter ratio. This dependence of mass transfer coefficient on the tube-to-particle diameter ratio is related with the wall effects, because the influence of the channeling near the channel wall is reduced in reactors with smaller particle.

The effect of the tube-to-particle diameter ratio is opposite if the Sherwood number is considered. This dependence can be explained by the Sherwood number definition in micro-channel packed bed reactors:

$$Sh = \frac{K_{MAT} D_{Particle}}{\mathfrak{D}_i}$$

The Sherwood number does not take into account the presence of the confining wall, thus it cannot be used to describe the dependence of the mass transport properties on the tube-to-particle diameter ratio.

2 Methodology

2.1 Introduction

The CFD results can be used to estimate Sherwood number and mass transfer coefficient, even if it is not possible to obtain their direct evaluation. Due to the difficult assessment of the Sherwood number three different methods to evaluate it are described in this chapter. These approaches are studied to understand their advantages and disadvantages and to comprehend if they can be applied to estimate the Sherwood number and the mass transfer coefficient in micro-channel reactors. The conventional geometry of a monolith reactor will be use to validate these different approaches.

2.2 Numerical methods to evaluate Sherwood number

The numerical methods proposed to estimate Sherwood number from the CFD data are:

- ✓ **Peripheral Average Mass Fraction method [PAMF]:** this method is based on a local mass balance at the catalytic wall.
- ✓ **Integral Mass Balance method [IMB]:** the global mass balance on the whole reactor and a one-dimensional model are used to evaluate the mass transfer coefficient.
- ✓ **Steady State Mass Balance [SSMB]:** this approach calculates the Sherwood number with a mass balance on an infinitesimal part of the reactor.

2.2.1 Peripheral Average Mass Fraction method [PAMF]

PAMF method is based on mass balance at the catalytic wall at steady state conditions:

$$IN - OUT + PROD = 0$$

The $IN - OUT$ term is composed by the diffusivity flux and can be written as:

$$IN - OUT = -\mathfrak{D}_i \frac{d\rho_i}{dn} \qquad [2.1]$$

where n represents the outward direction normal to the wall. The $PROD$ term is the reacting term.

Therefore:

$$-\mathfrak{D}_i \frac{d\rho_i}{dn} = R_i \qquad [2.2]$$

A first order kinetics is advised to simplify the problem allowing a direct relationship between the kinetic and the transport phenomena. This simplified reaction term can be modified to change the global reactivity and also to easily evaluate the Damkohler number. Due to the Damkohler number it is possible to understand if the reactor works in mass transfer conditions or in chemical regime. The first order kinetics constant can easily modify the operating conditions from one regime to the other. Therefore the reacting term can be written as:

$$R_i = \nu_i k_{CIN} MW_i C_i \qquad [2.3]$$

and the mass balance becomes:

$$-\mathfrak{D}_i \frac{d\rho_i}{dn} = \nu_i k_{CIN} MW_i C_i \qquad [2.4]$$

The diffusivity flux at the reacting wall [2.4] in heterogeneous simplified model is described with a linear term, which is composed by a driving force and the mass transfer coefficient. The difference between the density in bulk phase and the density on the catalytic wall is chosen as driving force.

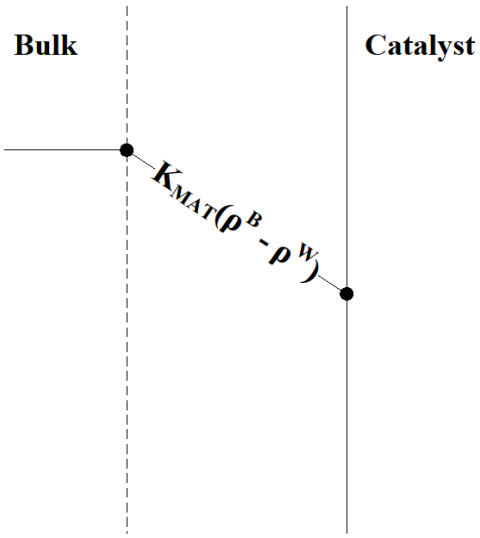

Figure 4: Linear expression for the diffusivity flux at the catalytic wall

As shown in equation [2.9] Sherwood number relates the diffusivity flux at the catalytic wall to the proportional flux based on the mass transfer coefficient. Thus the mass balance at the catalytic wall can be written also in this form:

$$K_{mat,i}(\rho_i^B - \rho_i^W) = -\mathfrak{D}_i \frac{d\rho_i}{dn} \qquad [2.5]$$

ρ_i^B is the cup-mixing average density over the channel cross-section S defined as:

$$\rho_i^B = \frac{\int_S \rho_i u dS}{\int_S u dS} \qquad [2.6]$$

where u represents the local velocity.

ρ_i^W is the peripheral average of density on the catalytic wall along the γ line, defined as:

$$\rho_i^W = \frac{\int_\gamma \rho_i \, d\gamma}{\gamma} \qquad [2.7]$$

On the basis of the equations [2.4] and [2.5] the mass balance for the kinetic controlling species can be written as:

$$K_{mat,i}(\rho_i^B - \rho_i^W) = -\nu_i k_{CIN} MW_i C_i = k_{CIN} \rho_i^W \qquad [2.8]$$

By introducing the dimensionless coefficients Sherwood number:

$$Sh = \frac{K_{mat,i} D_h}{\mathfrak{D}_i} \qquad [2.9]$$

and Damkohler number:

$$Da = \frac{k_{CIN} D_h}{\mathfrak{D}_i} \qquad [2.10]$$

The equation [2.8] can be written as:

$$Sh(\omega_i^B - \omega_i^W) = Da\omega_i^W \qquad [2.11]$$

The previous equation is based on mass fraction instead of density. This is a reasonable assumption because the density of the flow, at an established distant from the reactor entrance, it can be considered constant. Now it is possible to estimate the local Sherwood number as:

$$Sh = \frac{Da\omega_i^W}{(\omega_i^B - \omega_i^W)} \qquad [2.12]$$

Therefore the cup-mixing mass fractions and the wall mass fractions (peripheral average mass fractions) are calculated from CFD simulations. The cup-mixing mass fraction is evaluated as:

$$\omega_i^B = \frac{\int_S \varphi_x \omega_i dS}{\int_S \varphi_x dS} \qquad [2.13]$$

where φ_x is the normal component of the mass flux through the channel cross-section S:

$$\varphi_x = \rho_i u_x \qquad [2.14]$$

The wall mass fraction is estimated with this equation:

$$\omega_i^W = \frac{\int_P \omega_i d\gamma}{\gamma} \qquad [2.15]$$

where the value P is the peripheral length of the catalytic wall.

2.2.2 Integral Mass Balance method [IMB]

Sherwood number and mass transfer coefficient are evaluated with employing a 1D model for heterogeneous reactor. At steady state conditions and with negligible axial diffusivity fluxes, the mass balance for the gas phase is:

$$-u_{in} \frac{d\rho_i^B}{dx} - K_{mat,i} a_v (\rho_i^B - \rho_i^W) = 0 \qquad [2.16]$$

where u_{in} is the inlet velocity and a_v is the specific catalytic surface and it is defined as:

$$a_v = \frac{catalyticSurface}{reactorVolume} \qquad [2.17]$$

The hypothesis of a negligible axial diffusion depends on the operating conditions and reactor dimensions. The reactor back-mixing is described by the Péclet number, defined as:

$$Pe = \frac{uD_h}{\mathfrak{D}} \qquad [2.18]$$

where D_h is the hydraulic diameter, u is the velocity and $\mathfrak{D}$ is the diffusivity.

Péclet number compares the convective flux and the diffusivity flux. High Péclet number means that the convective fluxes are dominant, thus the reactor axial diffusivity can be avoid. For all reactors studied in this work is include between 50 and 300, thus equation [2.16] can be applied.

If the reaction is fast, the reactor works in mass transfer conditions and the assumption of a catalytic mass fraction close to zero can be applied:

$$\rho_i^W \to 0$$

$$-u_{in}\frac{d\rho_i^B}{dx} - K_{mat,i}a_v\rho_i^B = 0 \qquad [2.19]$$

Then the analytical solution of equation [2.19] is:

$$-\int_{\rho_i^{B,IN}}^{\rho_i^{B,OUT}} u_{in}\frac{d\rho_i^B}{\rho_i^B} = \int_0^L K_{mat,i}a_v dx \qquad [2.20]$$

$$-u_{in}\ln\left(\frac{\rho_i^{B,OUT}}{\rho_i^{B,IN}}\right) = K_{mat,i}a_v L \qquad [2.21]$$

The conversion is defined as:

$$\chi = \frac{\rho_i^{B,OUT} - \rho_i^{B,IN}}{\rho_i^{B,OUT}} \qquad [2.22]$$

thus the 1D analytical solution becomes:

$$-u_{in}\ln(1-\chi) = K_{mat,i}a_v L \qquad [2.23]$$

This equation is applied to the limiting reactant. The only information required from the CFD simulations is the conversion. Therefore the equation [2.24] can be used to evaluate the mass transfer coefficient and the global Sherwood number.

2.2.3 Steady State Mass Balance [SSMB]

This method is based on the global mass balance at steady state conditions. The mass balance is:

$$IN - OUT + PROD = 0$$

The *PROD* term is the reacting term and it describes reactants consuming. This method can be applied to evaluate the local Sherwood if a small volume, close to zero, is considered. The mass balance for this small volume is:

$$\dot{m}_i^{IN} - \dot{m}_i^{OUT} = k_{CIN}\rho_i^W A_{CAT} \qquad [2.25]$$

where A_{CAT} is the catalytic surface in this volume.

The chosen volume is the part of reactor included between two planes. These planes are cross-sections normal to the reactor main axis. To apply the balance at catalytic wall [2.4], the distance between these two plane must be close to zero. Therefore equation [2.25] becomes:

$$\dot{m}_i^{IN} - \dot{m}_i^{OUT} = -\mathfrak{D}_i \frac{d\rho_i}{dn} A_{CAT} \qquad [2.26]$$

The value of the diffusivity flux at the catalytic wall can be estimated:

$$\frac{\dot{m}_i^{IN} - \dot{m}_i^{OUT}}{A_{CAT}} = -\mathfrak{D}_i \frac{d\rho_i}{dn} \qquad [2.27]$$

and also the mass transfer coefficient [2.5]:

$$K_{mat,i} = \frac{\dfrac{\dot{m}_i^{IN} - \dot{m}_i^{OUT}}{A_{CAT}}}{(\rho_i^B - \rho_i^W)} \qquad [2.28]$$

where ρ_i^B and ρ_i^W are estimated as described for the PAMF method.

The SSMB method is different from the IMB method because the second one considers the conversion, estimated with the mass fraction, on the whole reactor. Instead the SSMB method is based on the difference between the inlet and outlet mass flux on an infinitesimal volume of the reactor.

2.3 Validation with monolithic structure

These different methods have been validated by reproducing the analytical solution for monolith reactors studied by Tronconi and Forzatti[21]. In their work, one-dimensional and two-dimensional models of monolith reactors for selective catalytic reduction (SCR) of $NO_{(x)}$ by NH_3 were developed.

$$4NO + 4NH_3 + O_2 \rightarrow 4N_2 + 6H_2O$$

These models were used to study circular, square and triangular geometry with a first order kinetics. The solutions of the two-dimensional model demonstrate that, as the reaction rate decreases from infinity to zero, the Sherwood number varies from the values of the Nusselt number characteristic of the Graetz-Nusselt problem with constant wall temperature to those with constant wall heat flux but with peripherally varying temperature. The solution of Graetz problem in circular ducts for constant wall temperature originally proposed by Grigull and Tratz[22] was adapted to describe Sherwood number:

$$Sh = Nu_{\infty,T} + 6.874(1000z^*)^{-0.488}\exp(-57.2z^*) \qquad [2.29]$$

where $z*$ is the dimensionless axial distance defined as:

$$z^* = (z\mathfrak{D}_i)/(u_m D_h^2) = (z/D_h)/(\mathrm{Re}\,Sc) \qquad [2.30]$$

For each geometry the values of $Nu_{\infty,T}$ are listed in the second column of Table 2.

Table 2: Asymptotic Sherwood number for different geometries and different Damkholer number

Tronconi and Forzatti [21]		
Geometry	Da =100	Da = 0.001
Circle	3.659	4.362
Square	2.977	3.087
Triangle	2.494	1.891

In their work Tronconi and Forzatti[21] evaluate the Sherwood number with simplified models and with all the following assumptions:

1. Irreversible first-order kinetics model at the catalytic wall: $r = k_{CIN} C_{NO}$
2. Identical condition within each channel implies that simulation of a single monolith channel is sufficient to represent the behavior of whole reactor.
3. Isothermal condition.
4. Laminar flow: $\mathrm{Re} < 2300$
5. Constant fluid properties.
6. Negligible axial diffusion.
7. Analytic solution of the flow field.

The hypothesis 5,6,7 are introduced only to apply the less complex one-dimensional and two-dimensional models. If these models can be used to estimate the Sherwood number in monolith reactors, also the CFD, in the same operating conditions, can be used to calculate the mass transfer coefficient. The CFD is a more detailed model than the one-dimensional and two-dimensional models. Therefore the last assumptions can be ignored, but the results and the Sherwood number estimated must be the same.

The monolith reactor geometry is described in Figure 5 and in Figure 6:

Figure 5: Monolith reactor dimensions

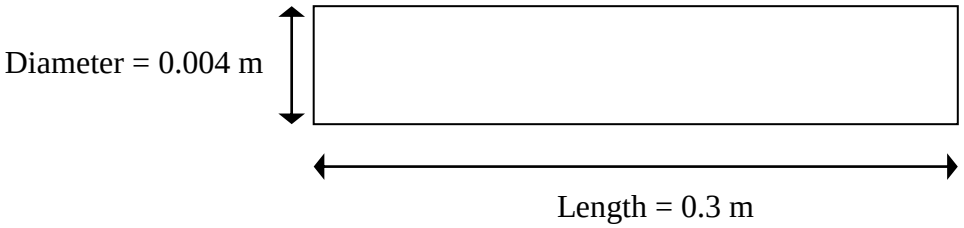

The channel cross-sections are circular, triangular and square with the same hydraulic diameter:

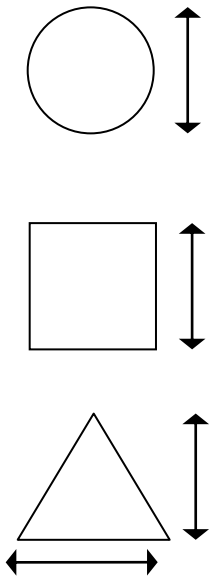

Diameter:	0.004	m
Side:	0.004	m
Side:	0.0034641	m
Height:	0.006	m

Figure 6: Duct geometries

Exploiting axial symmetry of these sections, it is possible to reduce the simulations CPU time. The meshes of the simulated geometries are shown in Figure 7 -Figure 9:

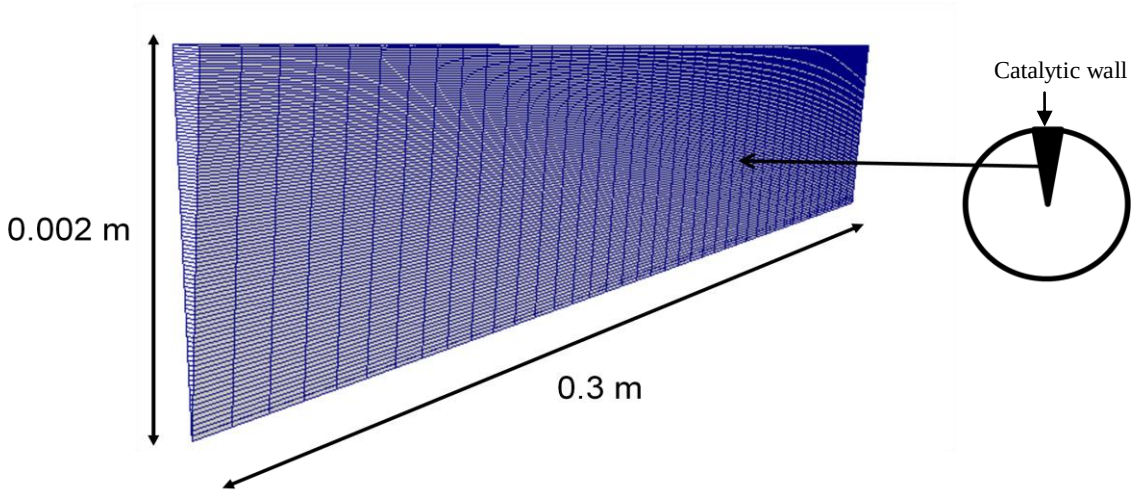

Figure 7: Mesh for the circular duct

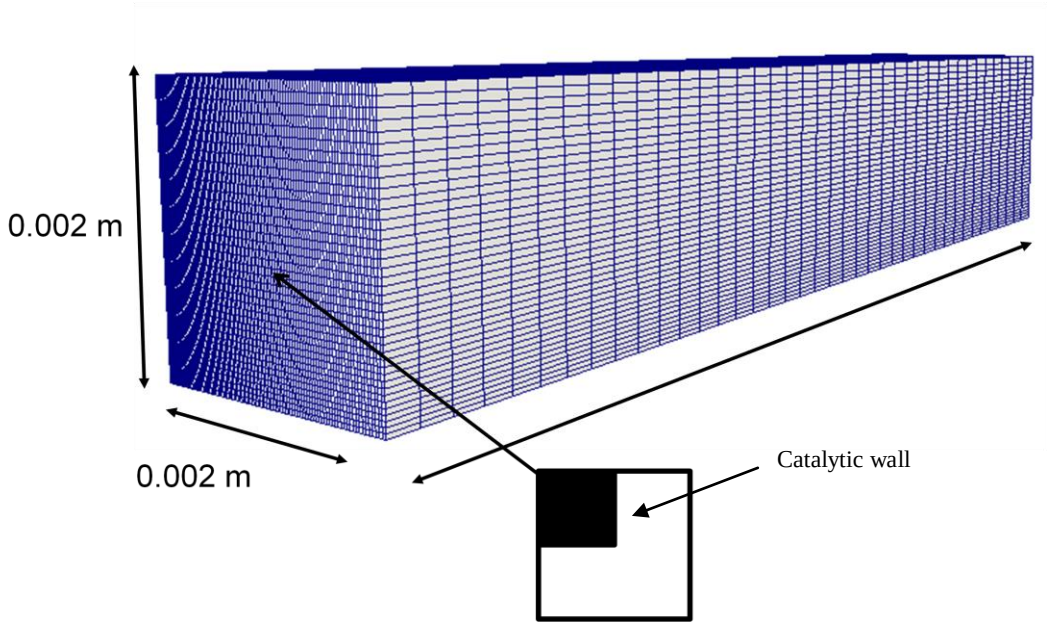

Figure 8: Mesh for the square duct

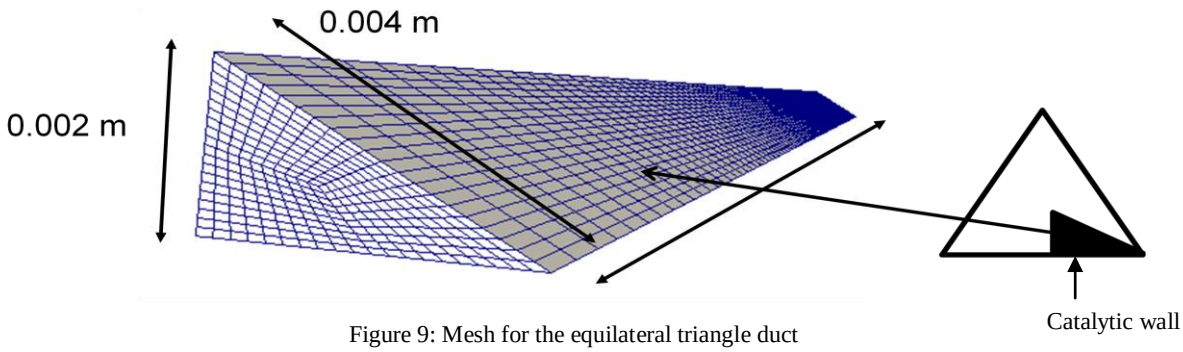

Figure 9: Mesh for the equilateral triangle duct

The operating conditions are reported in Table 3:

Table 3: Operating conditions

	Value	Unit dimension
Temperature	653	K
Pressure	101325	Pa
Velocity	4	m/s
Inlet mass fraction		
Argon (AR)	0.5	
Oxygen (O_2)	0.15	
Nitric oxide (NO)	0.1	
Ammonia (NH_3)	0.25	

As already mentioned, the reaction rate depends on the oxygen NO concentration, which is the limiting reactant. Moreover the Argon is the inert species.

The last parameter imposed for the CFD simulation is the kinetic constant. These simulations must be run in mass transfer regime. For this reason the Damkohler number [2.10], that describes the comparison between the reaction rate and the diffusivity flux, must as high as possible. First of all the methods validation is focus on asymptotic value of Sherwood number at the mass transfer regime. Therefore the chosen kinetic constant is:

$$Da \cong 100$$

$$r = 1.98 C_{NO} \quad \frac{Kmol}{m^2 s}$$

2.3.1 Mesh dependence analysis

First of all the effect of the mesh on these three methods is analyzed. The aim of this section is to find the smallest number of cells, which can describe the monolith reactor, without any influence on the Sherwood number estimated.

2.3.1.1 Peripheral Average Mass Fraction method [PAMF]

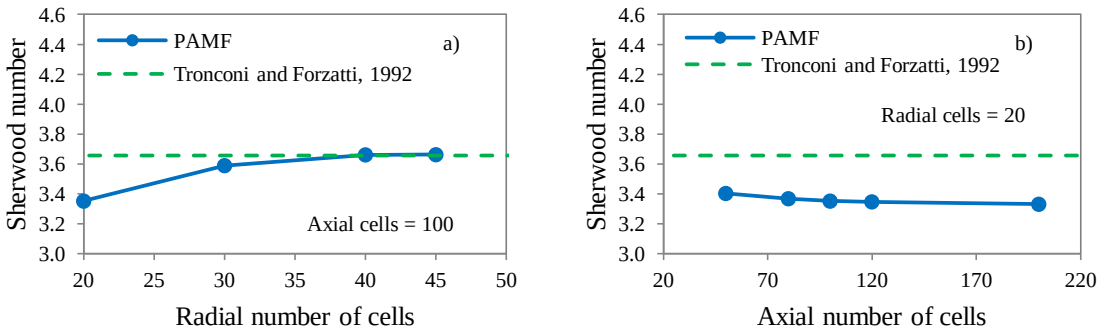

Figure 10: Analysis of the mesh effect on the Sherwood number estimated with the PAMF method

Figure 10 shows the effect of the mesh on the PAMF method. The plot a) describes the effect of increasing the radial number of cells, keeping the axial number of cell. The Sherwood number estimated reaches an asymptotic value, which does not depend on the mesh. The plot b) shows that if the number of axial cells increases, keeping the radial number constant, the Sherwood number reaches a wrong asymptotic value. This difference is related to the estimation of the cup-mixing mass fraction. As shown in the equation [2.13] the cup-mixing mass fraction depends on the velocity field.

For this reason the PAMF method is more depending on the radial mesh than on the axial mesh, because the correct cup-mixing mass fraction value can be estimated only if the radial number of cells can describe the velocity field on the cross-section. This effect is described in Table 4.

Table 4: Cup-mixing mass fraction and wall mass fraction VS radial number of cells with 100 axial cells.

Number of cells	NO mass fraction	
Radial	Wall (x1e-05)	Cup-mixing (x1e-04)
10	2.479	7.531
15	2.534	7.774
30	2.482	7.160
40	2.497	7.067
45	2.503	7.082

Table 4 shows that the cup-mixing mass fraction is more affected from the number of cells than the wall mass fraction. For this reason the PAMF method requires a more detailed description of the radial profile than of the axial profile to estimate the Sherwood number.

2.3.1.2 Integral Mass Balance method [IMB]

The dependence on the mesh of the IMB method is described in Figure 11.

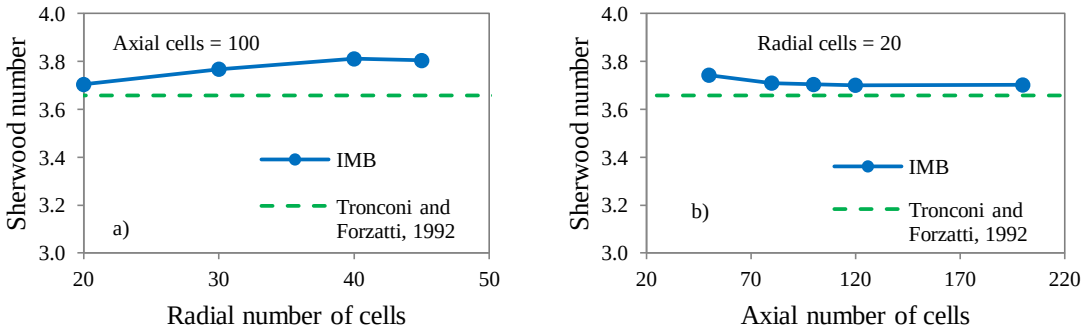

Figure 11: Analysis of the mesh effect on the Sherwood number estimated with the IMB method

Figure 11 shows that the IMB method always reaches an asymptotic value. The IMB method is based on a mass balance on the whole channel.

For this reasons this method can estimated the Sherwood number once the number of cell considered is bigger than 4000, as shown in Figure 12:

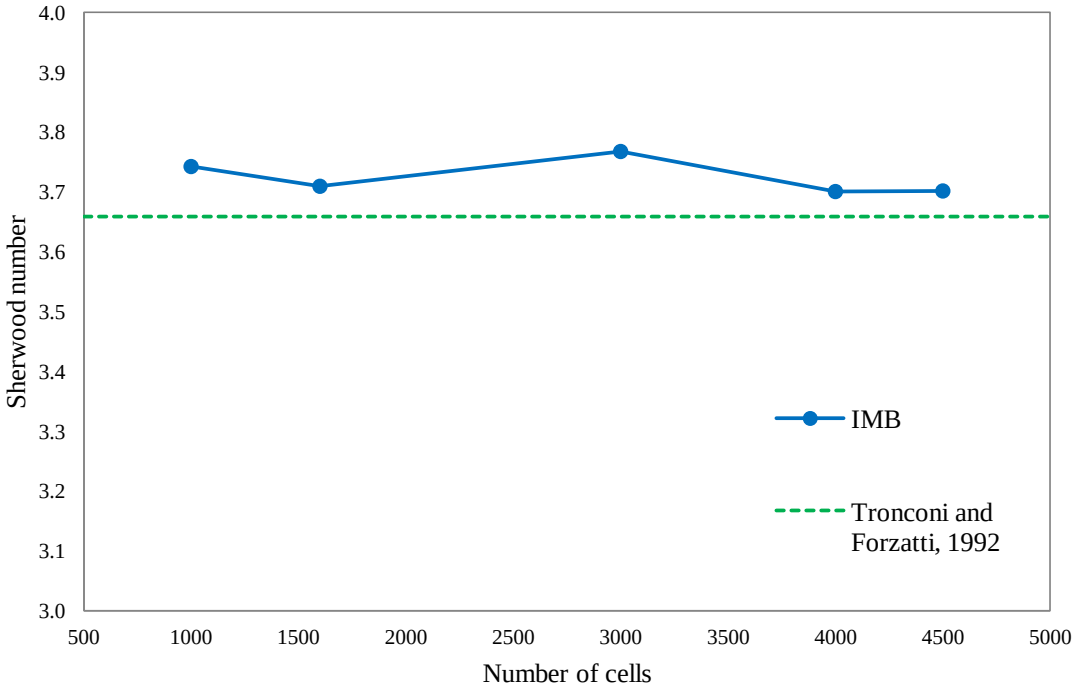

Figure 12: Mesh convergence check for IMB method

2.3.1.3 Steady State Mass Balance [SSMB]

The dependence on the mesh of the SSMB method is described in Figure 13.

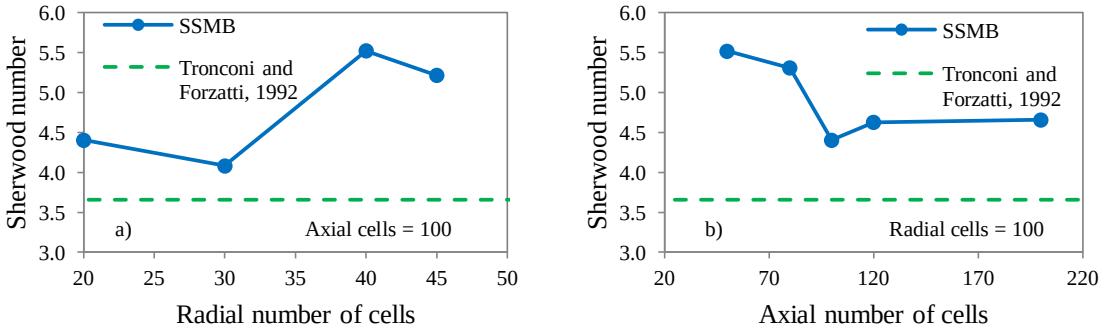

Figure 13: Analysis of the mesh effect on the Sherwood number estimated with the SSMB method

Figure 13 shows that the SSMB method is more affected by the axial number of cells than with by radial number of cells. This effect depends on the infinitesimal volume considered for the mass balance. The smallest distance between the two planes, used to select the volume for the mass balance, is the axial cell length. This method can be applied only if the volume is close to zero.

Therefore the Sherwood number reaches an asymptotic value only if the number of axial cells is high enough to guarantee a cell length small enough. Obviously, this effect influences also the total number of cells, as shown in Figure 14.

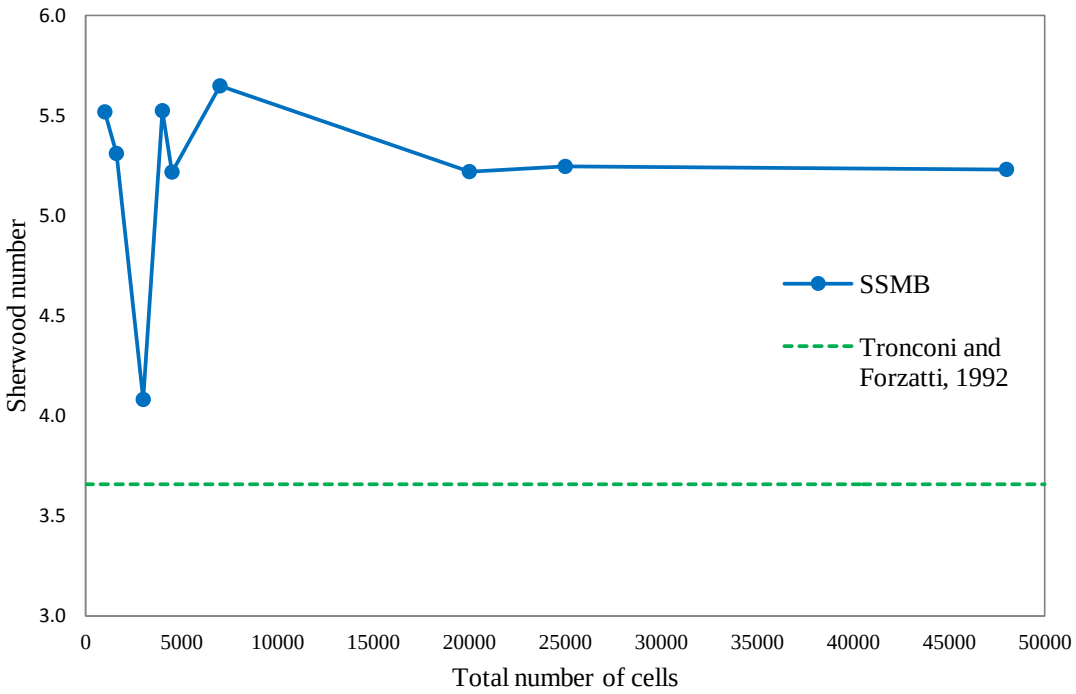

Figure 14: Mesh convergence check for SSMB method

2.3.2 Asymptotic Sherwood number

In their work, Tronconi and Forzatti [21], demonstrate that the asymptotic value of Sherwood number is reached when the dimensionless length of the channel is $z^* \geq 0.2$. Therefore all the results describes in this paragraph are estimate for $z^* \geq 0.2$. The considered equation is the solution of the Graetz-Nusselt problem with constant wall temperature and the asymptotic $Nu_{\infty,T}$ calculated by Tronconi and Forzatti[21]:

$$Sh = Nu_{\infty,T} + 6.874(1000z^*)^{-0.488}\exp(-57.2z^*)$$

2.3.2.1 Peripheral Average Mass Fraction method [PAMF]

The PAMF method is used to estimate the asymptotic value of Sherwood number for different geometries, in mass transfer regime. The results are shown in Table 5:

Table 5: Asymptotic Sherwood number for different geometries estimated with PAMF method

	This work	Tronconi and Forzatti [21]	Shah and London [23]
Geometry		Asymptotic Sherwood for Da = 100	
Circle	3.661	3.659	3.657
Square	2.980	2.977	2.976
Triangle	2.492	2.494	2.491

The main disadvantage of PAMF method is connected to the calculation of the wall mass fraction. The wall mass fraction can be estimated if this value on every catalytic faces of any catalytic cells is evaluated. Once these values are calculated with the CFD simulation, the peripheral average on the catalytic wall can be estimated. For simple geometries, as circular or square duct, at a fixed distance from the reactor entrance, the catalytic wall is a square or a circle and the mean value can be evaluated, but for more complex geometry the length of the catalytic wall may not be calculated.

2.3.2.2 Integral Mass Balance method [IMB]

The main advantage of this method is that wall mass fraction is not considered to calculate Sherwood number and thus it does not require the definition of the length of the catalytic wall. Therefore it can be applied to every kind of geometry, also complex geometry as packed bed. The different geometries are considered in these parameters:

reactor length: L

specific catalytic surface: a_v

On the contrary this approach can be used only in mass transfer regime. As described before, the equation [2.19] has an analytical solution only if the wall mass fraction is close to zero.

Moreover the IMB method is that it cannot calculate the local Sherwood number at any axial distance, but the Sherwood number is assumed to be constant in the whole reactor. Since the estimation of the Sherwood number is made on the all reactor length, the asymptotic Sherwood number is influence also by the entry region. Therefore the asymptotic Sherwood number is overestimated. This effect can be reduced if the reactor length is extended as shown in Table 6.

Table 6: Entry region effect on asymptotic Sherwood for different reactor length

Reactor length [m]	Asymptotic Sherwood number
0.150	4.030
0.300	3.812
0.400	3.808
0.500	3.737
0.550	3.707
0.650	3.704
0.750	3.682
0.800	3.685
0.840	3.680

The difference between the solution estimated by Tronconi and Forzatti[21] and IMB method could not be zero because this approach is developed with different hypothesis, as discussed before.

Table 7: IMB method for different channel geometries

	This work	Tronconi and Forzatti [21]	Difference
Geometry	Asymptotic Sherwood for Da = 100		
Circle	3.682	3.659	0.023
Square	3.012	2.977	0.035
Triangle	2.513	2.494	0.019

As shown in Table 7 the asymptotic Sherwood number estimated with the IMB method has a difference. To verify if this offset can be considered acceptable or not, a one-dimensional simulations has been carried out, comparing the mass fraction profile of the NO species.

The one-dimensional model equations are:

Gas phase species mass balance:

$$\frac{\partial \omega_i^B}{\partial t} = -\frac{G}{\rho_g \varepsilon}\frac{\partial \omega_i^B}{\partial x} - a_v K_{mat,i}(\omega_i^B - \omega_i^W) \qquad [2.31]$$

Solid phase species mass balance:

$$0 = -a_v \rho_g K_{mat,i}(\omega_i^B - \omega_i^W) + \sum_{j=1}^{Nreaction} \nu_{i,j} R_j \alpha_{cat} \qquad [2.32]$$

Where a_v and α_{cat} are parameters that describe the monolith reactor geometry.

The one-dimensional model describes the monolith channel in the same operating condition, with the same kinetics constant and hypothesis described in this chapter. The expressions of Sherwood number, for circular duct, implemented in the one-dimensional model are:

Tronconi and Forzatti, 1992: $Sh = 3.659 + 6.874(1000\ z^*)^{-0.488}\exp(-57.2\ z^*)$

IMB method: $Sh = 3.682 + 6.874(1000 z^*)^{-0.488}\exp(-57.2 z^*)$

As discussed before this equation is a modified solution of the Graetz-Nusselt problem with constant wall temperature for circular duct.

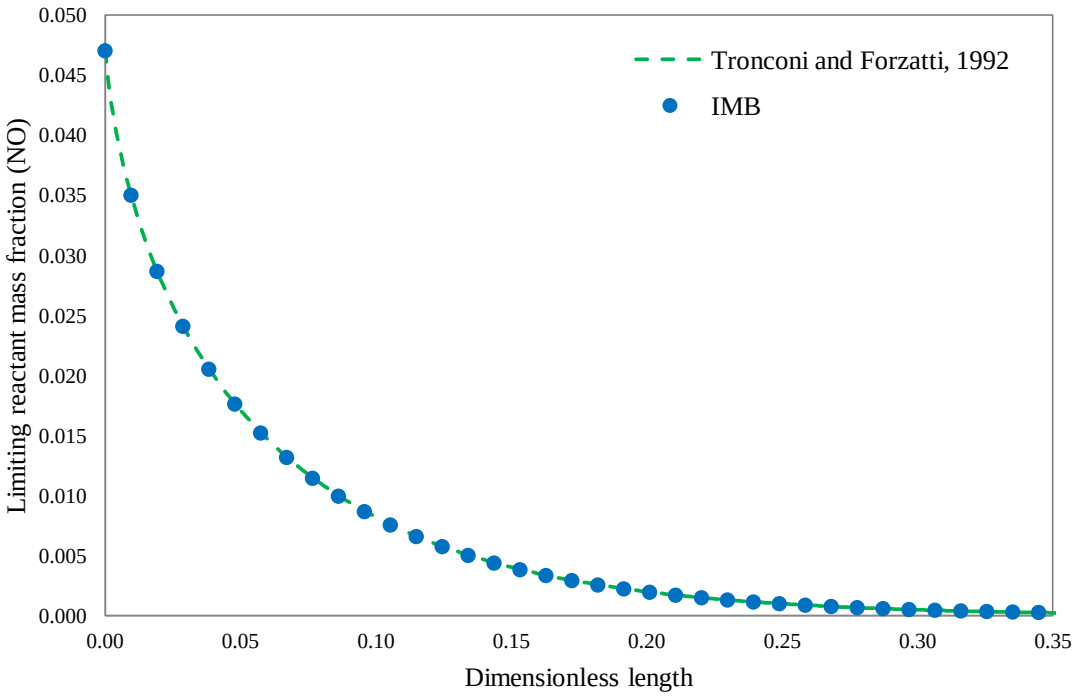

Figure 15: Asymptotic Sherwood comparisons with 1D model for IMB method

Figure 15 shows that an offset of 0.023 on the asymptotic value of Sherwood number can be considered acceptable.

2.3.2.3 Steady State Mass Balance [SSMB]

Table 8 shows the comparison between the asymptotic Sherwood numbers:

Table 8: Asymptotic Sherwood number for the SSMB method

	This work	Tronconi and Forzatti [21]	Offset
Geometry	Asymptotic Sherwood for Da = 100		
Circle	5.231	3.659	1.572

Table 8 shows that the error is not negligible. In this case the offset is higher than in the previous one. In the same way the one-dimensional model has been applied to verify if the offset is acceptable or not. The expressions of Sherwood number, for circular duct, are:

Tronconi and Forzatti, 1992: $Sh = 3.659 + 6.874(1000z^*)^{-0.488}\exp(-57.2z^*)$

SSMB method: $Sh = 5.231 + 6.874(1000z^*)^{-0.488}\exp(-57.2z^*)$

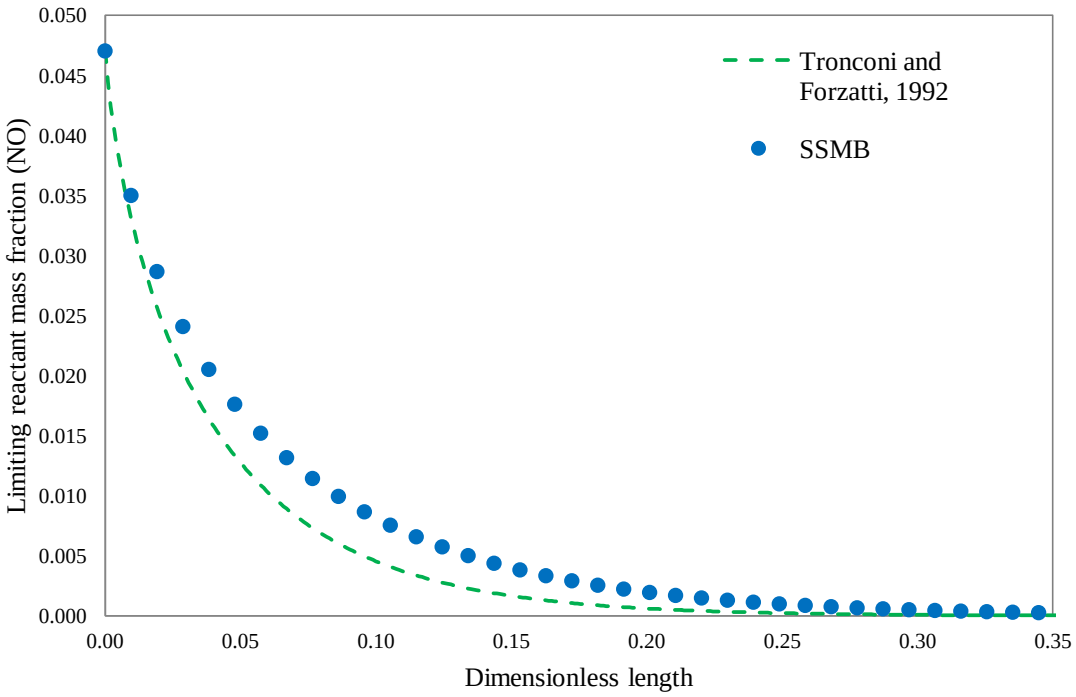

Figure 16: Asymptotic Sherwood comparisons with 1D model for SSMB method

The results of the one-dimensional model have demonstrated that the offset of SSMB is significant. The error depends on the calculated values of cup-mixing density, wall mass fraction and global mass flux.

- ✓ The low volumetric flow rate in each monolith channel (e.g. $5*10^{-05}\ \frac{m^3}{s}$) increases the uncertainty non only the global mass flux but also on the cup-mixing density, which depends on the mass flow rate.
- ✓ Moreover the SSMB method requires to work with an infinitesimal volume that mean a variation of the global mass flux extremely low (e.g. $\dot{m}_i^{IN} - \dot{m}_i^{OUT} = 2.104*10^{-13}$) making the numerical errors related to the CFD simulation not anymore negligible.
- ✓ Finally the reactor works in mass transfer regime, then the wall mass fraction is close to zero

Due to these disadvantages and the high number of cells required this method could not be applied to study Sherwood number and mass transfer coefficient, in these operating conditions.

2.3.3 Local Sherwood number

The equation [2.29] allows estimating the local Sherwood number in every point of the reactor. In this paragraph PAMF, IMB and SSMB methods are used to calculate the local Sherwood number and their results are compared with the analytical solution.

2.3.3.1 Peripheral Average Mass Fraction method [PAMF]

One of the advantages of this method is that it is able to estimate the local Sherwood number. Figure 21 shows the comparisons between the Sherwood number estimated by the PAMF method and that estimated by Tronconi and Forzatti[21].

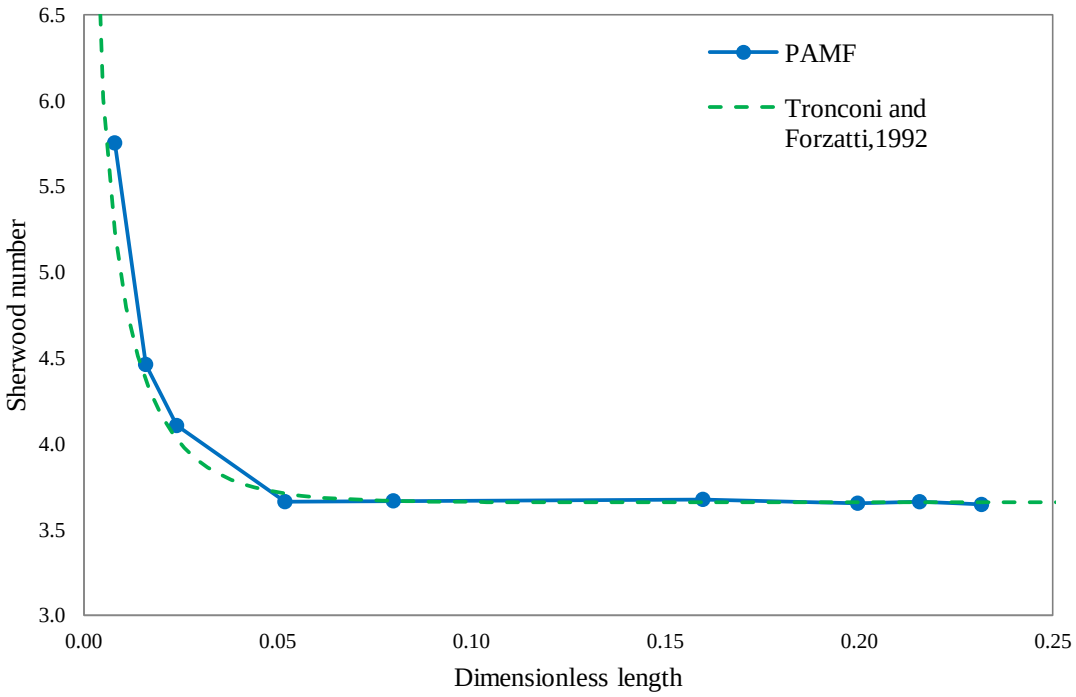

Figure 17: Axial profile of Sherwood number in for circular duct with PAMF

The small difference in the entry region can be correlated with the hypothesis of constant flow proprieties and analytical flow field solution applied by Tronconi and Forzatti [21].

2.3.3.2 Integral Mass Balance method [IMB]

As discussed before, this method considers the whole reactor. For this reasons the IMB method cannot calculate the local Sherwood number and the axial profile inside the monolith reactor. This is the main disadvantage of this approach. This disadvantage can be partially overcome if the global mass balance is applied not to the whole reactor, but at different reactor length. The axial profile estimated with the IMB method is shown in Figure 18.

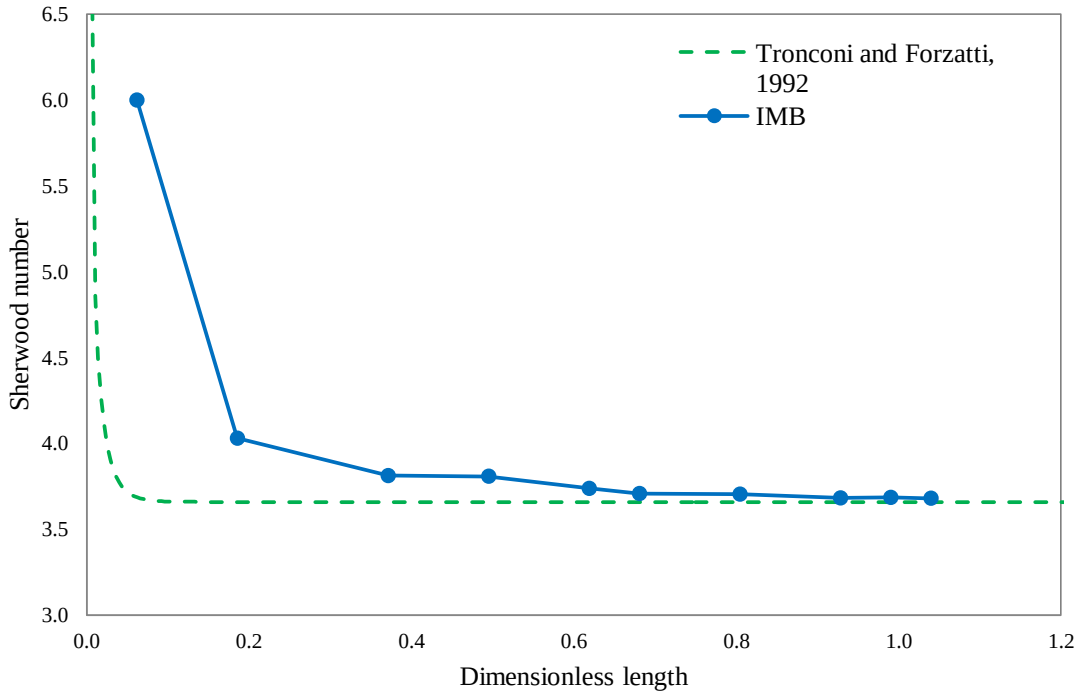

Figure 18: Axial profile for the monolithic reactor estimated with the IMB method

Figure 18 shows that the IMB method cannot be used to evaluate the local Sherwood number, because it is based on a mass balance on the whole reactor.

2.3.3.3 Steady State Mass Balance [SSMB]

The local Sherwood number can be estimated with this method as shown in Figure 19.

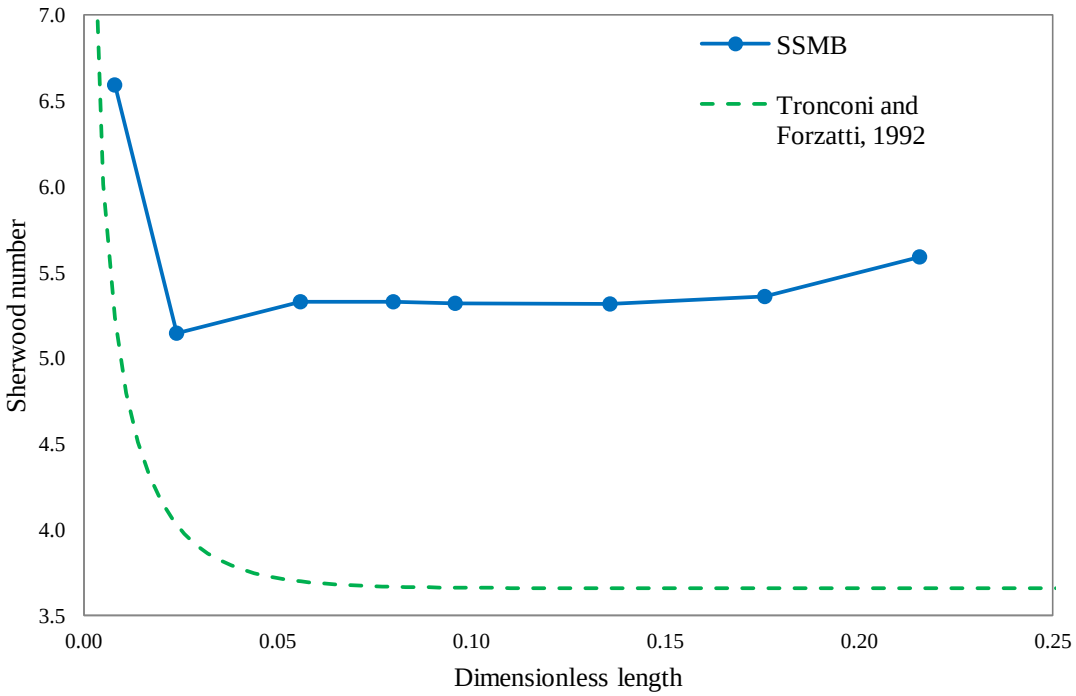

Figure 19: Axial profile of Sherwood number in for circular duct with IMB

The SSMB method can take into account the entry region effect and the axial trend of Sherwood number inside a monolith reactor. However the main problems of this approach are related to the offset and to the numerical errors of the CFD simulation, as discussed before, and that an asymptotic value of the Sherwood number is not reached (Figure 19).

2.3.4 Chemical regime

As described before, due to the hypothesis of the first order kinetics, the rate of reaction can be modified according to different Damkohler numbers. Therefore the chemical regime will be analyzed in this paragraph.

$$Da \cong 1 \qquad\qquad Da \cong 0.01$$

$$r = 0.0198 C_{NO} \ \frac{Kmol}{m^2 s} \qquad\qquad r = 0.000198 C_{NO} \ \frac{Kmol}{m^2 s}$$

2.3.4.1 Peripheral Average Mass Fraction method [PAMF]

The PAMF method is used to estimate the Sherwood number in chemical regime as well as the axial trend inside the reactor is investigated.

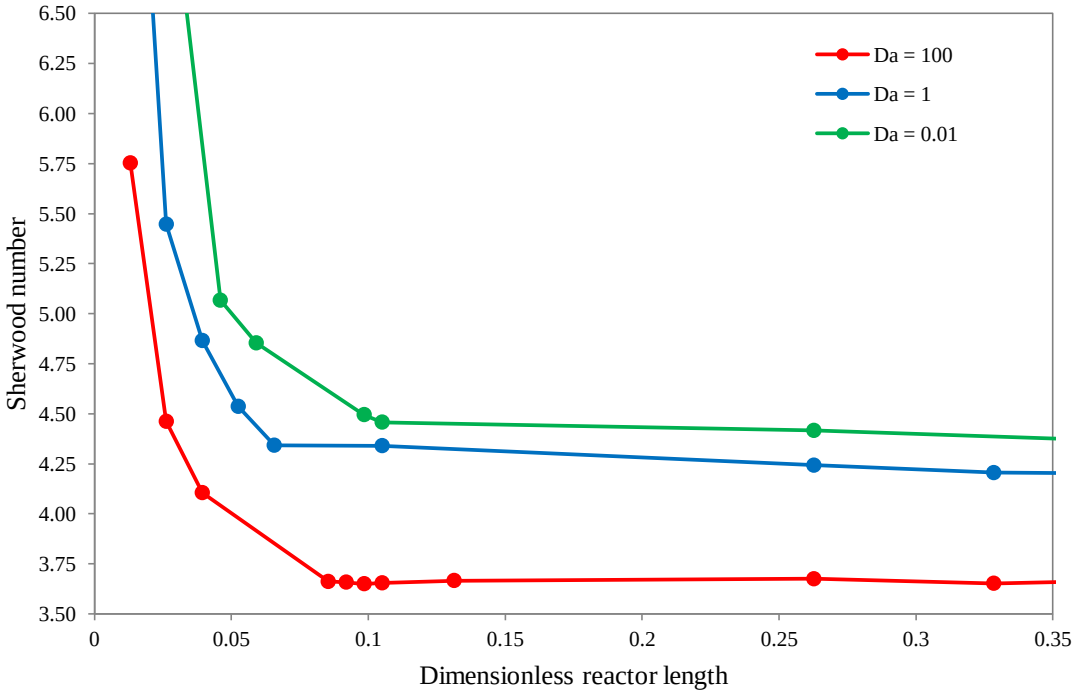

Figure 20: Sherwood axial profile for different Damkohler number

Figure 20 shows like that Sherwood number decrease rapidly along the entry region of the channel until an asymptotic value is reached. As observed by Tronconi and Forzatti, the asymptotic Sherwood number is reached for $z^* \geq 0.2$. Moreover the asymptotic value of Sherwood number, for the same geometry channel, is related with Damkohler number.

This correlation between the asymptotic Sherwood number and the Damkohler number has been studied for different geometries.

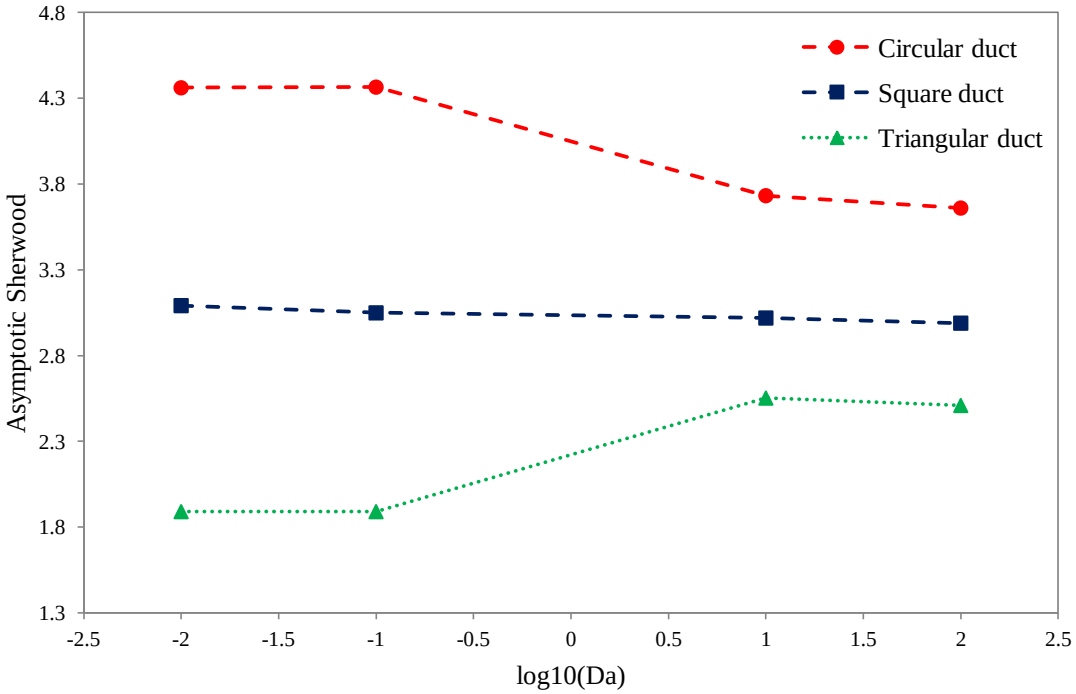

Figure 21: Influence of the Damkohler number and the channel geometry on Sherwood number with PAMF

As shown in Figure 21 the effect of Damkohler number on the asymptotic Sherwood number is different in terms of value and in terms of trend for the three geometries. For the triangular duct increasing the Damkohler number increases the Sherwood number. In the case of the square channel the effect is reduced and for the circular duct the increasing of Damkohler number decreases the Sherwood number.

2.3.4.2 Integrate Mass Balance method [IMB]

As described before, the IMB method can be applied only in mass transfer regime due to the hypothesis of wall mass density close to zero (eq. [2.19]).

Table 9: Geometry effect on the asymptotic Sherwood number with IMB method

	This work	(Tronconi and Forzatti,1992)[21]	Offset
Geometry	Asymptotic Sherwood for Da = 100		
Circle	3.682	3.659	0.023
Square	3.012	2.977	0.035
Triangle	2.513	2.494	0.019

2.3.4.3 Steady State Mass Balance [SSMB]

The SSMB method can be applied also in chemical regime and the results are shown in Figure 22.

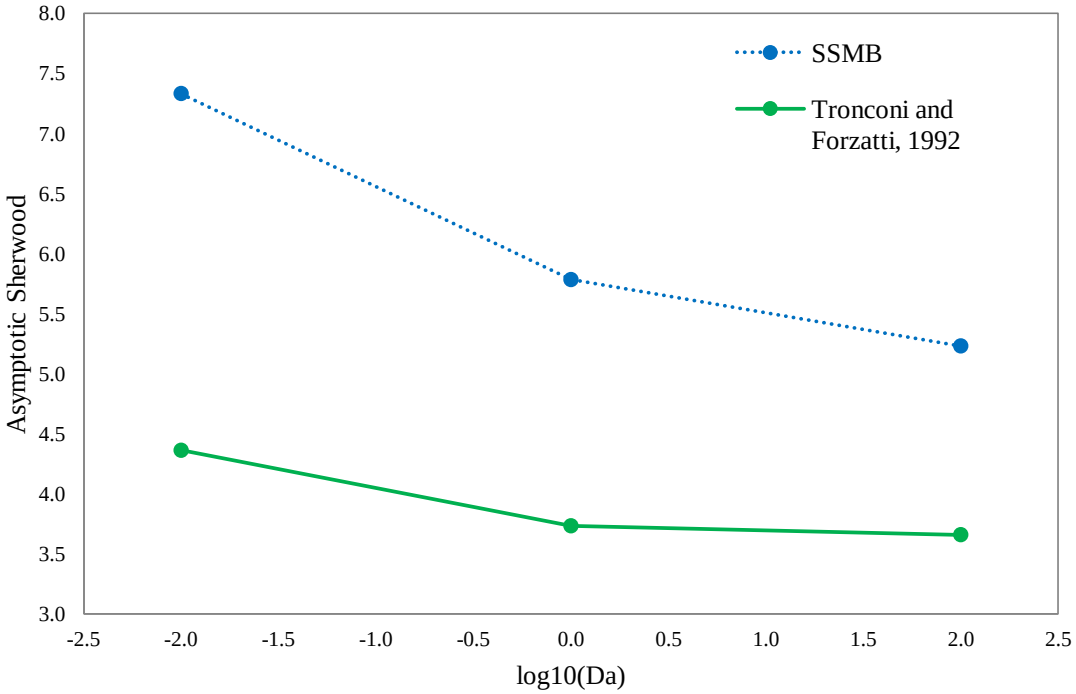

Figure 22: Influence of the Damkohler number on Sherwood number with PAMF

Also in this case the problems of this method are the numerical errors and the offset with the analytical solution, related with them. Due to these errors the trend that describes the relation between the Damkohler number and the asymptotic Sherwood number is not achieved.

This method has been applied also with other geometries:

Table 10: Geometry effect on the asymptotic Sherwood number with SSMB method

	This work	Tronconi and Forzatti [21]	Offset
Geometry	Asymptotic Sherwood for Da = 100		
Circle	5.231	3.659	1.572
Square	6.068	2.977	3.091
Triangle	4.315	2.494	1.821

Due to the offset the SSMB method cannot distinguish *a priori* between the different duct geometries.

2.4 Extension to more complex geometries

IMB and PAMF methods have been applied to more complex geometries to verify if they can be used to study the mass transfer coefficient in complex geometries, as micro-channel packed bed. These channels are also used to analyze the effect of inert and reacting sphere on Sherwood number. For these reasons two different geometries are developed.

The first one is a circular duct, with spheres inside. The center of every sphere is on the symmetry axis of the channel. The geometry of this channel is described in Figure 23 and Figure 24:

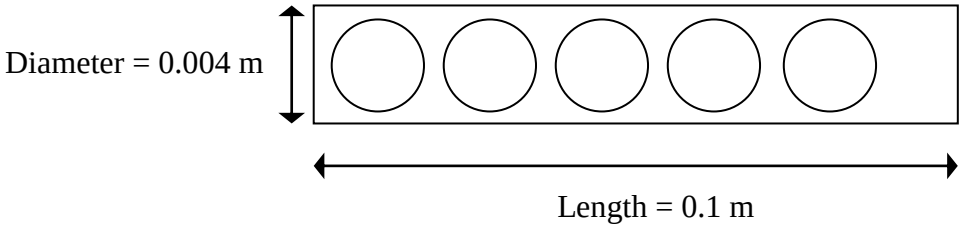

Figure 23: Circular duct with spheres

The sphere's diameter is 0.003 m and the distance between the centers of the spheres is 0.004. In the channel there are 24 spheres.

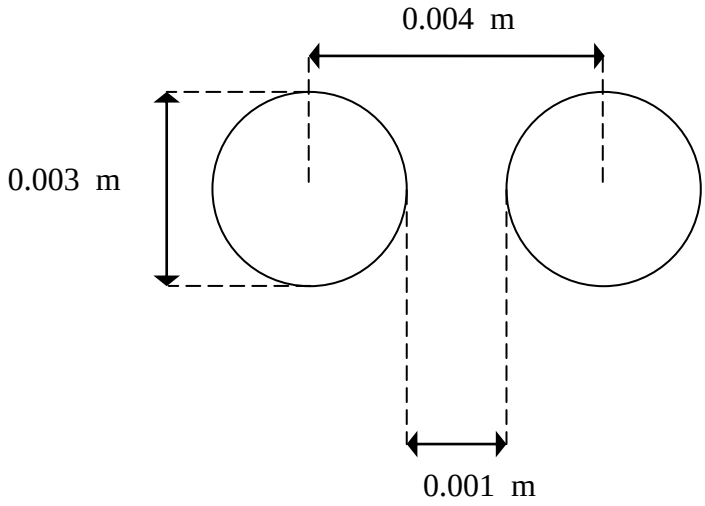

Figure 24: Spheres position in the circular duct

The second geometry is a square duct with 32 spheres inside. In this geometry, the centers of the spheres are not on the main axis, but their position create a more complex geometry without any symmetry. The geometry of this channel is shown in Figure 25 and Figure 26:

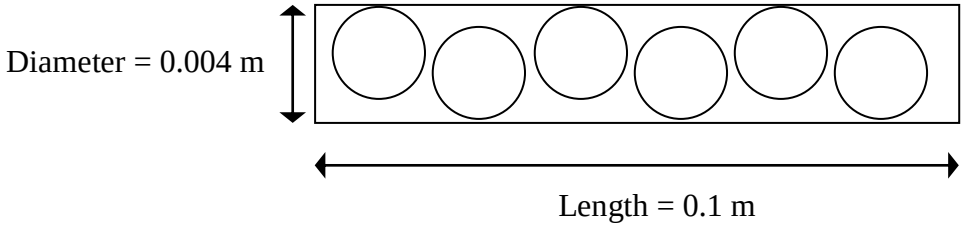

Figure 25: Square duct with spheres

Also in this geometry the sphere diameter is 0.003:

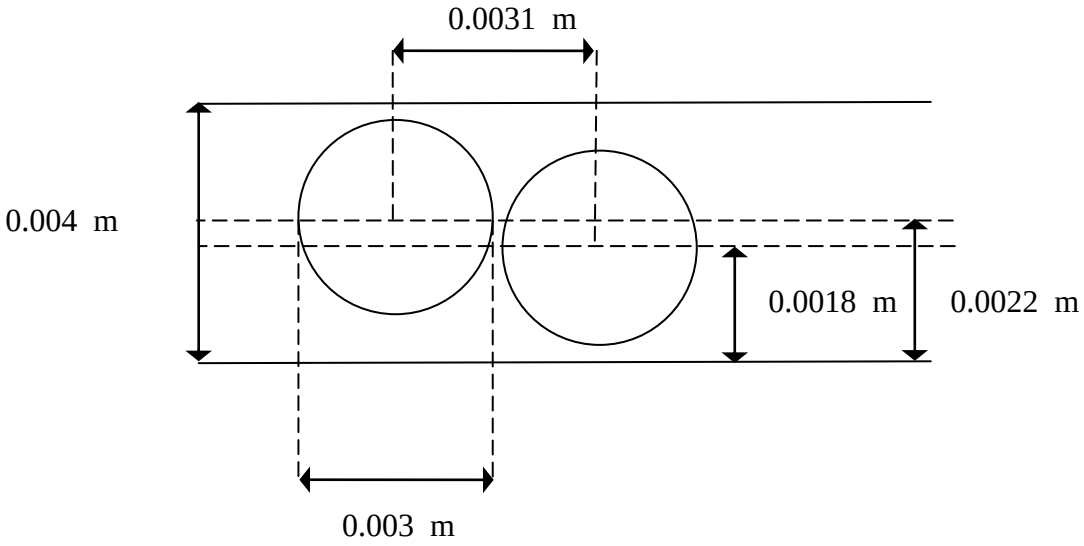

Figure 26: Spheres positions in the square duct

2.4.1 Inert spheres

These complex geometries are used to create a reacting wall channel with inert spheres inside. These studies are developed to analysis the effect of the flow field on the Sherwood number. All the simulations are run with the same operating condition described before. For this reasons the results can be compared with the analytical solution of the empty channel[21].

The PAMF and IMB methods are used to evaluate the asymptotic Sherwood number and the results are described in Table 11:

Table 11: Asymptotic Sherwood number for circular duct with inert spheres

Asymptotic Sherwood number			
	PAMF method	IMB method	Difference
Circular duct	11.675	13.961	2.286
Square duct	7.569	16.396	8.827

If compared with the offset for monolith reactor described before, the differences between the Sherwood numbers estimated with the IMB method and with the PAMF method now are significant. The error is related to the PAMF method. As shown before, this approach can evaluate the Sherwood number at every axial distance of the reactor., but the estimation of the mass transfer coefficient requires the calculation of the cup-mixing mass fraction (eq. [2.13]). This value is straightly connected with the velocity and the flow field.

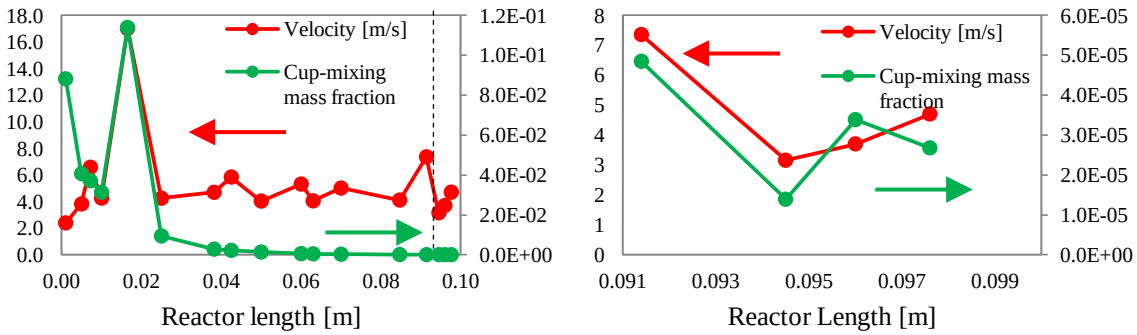

Figure 27: Velocity and cup-mixing mass fraction in the square duct with spheres

Figure 27 shows the velocity and cup-mixing mass fraction along the axial profile. The axial profile should reach the asymptotic value for the velocity at the end of the reactor, but Figure 27 shows that this does not happen.

Due to the presence of the spheres the velocity cannot reach an asymptotic value and this behavior has effect on the Sherwood number estimated.

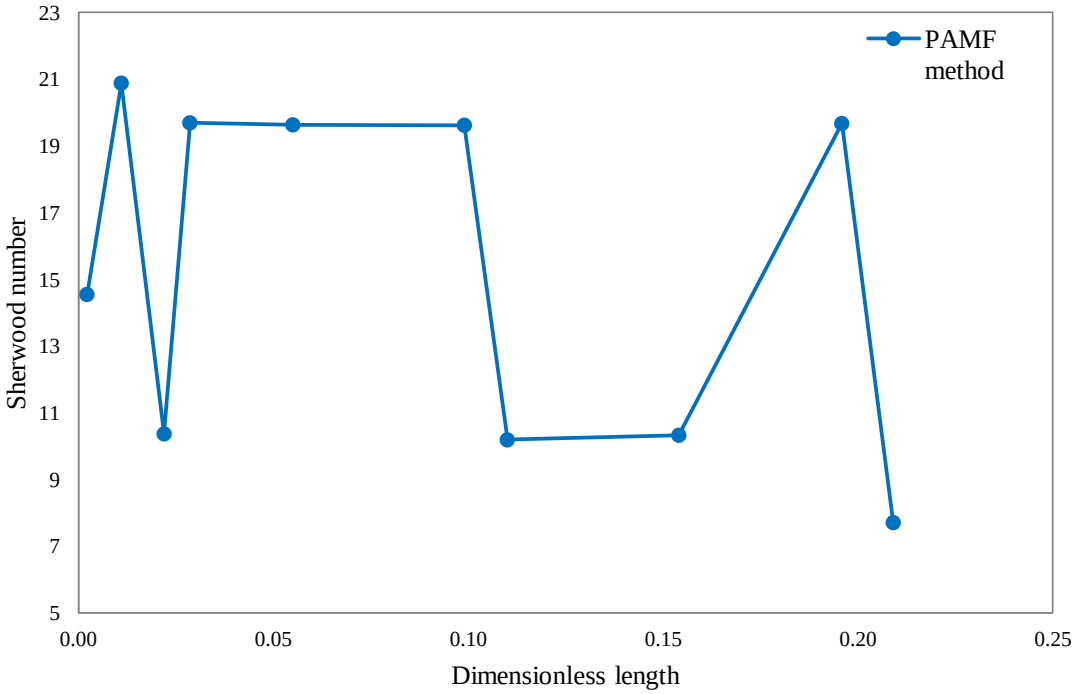

Figure 28: Axial profile of Sherwood number in the square duct with inert spheres estimated with PAMF method

Figure 28 shows that the Sherwood number estimated with the PAMF method depends on the velocity field. Higher Sherwood numbers are related with higher velocity as shown in Figure 29.

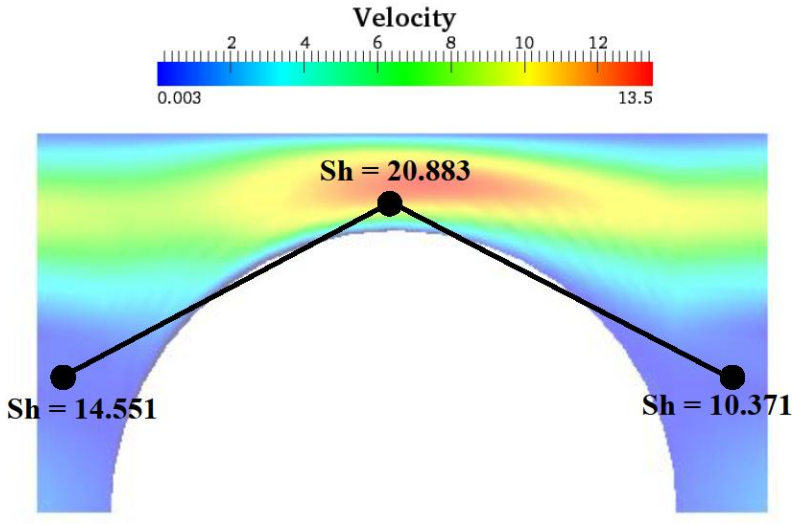

Figure 29: Effect of the velocity field on the Sherwood number estimated with the PAMF method

PAMF method is not suitable investigate Sherwood number and mass transfer coefficient in this kind of reactors with complex geometry, because the velocity and cup-mixing mass fraction do not reach asymptotic values. This problem is exceeded if the Sherwood number is calculated with the IMB method. This approach has the advantage that the mass balance considers the whole reactor, thus the not constant velocity field has a no effect on the Sherwood number estimated. The Sherwood number calculated with the IMB method can be considered as a mean Sherwood number weighted on the velocity field, as show in Figure 30.

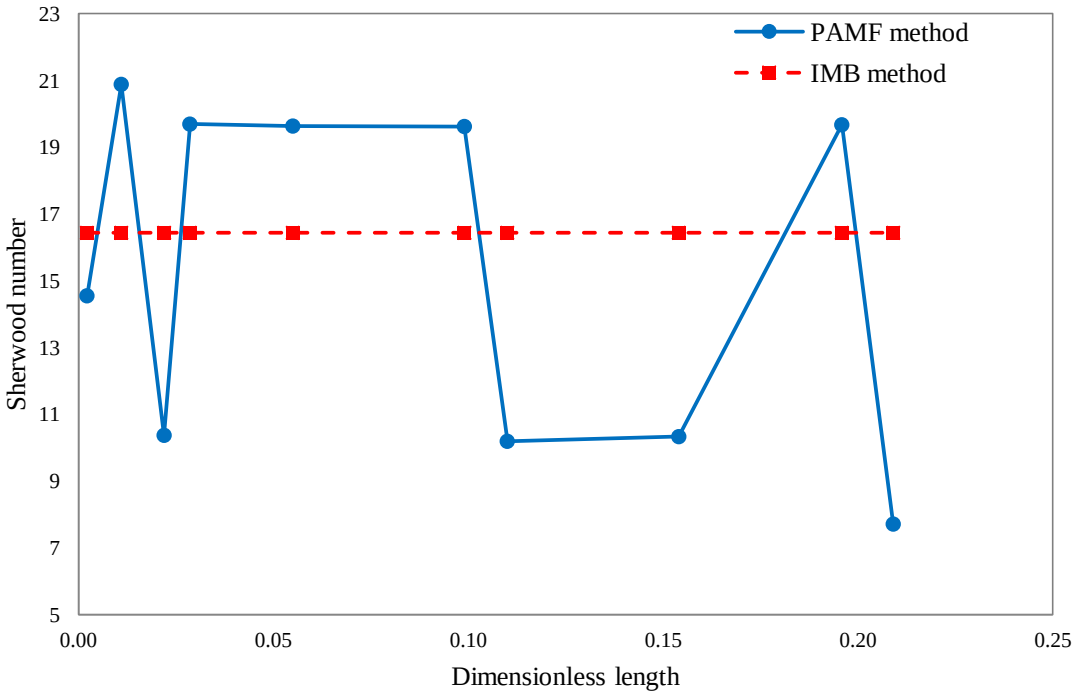

Figure 30: Comparisons of the axial profile of Sherwood number in the square duct with inert spheres estimated with PAMF method and with IMB method

Figure 30 shows that the Sherwood number estimated with the IMB method can describe the mass transfer phenomena inside these reactors with complex geometries.

Once it is understand that the right value of the Sherwood number can be estimated with the IMB method the flow field effect on mass transfer coefficient in these channels can be studied.

Table 12: Flow field effect on Sherwood number for complex geometries with inert spheres

		Channel with spheres	
	Empty channel	Circle	Square
Asymptotic Sherwood number	3.659/2.997	13.961	16.396

In Table 12 the asymptotic Sherwood number evaluated with the IMB method are compared. Therefore the values of Sherwood number in Table 12 show that mass transfer phenomena are supported by the presence of the spheres. This effect can be explained if the velocity field is analyzed:

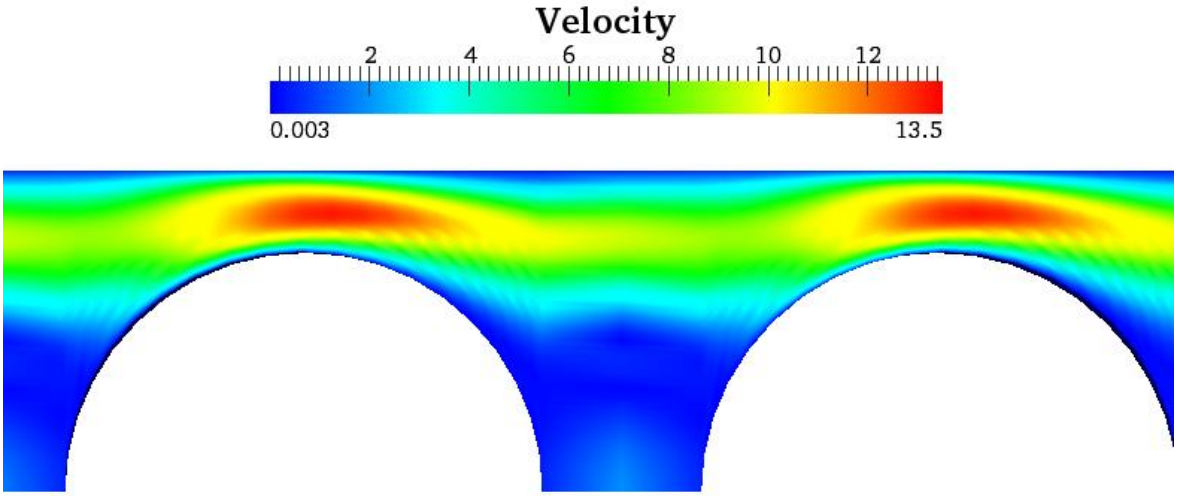

Figure 31: Velocity field in the circular duct with spheres

Figure 31 shows that the velocity near the wall is higher than in the center of the channel. This means that the spheres create preferential paths that concentrate the reactants near the catalytic wall. Therefore a bigger amount of reactants reach the catalyst. Due to the mass transfer regime this effect is described by greater Sherwood number and mass transfer coefficient.

Moreover in Table 12 is shown that Sherwood number is higher in square channel than in the circular duct. This effect depends on the corners of the square section. The cornered section creates preferential path that has positive influence on the mechanism thought with the reactants reach the catalytic wall (Figure 32).

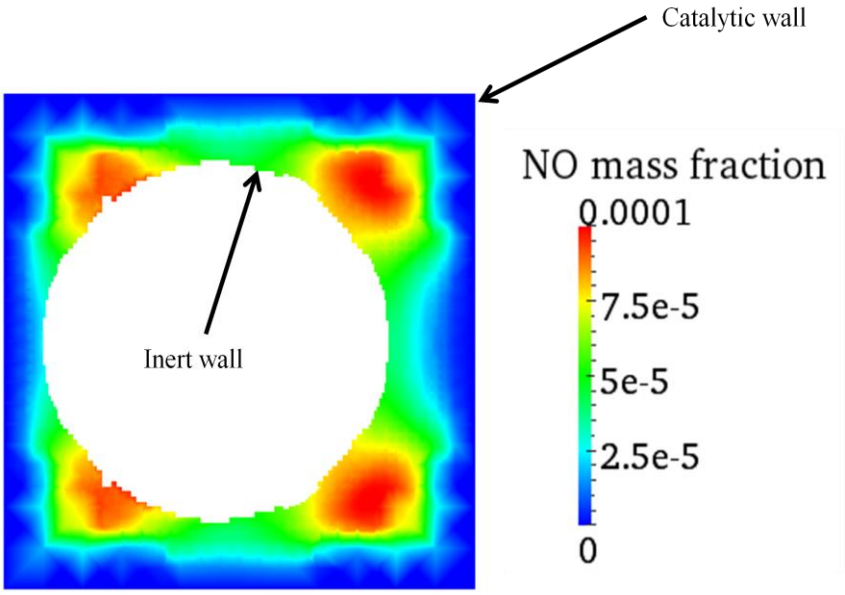

Figure 32: Cross section of the square channel with inert spheres

2.4.2 Catalytic spheres

The complex geometries are now used to analyze the effect of reacting spheres inside a circular and a square inert channel. These geometries are similar to a simple packed bed and these CFD simulations can be used to have an overview of the mass transport phenomena inside packed bed with characteristic dimensions of a micro-channel reactor.
The results are shown in Table 13:

Table 13: Asymptotic Sherwood number for circular duct with catalytic spheres

Asymptotic Sherwood number			
	PAMF method	IMB method	Difference
Circular duct	19.767	16.438	3.329
Square duct	6.014	10.387	4.373

Also in this case the difference between the PAMF method and the IMB method is significant. As discussed before, the error is associated with the PAMF method and the cup-mixing mass fraction that is straightly connected with the velocity field.
Table 14 shows the of the Sherwood numbers for the two complex geometries:

Table 14: Flow field effect on Sherwood number for complex geometry with catalytic spheres

	Circle	Square
Asymptotic Sherwood number	16.438	10.384

The trend of Sherwood number, in this case, is opposite to those observed in the Table 12.

This effect depends on the flow field and on the preferential path developed near the external wall, as shown in Figure 31.

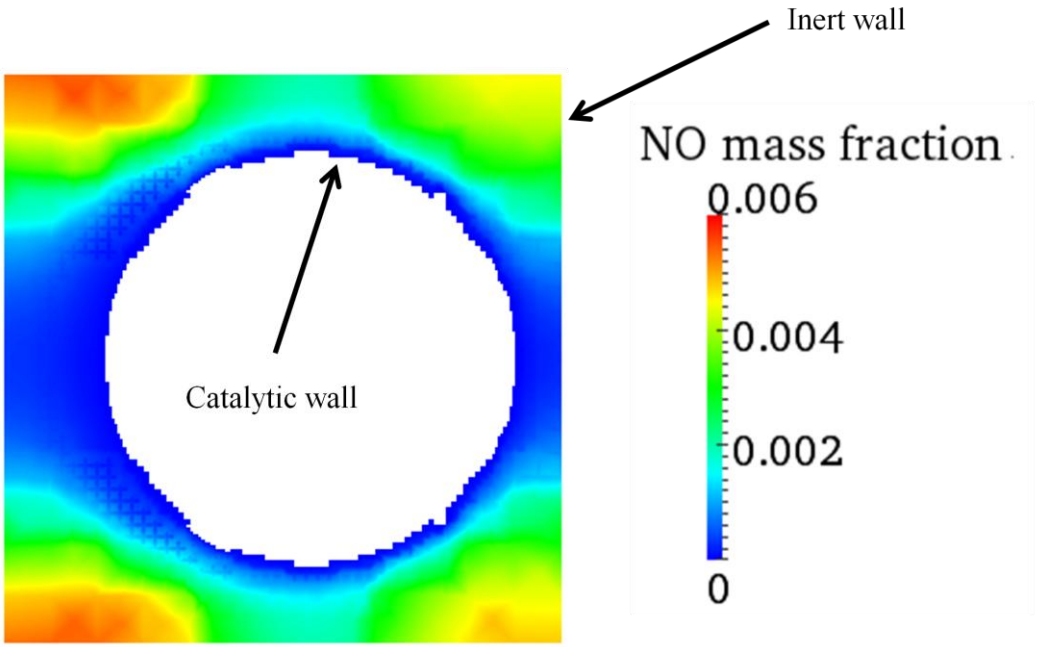

Figure 33: Cross section of the square duct with reacting spheres

Figure 33 shows the effect of preferential path on the Sherwood numbers. The preferential path near the corners of the channel creates flux of reactant (NO) that cannot reach the catalytic surface of the sphere. In this case the cornered section has a negative effect on the mechanism thought which the reactants reach the catalytic wall. Due to the mass transfer regime this effect is represented by a smaller Sherwood number for the square duct.

3 Mass transfer phenomena and pressure drops

3.1 Introduction

At the beginning of this chapter, the methodology to generate a model of a random packing of spheres is described. This methodology was developed by Freund et al. [24, 25] to create random packing models for reactor with geometry and dimensions similar to industrial applications. This approach will be used to generate a micro-channel packed bed reactor. Then the void fraction will be analyzed. The results will be compared with different experimental correlations developed to predict the mean void fraction of a packed bed (e.g. Dixon[26], Foumeny et al.[27], Haughey and Beveridge[28]). This comparison can establish if the generated model for the micro-channel reactor is an acceptable description of a real packed bed, because the bed porosity is the only property, related to the random packing, which can be easily analyzed. Once the feasibility of the micro-channel is verified, the properties of this unconventional device will be studied. The pressure drops are estimated with the CFD simulations and the mass transfer phenomena are analyzed with Global Mass Transfer method (IMB) described in chapter 2. Finally the pressure drops and the Sherwood number calculated will be compared with the correlations developed for industrial dimensions packed bed (e.g. Ergun [13], for the pressure drops, or Yoshida et al. [2] for the Sherwood number).

Due to the very unconventional geometry of micro-channels respect to traditional reactors, mass transfer coefficients may be different from the value of conventional packed bed. For this reason the aim of this chapter is to verify whether these correlations are able to describe transport phenomena inside micro-channel reactors.

3.2 Numerical construction of random packing model

The most common type of fixed bed in industry is a random arrangement of particle inside confining circle or square section tubes. Especially for low tube-to-particle diameter ratio the random packing has attracted much experimental and numerical analysis. The numerical studies were performed for packing consisting of spherical particle, due to the easiest way to generate the packing. The random packing is complex to create it can be generated only if one is interested in the "statistical" mean properties and not in the complete 3D structure. Ad described by Freund et al.[25], a two-step Monte Carlo process based on the algorithm of Soppe[29] is implemented to create the random packing. This approach has the advantage that is less time and money consuming then experimental method such as X-ray computer tomography (CT) [30] or magnetic resonance imaging (MRI) [31] that generates the 3D bitmap of the geometry.

This technique imitates the technical filling process to create the bed. Spherical particles of uniform size distribution are successively dropped into a circle or square cross-section tube. They stop as soon as they come into contact with any other sphere. During this *raining* process, a loose (and non-physical) packing is generated, because the spheres arrangement has not reach the mechanical stability and the mean bed porosity is not asymptotic.

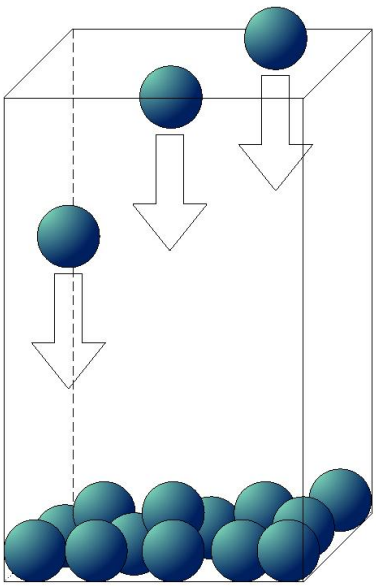

Figure 34: Dropping spheres in square channel

After this *raining* step the packing is compressed by rearranging the spheres with an increase probability into the direction of gravity. The process stops after meeting the convergence criteria that accounts for the change in potential energy and for the plausibility of the sphere positions (e.g, mechanical stability). The bed geometry is:

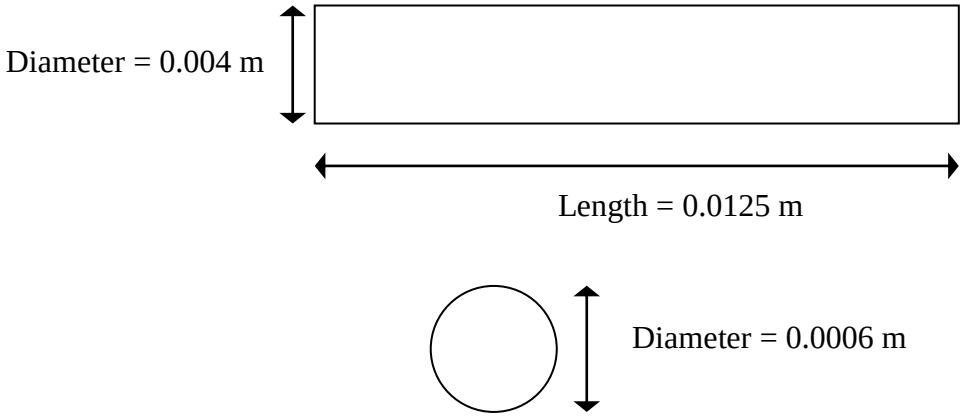

Figure 35: Micro-channel geometry with 600 micron sphere diameter

And the micro-channel reactor created with the methodology developed by Freund et al.[24, 25] is:

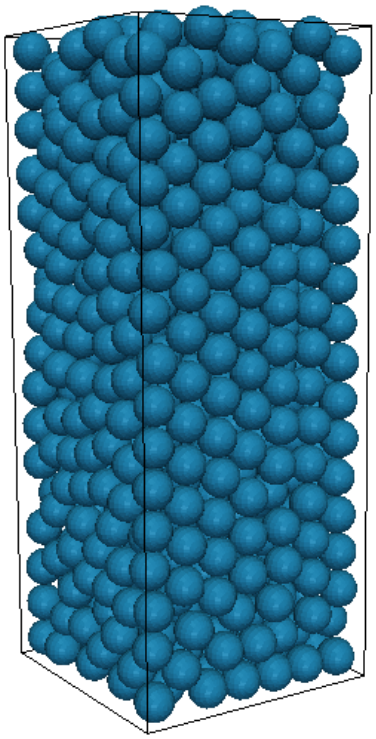

Figure 36: Micro-channel packed bed solid mesh

Once the spheres particle mesh is developed the mesh of the fluid region, around the spheres, has to be generated.

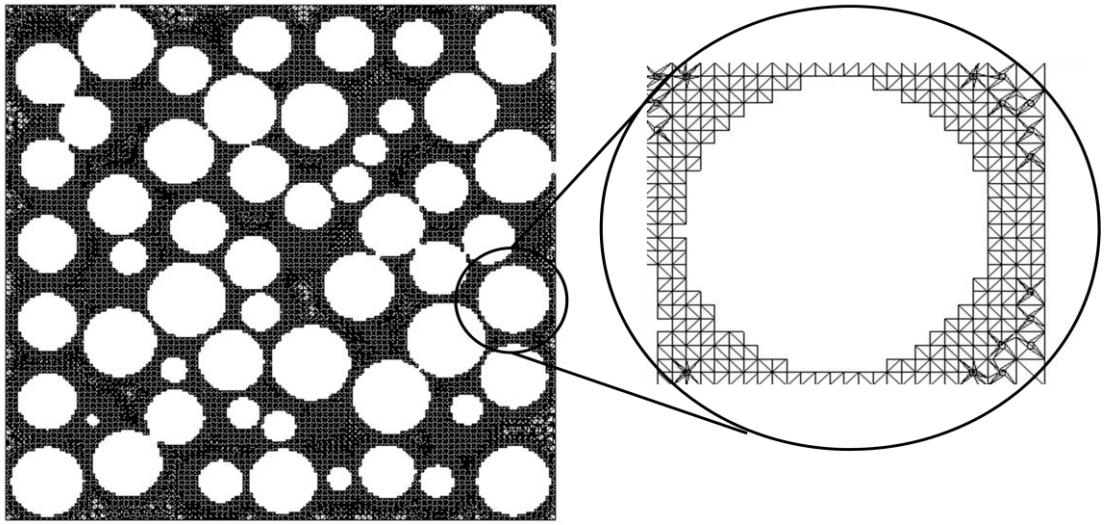

Figure 37: Micro-channel packed bed fluid mesh

The high number of cells, ~2000000, required depends on the small distance between the sphere and on the high number of spheres in the bed. In this micro-channel there are more or less 2500 spheres and, to the distinguish one from the others, the number of cells near the wall of the spheres must be high.

3.2.1 Mesh convergence analysis

The mesh depending analysis must be considered the properties studied. In this thesis the micro-channel pressure drops and mass transfer phenomena are analyzed, thus the Sherwood number and the pressure drops are considered. In Figure 38 the mesh depending is analyzed considering the pressure drops.

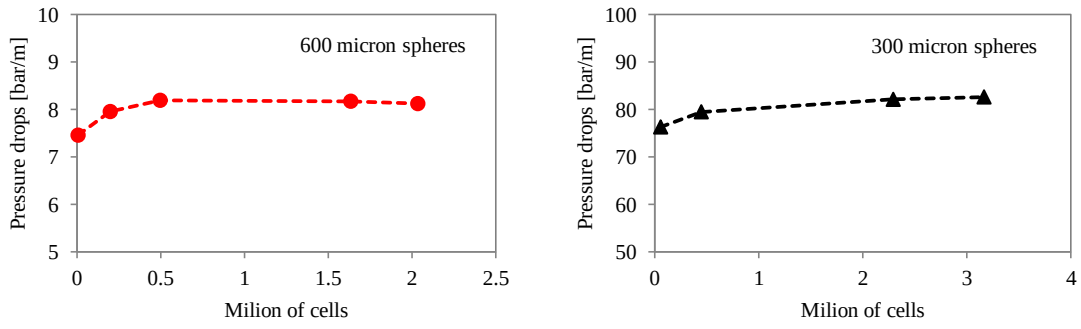

Figure 38: Mesh depending considering the pressure drops (Re = 77)

In Figure 39 the mesh depending analysis is carried out considering the asymptotic Sherwood number.

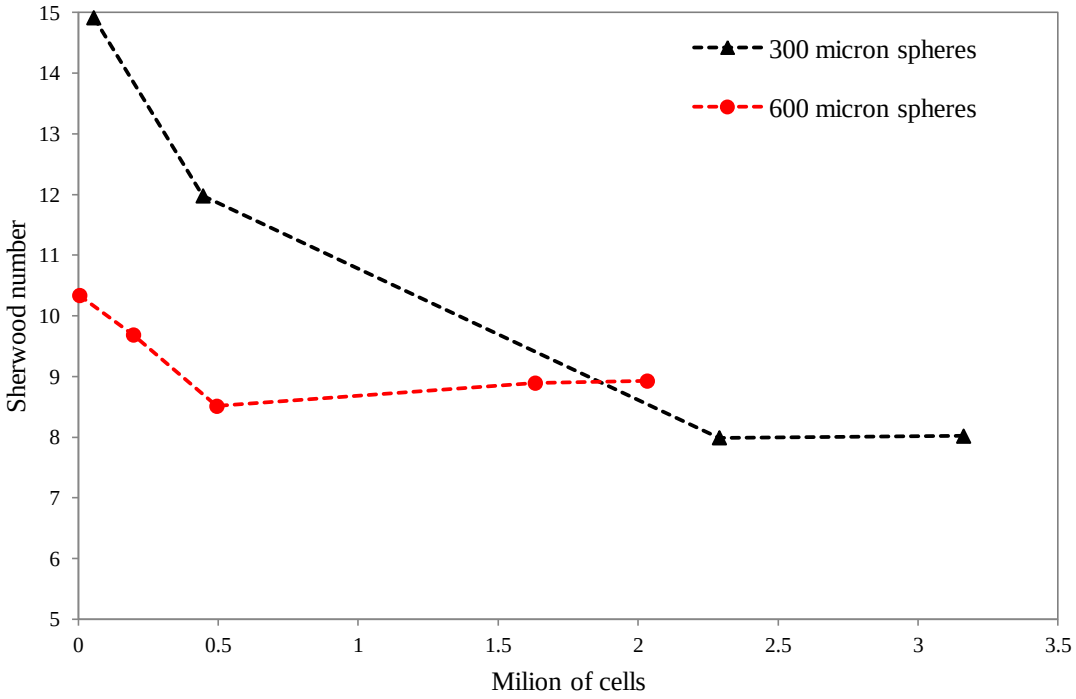

Figure 39: Mesh convergence analysis based on Sherwood number for the micro-channel reactors (Re = 77)

Figure 38 and Figure 39 show the mesh convergence check for both the considered micro-channel reactors. The number of cells requires to describe the pressure drops is smaller, thus the high number of cells is related to the mass transfer.

As discussed before, the number of cells required depends on the small distance between the spheres and describing the distance between every single sphere is possible only if the mesh grid is enough detailed. The area of every single sphere must be properly described because the mass transfer coefficient and the Sherwood number depends on it. For this reason ad mesh independent Sherwood number can be estimated only with a high number of cells. The high number of cells for these meshes (e.g ~2mln cells for 0.6 mm spheres diameter channel, ~ 2.3mln cells for 0.3 mm spheres channel) require also an high computational time.

3.3 Validation of the correlation for the void fraction

Once the micro-channel reactor and the fluid mesh are created, the bed porosity can be analyzed to verify if the generated packed bed is an acceptable description of a real packed bed. The void fraction for packed bed is defined as:

$$\varepsilon = \frac{V_{Void}}{V_{Total}} = \frac{V_{Total} - V_{Spheres}}{V_{Total}} \qquad [3.1]$$

For a square duct with sphere inside the void fraction is:

$$\varepsilon = 1 - N_{Spheres} \frac{\pi \frac{D_{Particle}^3}{6}}{D_{Tube}^2 L} \qquad [3.2]$$

The void fraction could not be evaluated *a priori* because the number of spheres $N_{Spheres}$ in the micro-channel is unknown. For this reason different experimental correlation were developed to estimate the void fraction without knowing the number of spheres.

The mean bed porosity, estimated with the packed bed generation, can be compared with the asymptotic values evaluated with some correlations developed for packed bed with conventional dimensions. The first considered correlation was developed by Dixon [26]. This equation depends on the tube-to-particle diameter ratio:

$$\varepsilon = 0.4 + 0.05\left(\frac{D_{Tube}}{D_{Particle}}\right)^{-1} + 0.412\left(\frac{D_{Tube}}{D_{Particle}}\right)^{-2} \qquad \frac{D_{Tube}}{D_{Particle}} > 2 \qquad [3.3]$$

$$\varepsilon = 0.528 + 2.464\left[\left(\frac{D_{Tube}}{D_{Particle}}\right)^{-1} - 0.5\right] \qquad 1 + \frac{\sqrt{3}}{2} \le \frac{D_{Tube}}{D_{Particle}} \le 2 \qquad [3.4]$$

$$\varepsilon = 1 - 0.667\left(\frac{D_{Tube}}{D_{Particle}}\right)^{-3}\left[2\left(\frac{D_{Tube}}{D_{Particle}}\right)^{-1} - 1\right]^{-0.5} \qquad \frac{D_{Tube}}{D_{Particle}} \le 1 + \frac{\sqrt{3}}{2} \qquad [3.5]$$

The micro-channels considered have this tube-to-particle diameter ratio:

$$\frac{D_{tube}}{D_{particle}} = \frac{0.004}{0.0006} \cong 6.7 \qquad \frac{D_{tube}}{D_{particle}} = \frac{0.004}{0.0003} \cong 13.3$$

Therefore the equation used in Table 15 is the equation [3.3].

The second experimental correlation for the void fraction considered was developed by Foumeny et al.[27]:

$$\varepsilon = 0.383 + \frac{0.254\left(\frac{D_{Tube}}{D_{Particle}}\right)^{-0.923}}{\sqrt{0.723\left(\frac{D_{Tube}}{D_{Particle}}\right)-1}} \qquad \frac{D_{Tube}}{D_{Particle}} > 1 + \frac{\sqrt{3}}{2} \qquad [3.6]$$

The last examined equation was proposed by Haughey and Beveridge [28]:

$$\varepsilon = 0.39 + 0.07\left(\frac{D_{Tube}}{D_{Particle}}\right)^{-1} + 0.54\left(\frac{D_{Tube}}{D_{Particle}}\right)^{-2} \qquad \frac{D_{Tube}}{D_{Particle}} > 2 \qquad [3.7]$$

Now these values can be compared with the void fraction calculated while the packed bed was generated:

Table 15: Micro-channel reactor void fraction VS experimental correlations

	Void fraction			
Tube-to-particle diameter ratio	Exact	Dixon[26]	Foumeny et al.[27]	Haughey and Beveridge[28]
6.7	0.41	0.417	0.406	0.413
13.3	0.40	0.406	0.391	0.398

Table 15 shows that the void fraction of the random packing models for the micro-channels are similar to the bed porosity predicted by the experimental correlations. These results demonstrate that the experimental correlations, developed for conventional packed bed reactor, can be applied to micro-channel reactors.

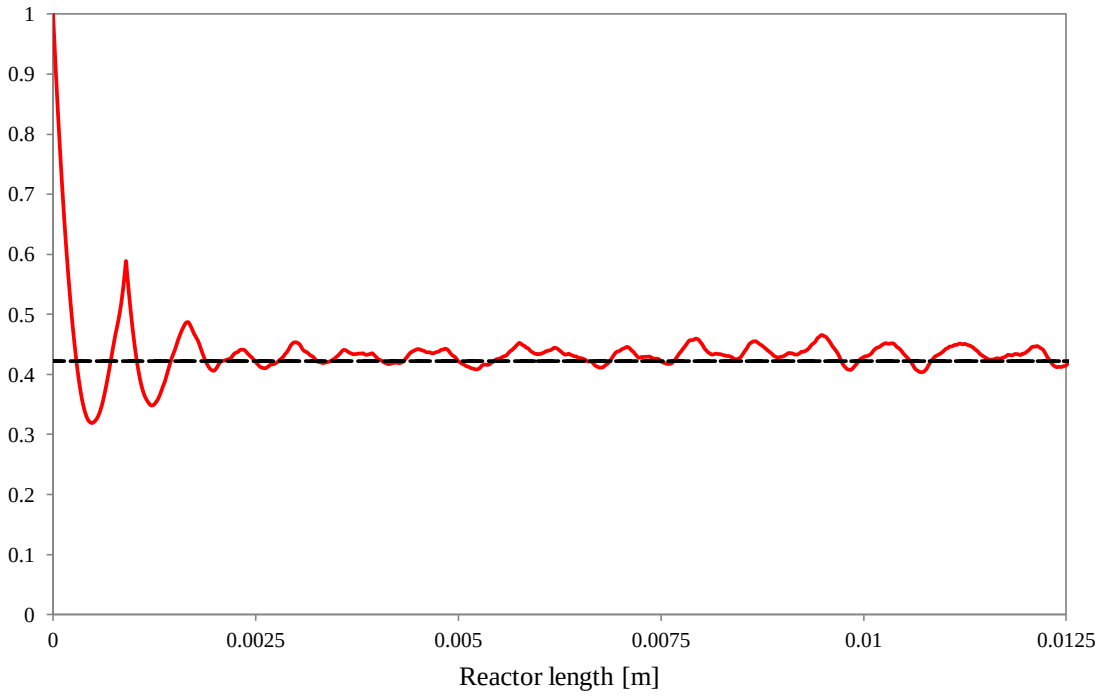

Figure 40: Axial void fraction for 600 μm diameter spheres

Figure 40 shows the axial profile of the void fraction. The straight line describes the mean value considered in Table 15. The axial profile of the void fraction demonstrates that the generated bed has a good arrangement of the spheres, because after an entry region the bed porosity reaches an asymptotical value.

3.4 Validation of the correlation for the pressure drops

Pressure drops are studied with the introduction of a dimensionless number called *friction factors*, as described by Bird et al.[13]. If a fluid flows in a duct, there will be a force applied by the fluid on the solid surface. This force can be split in two terms:

$$F_{TOT} = F_S + F_M \qquad [3.8]$$

The first one F_S describes the forces that are exerted by the fluid even if it is stationary. The second one F_M represents the forces associated with the motion of the fluid.

As shown by Bird et al.[13] the magnitude of second term is proportional to a characteristic area A and to kinetics energy K per unit volume:

$$F_M = AKf \qquad [3.9]$$

where the proportionally constant f is call *friction factor*. Note that this equation is not a law of fluid dynamics but only a definition of *friction factor*. This is a useful definition, because the dimensionless number f can be written as a function of Reynolds number and of the characteristic dimensions of the considered channel.

If an empty channel is considered the parameter involved in equation [3.9] are:

$$A = 2\pi RL \qquad [3.10]$$

$$K = \frac{1}{2}\rho\langle v\rangle^2 \qquad [3.11]$$

and the F_M force can be written as:

$$F_M = \Delta PA = \Delta P\pi\frac{D^2}{4} \qquad [3.12]$$

From the equations [3.9] and [3.12] the *friction factor* for a empty channel can be estimated as:

$$f = \frac{1}{4}\left(\frac{D}{L}\right)\frac{\Delta P}{\frac{1}{2}\rho v_0^2} \qquad [3.13]$$

As shown by Bird et al. [13] a "tube bundle" model can describe a packed bed. The pressure drops for a single tube are:

$$\Delta P = \frac{1}{2}\rho\langle v\rangle^2\left(\frac{L}{R_h}\right)f_{tube} \qquad [3.14]$$

From the equation [3.13] and [3.14] the *friction factor* of the whole packed bed is calculated as:

$$f = \frac{1}{4}\frac{D_p}{R_h}\frac{\langle v\rangle^2}{v_0^2} f_{tube} = \frac{1}{4}\frac{D_p}{R_h}\frac{1}{\varepsilon^2} f_{tube} \qquad [3.15]$$

The void fraction ε is introduced as a result of the superficial velocity:

$$v_0 = \varepsilon\langle v\rangle \qquad [3.16]$$

The hydraulic diameter R_h of a packed bed is defined as:

$$R_h = \frac{\varepsilon}{1-\varepsilon}\frac{D_p}{6} \qquad [3.17]$$

From the equations [3.15] and [3.17] the *friction factor* for the packed bed can be expressed as:

$$f = \frac{3}{2}\left(\frac{1-\varepsilon}{\varepsilon^3}\right) f_{tube} \qquad [3.18]$$

The f_{tube} is the experimental parameter calculated in different flow conditions.

3.4.1 Ergun equation

The f_{tube} can be modified to describe different flow condition and it value is evaluated by experimental data. All the simulations in this thesis work in laminar conditions, thus for laminar flow in tubes the *friction factor* is define as:

$$f_{tube} = \frac{16}{\mathrm{Re}_h} = \frac{16}{\frac{\rho v_0 R_h}{\mu}} \qquad [3.19]$$

If the constant value 16, is replaced by the value 100/3 this equation can describe the *friction factor* for packed bed in laminar flow conditions. The equation [3.9] can be modified with this value for the *friction factor* and the results is the Blake-Kozeny equation for the pressure drops in laminar conditions for packed bed:

$$\frac{\Delta P}{L} = 150\left(\frac{\mu v_0}{D_p^2}\right)\frac{(1-\varepsilon)^2}{\varepsilon^3} \qquad [3.20]$$

The Ergun equation, as demonstrated by Bird et al. [13], is an empirical superposition of asymptotes. For smaller inlet velocity v_0 the Ergun equation corresponds with the Blake-Kozeny equation (eq. [3.20]), for higher inlet velocity v_0 matches the Burke-Plummer equation, introduced for high turbulent flow.

The Burke-Plummer equation is:

$$\frac{\Delta P}{L} = \frac{7}{4}\left(\frac{\rho v_0^2}{D_p}\right)\frac{1-\varepsilon}{\varepsilon^3} \qquad [3.21]$$

Therefore the Ergun equation, that can describe the transition regime, is:

$$\left(\frac{\Delta P \rho}{G_0^2}\right)\left(\frac{D_p}{L}\right)\left(\frac{\varepsilon^3}{1-\varepsilon}\right) = 150\left(\frac{1-\varepsilon}{D_p G_0/\mu}\right) + \frac{7}{4} \qquad [3.22]$$

This equation has been applied with success to gas flow through packed bed columns by using an average value of gas density at the arithmetic average of the end pressures. Note that in all this equations G_0 and v_0 are hypothesized constant through the whole reactor length, whereas these values change through the bed for compressible fluids.

The Ergun equation has a good arrangement with experimental data over the range:

$$0.1 < \frac{D_p G_0}{(1-\varepsilon)\mu} < 10^5$$

As described before, the dimensions of the micro-channel analyzed in this work are:

$$D_p = 0.006\ m$$

$$\varepsilon = 0.41$$

And the range of inlet velocity considered is:

$$1 \le v_0 \le 10\ m/s$$

Therefore the Ergun equation can be applied to micro-channel, because the Reynolds range is:

$$21 < \frac{D_p G_0}{(1-\varepsilon)\mu} < 236$$

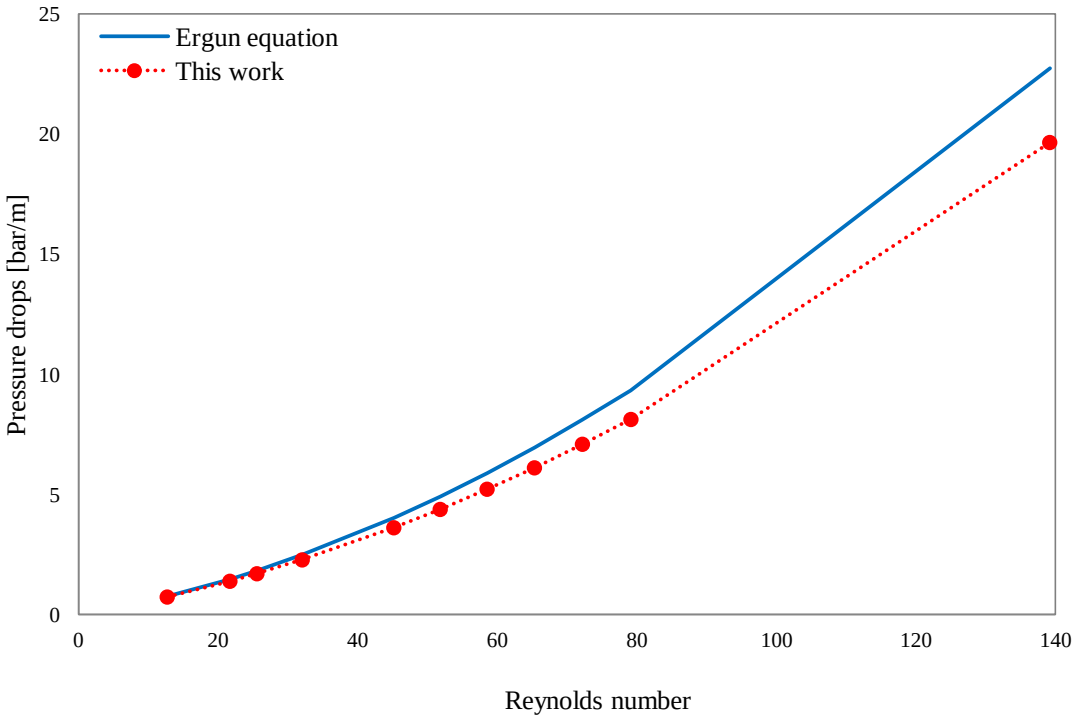

Figure 41: Ergun VS This work

Figure 41 shows the comparison of the Ergun equations with the pressure drops calculated with catalyticFoam [4, 5]. It is observed that the Ergun equation overestimate the pressure drops for this micro-channel. This difference is related to preferential paths developed near the external wall of the channel. The velocity field of this micro-channel can be analyzed with the CFD simulation:

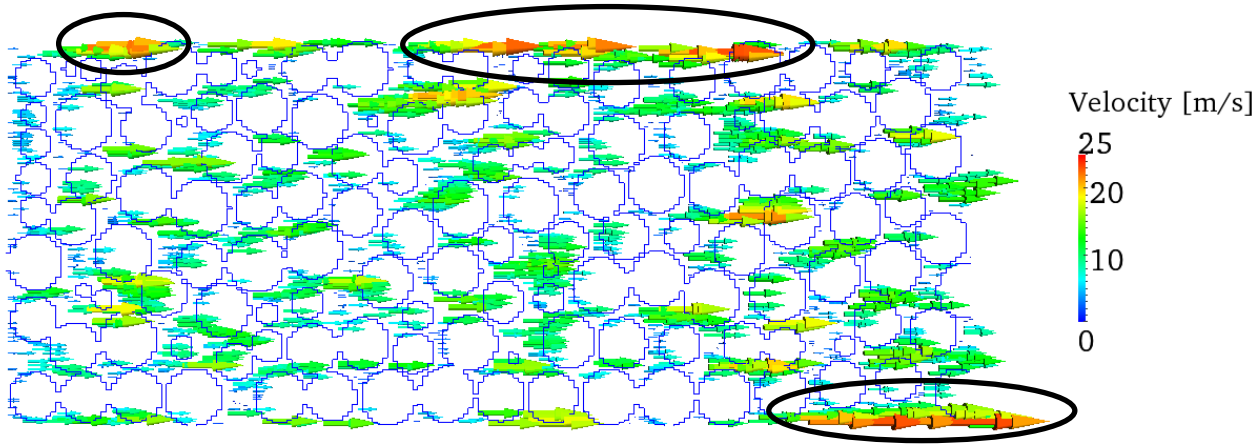

Figure 42: Velocity field in micro-channel. (Re = 70)

Figure 42 shows that the external wall creates preferential paths and their presence has effect on the flow rates and on the pressure drops. For these reasons Ergun equation cannot describe the pressure drops of this micro-channel reactor.

3.4.2 Wall effects

The influence of the container wall on the pressure drop of packed bed was investigated by Eisfeld et at. [3]. In their work was demonstrated that the tube-to-particle diameter ratio has effect on the pressure drops because any packed bed is bounded by confining walls. In their work, Eisfeld et al.[3] explain that the wall effect is important only for tube-to-particle diameter ratio lower than 10. The micro-channel considered has this tube-to-particle diameter ratio:

$$\frac{D_{tube}}{D_{particle}} = \frac{0.004}{0.0006} \cong 6.7$$

The wall effect can be attributed to two counteracting effects. The first one is the increasing local flow rate, as shown in Figure 42, due to an increased local void in their neighborhood. The second one is that the local velocity can be reduced to zero due to the wall friction. The relation between these two effects is described by the boundary layer theory explained by Eisfeld [32]. According to this theory the first effect is dominant at low Reynolds numbers, because the wall friction reaches far into the reactor. At high Reynolds number the wall friction is restricted to small boundary layer, therefore the second effect becomes dominant.

Due to this results Eisfeld et al. [3] develop a new correlation for the pressure drops for a packed bed, where the wall effect is considered. The pressure drops are expressed with the *modified friction factor* that is defined as:

$$f_m = 2f \qquad [3.23]$$

where f is *the Fanning Friction Factor*, defined in the equation [3.9]. The pressure drops, if the equation [3.14] is considered, become:

$$\frac{\Delta P}{L} = \frac{f_m \rho \langle v \rangle^2}{D_p} \qquad [3.24]$$

Eisfeld defines the *modified friction factor* as:

$$f_m = \frac{K_1 A_W^2}{\mathrm{Re}} \frac{(1-\varepsilon)^2}{\varepsilon^3} + \frac{A_W}{B_W} \frac{(1-\varepsilon)}{\varepsilon^3} \qquad [3.25]$$

where the parameter are:

$$A_W = 1 + \frac{2}{\frac{3D_{tube}}{D_{Particle}}(1-\varepsilon)} \qquad [3.26]$$

$$B_W = \left[k_1 \left(\frac{D_{Particle}}{D_{Tube}} \right)^2 + k_2 \right]^2 \qquad [3.27]$$

$$\mathrm{Re} = \frac{\rho v D_{Particle}}{\mu} \qquad [3.28]$$

This is an Ergun-type equation where the wall effect to the hydraulic radius is accounted for analytically by the coefficient A_W. The function B_W is introduced, describing empirically the void fraction effect of the wall at high Reynolds numbers. These numerical parameters:

$$K_1 = 154$$

$$k_1 = 1.15$$

$$k_2 = 0.87$$

are fitting coefficients developed with experimental database. The Eisfeld equation can be used to predict pressure drops for packed bed with these operating conditions and geometries:

$$0.01 < \mathrm{Re} < 17635$$

$$1.624 \le \frac{D_{Tube}}{D_{Particle}} \le 250$$

$$0.330 \le \varepsilon \le 0.882$$

The operating range for the micro-channel considered is:

$$13 < \mathrm{Re} < 140$$

$$\frac{D_{Tube}}{D_{Particle}} \cong 6.7$$

$$\varepsilon \cong 0.41$$

For this reason the pressure drops evaluated with catalyticFoam can be compared with the Eisfeld equation.

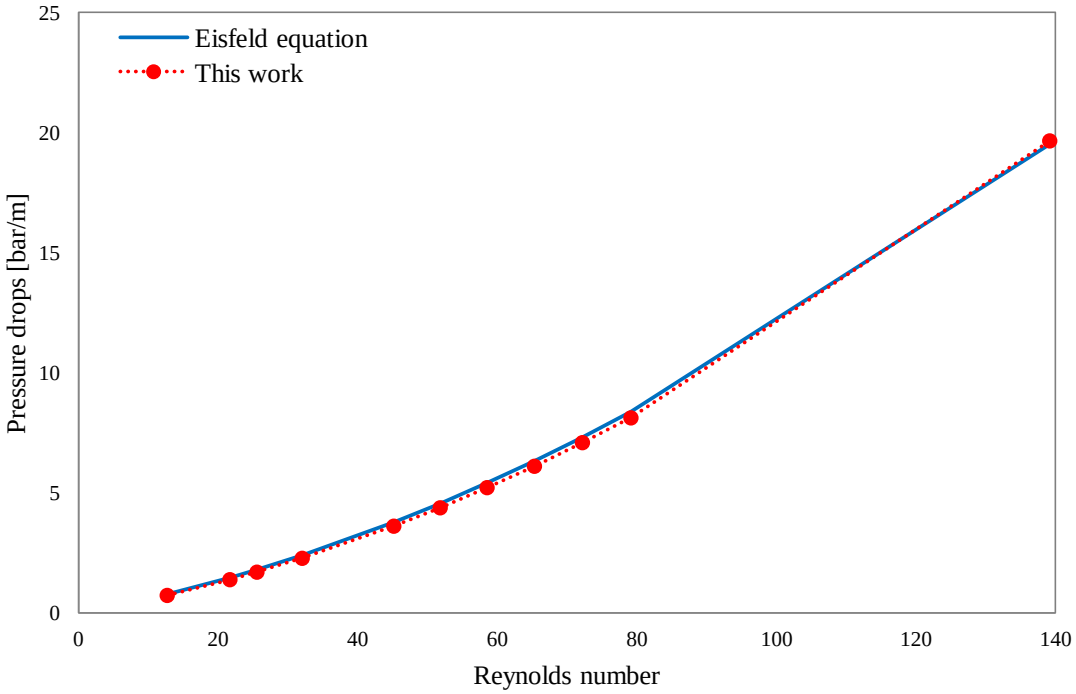

Figure 43: Eisfeld VS This work

Therefore, as shown in Figure 43, the pressure drops in micro-channel reactor can be described by equations where the wall effect is considered, such as the Eisfeld correlation.
The pressure drops in the micro-channel reactor are compared with the Foumeny equation[20]. This comparison can verify if the pressure drops for the micro-channel reactor are influenced by the wall effect. This pressure drops correlation is developed considering the wall effect. The different between the Eisfeld correlation and the Foumeny correlation is related to the parameter A_W . In the Eisfeld equation this parameter depends on the tube-to-particle diameter ratio (eq. [3.26]) instead in the Foumeny correlation it is a constant value (eq. [3.29]). If the pressure drops in micro-channel are strongly affected by the wall effect also the Foumeny equation could be used to predict the pressure drops in this unconventional reactor.

The Foumeny equation describes the pressure drops in term of *modified friction factor*:

$$f_m = \frac{(1-\varepsilon)}{\varepsilon^3}\left[\left(\frac{\frac{D_{Tube}}{D_{Particle}}}{0.355\frac{D_{Tube}}{D_{Particle}}+2.28}\right)+\frac{130}{\mathrm{Re}}\right] \qquad [3.29]$$

where the Reynolds number is defined as:

$$\mathrm{Re} = \frac{\rho v_0 D_p}{\mu(1-\varepsilon)} \qquad [3.30]$$

The Foumeny equation can be applied in these ranges:

$$3 \le \frac{D_{Tube}}{D_{Particle}} \le 25$$

$$5 \le \mathrm{Re} \le 8500$$

The operating conditions of the micro-channel reactor considered are in the application range.

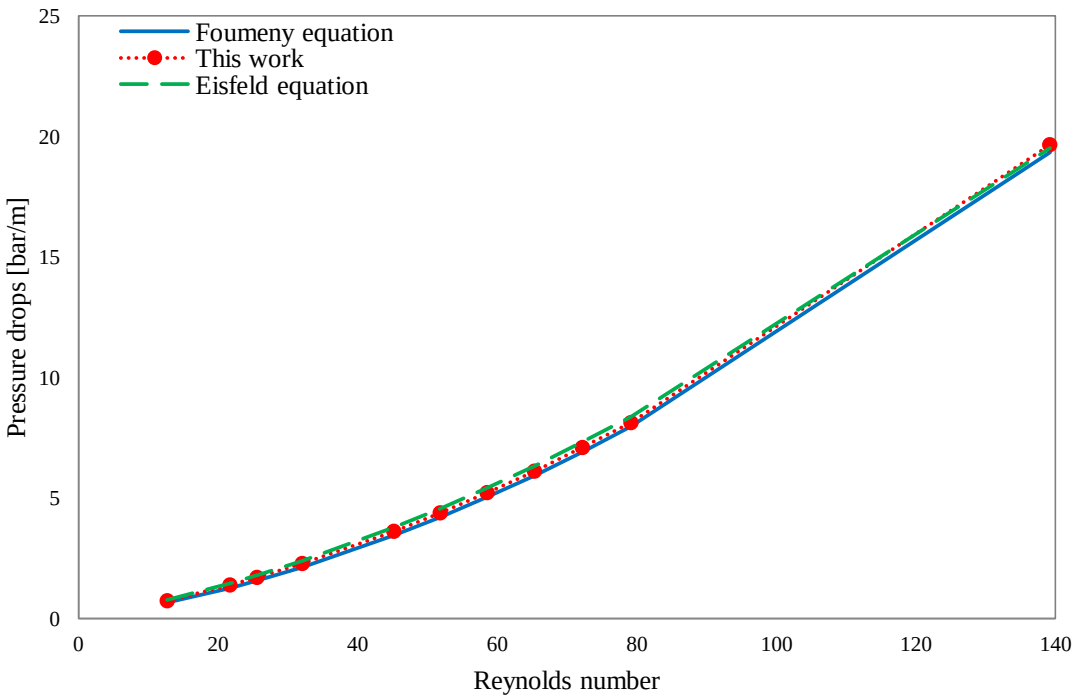

Figure 44: Foumeny and Eisfeld VS This work

Figure 44 shows that also this correlation can describe the pressure drops in micro-channel reactor. Therefore the pressure drops in these unconventional reactors can be predicted by correlations that considered the wall effect, because pressure drops are strongly influenced by this phenomenon.

3.4.2.1 Micro-channel with 300 μm spheres

The dependence of the pressure drops on the wall effect can be verified if a micro-channel with different particle diameter is considered. The new micro-channel geometry is shown in Figure 45:

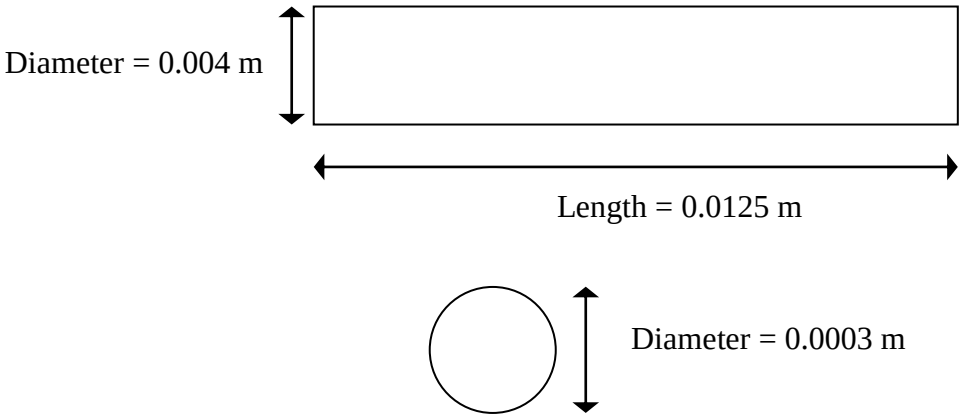

Figure 45: Micro-channel packed bed geometry with 300 μm spheres diameter

This micro-channel has a smaller particle diameter, thus the pressure drops in this reactor are bigger than in the micro-channel reactor with 600 μm diameter spheres. For this reason the considered range of Reynolds number is:

$$13 < \mathrm{Re} < 90$$

This range of Reynolds number is reduced from those considered for micro-channel with 600 μm spheres. The upper value of Reynolds number is decreased because, as shown in Figure 46, is related to huge pressure drops. Therefore investigating higher Reynolds numbers has no sense from a technological and industrial point of view. The geometry properties for the micro-channel considered are:

$$\frac{D_{Tube}}{D_{Particle}} \cong 13.3$$

$$\varepsilon \cong 0.40$$

Thus the Eisfeld[3] and the Ergun[13] equations can be applied to study the pressure drops in this micro-device.

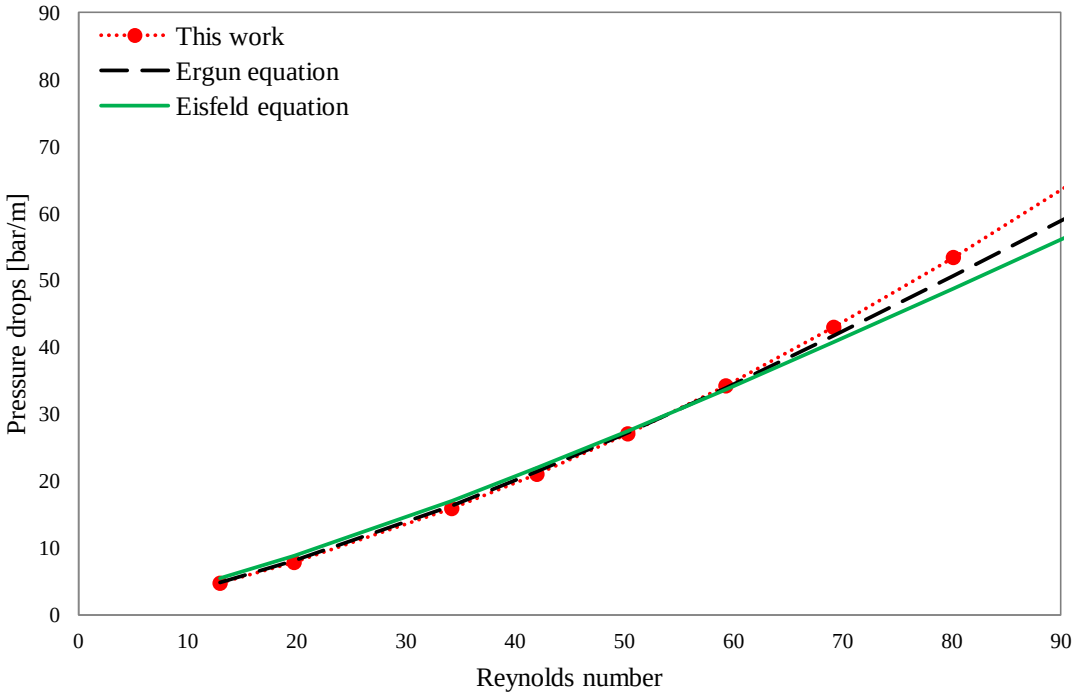

Figure 46: Pressure drops in a micro-channel reactor with 300 µm sphere diameter

Figure 46 shows that all the considered experimental correlations can describe the pressure drops in the micro-channel. This effect is related to the high value of the pressure drops in this unconventional device. Reducing the particle diameter increase the pressure drops, then the difference between the correlations is negligible. Due to the high value of the pressure drops the wall effect has an insignificant influence, thus the pressure drops in micro-channel with very small spheres can also be described by correlations that do not take into account the wall effect, as the Ergun equation.

To verify that the difference between the correlations is negligible the pressure drops in the packed bed described in Figure 47 are studied.

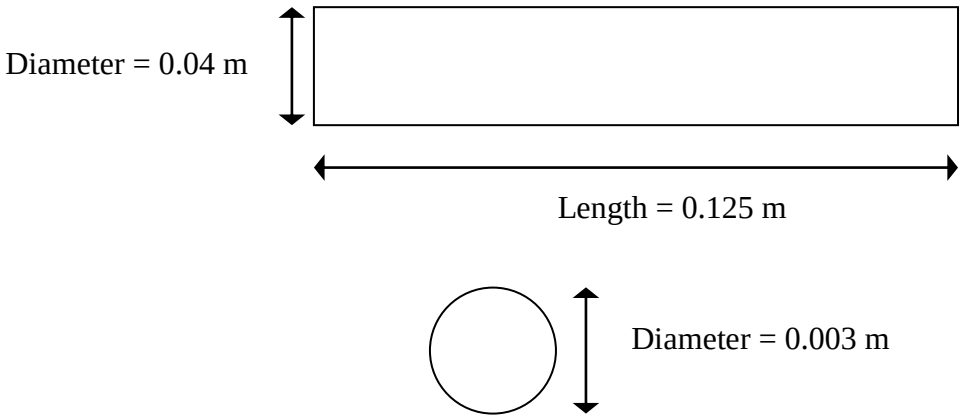

Figure 47: Packed bed geometry with spheres diameter of 0.003 m

This reactor has the same tube-to-particle diameter ratio of the micro-channel with 300 μm diameter spheres, but with the dimensions of a conventional packed bed reactor. The pressure drops for this packed bed are describes in Figure 48:

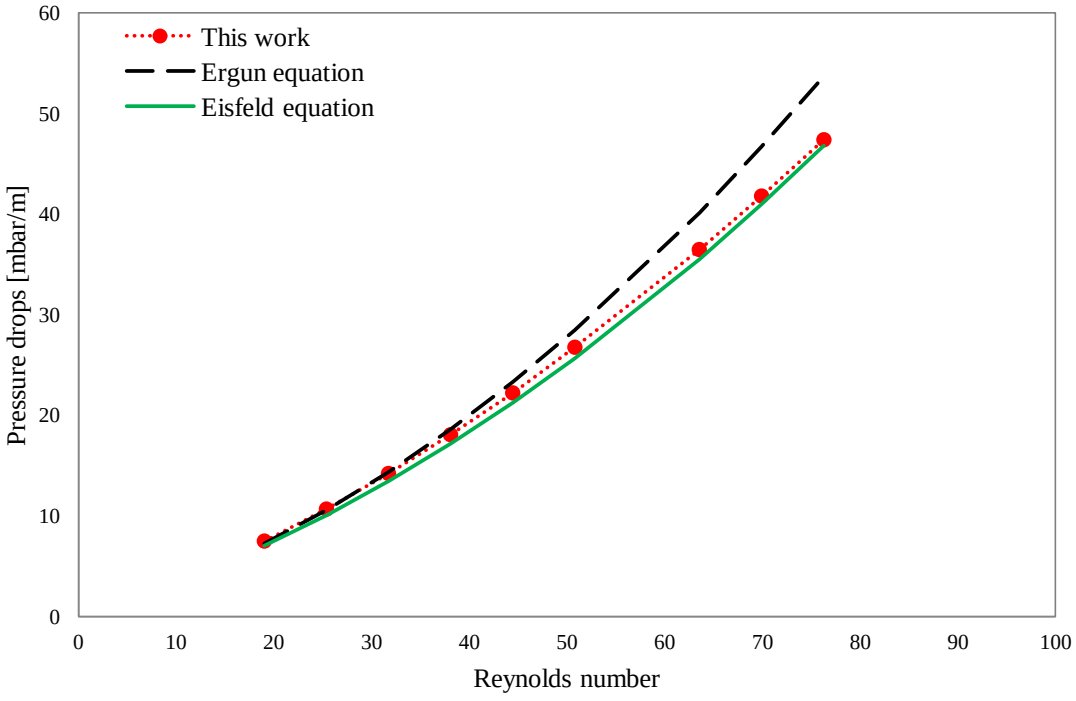

Figure 48: Pressure drops in a micro-channel reactor with 3 mm sphere diameter

In Figure 48 is shown that the difference between the correlations is significant because the pressure drops for this reactor are smaller than in the micro-channel reactor (mbar instead of bar). The pressure drops for this packed bed, at the considered operating conditions, are controlled by the wall effect. For this reason the pressure drops are described by the Eisfeld equation.

3.5 Analysis of Sherwood number

In the following paragraphs three different reactor geometries are studied:

1. Micro-channel reactor with 0.0006 m diameter spheres: Figure 35
2. Micro-channel reactor with 0.0003 m diameter spheres: Figure 45
3. Conventional packed bed reactor with 0.006 m diameter spheres: Figure 57

All the characteristic dimensions of the considered packed bed reactors are shown also in Figure 49:

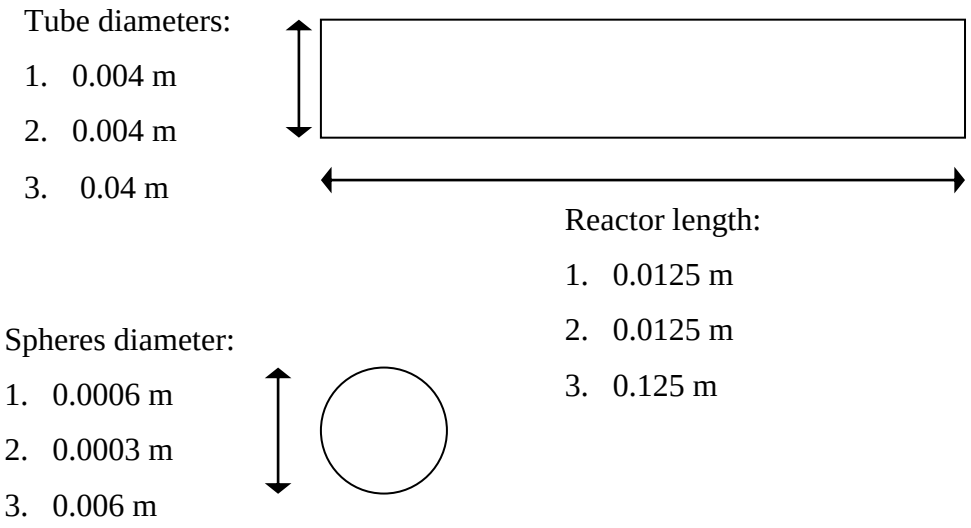

Figure 49: Geometry of all the considered reactors in the mass transfer coefficient anlysis

3.5.1 Operating conditions

First, as shown in Figure 39, the results do not depend on the mesh, thus the results presented in this paragraph are independent from the grid. Second, the mass transport properties can be studied if the reactor works in external mass transfer regime, which is described by high Damkohler number. Therefore the CFD simulations must be carried out in the optimal operating conditions to analyze mass transfer phenomena. For this reason a first order kinetic constant is considered for this reaction:

$$2H_2 + O_2 \rightarrow 2H_2O$$

The reaction rate is:

$$r = k_{CIN} C_{O_2} \frac{Kmol}{m^2 s}$$

The kinetic constant k_{CIN} and the related Damkohler number are described in Table 16:

Table 16: Damkohler number for different particle diameter

	Particle diameter [m]			
	0.0003	0.0006	0.003	0.006
Kinetic constant [m/s]	100	100	100	100
Damkohler number	469	939	4695	9389

The aim of this work is to investigate the only external mass transfer coefficient, thus the micro-channel reactor is simulated in isothermal condition, with a constant temperature of 553 K. Table 17 shows the inlet flow composition:

Table 17: Operating conditions for micro-channel reactor

	Molar fraction
Nitrogen (N_2)	0.95
Oxygen (O_2)	0.014
Hydrogen (H_2)	0.036

The nitrogen is chosen as the inert species and the oxygen is the limiting reactant. Due to the mass transfer regime the concentration of limiting reactant at the catalytic wall is zero. This information can be used to verify if at these operating conditions the reactors works in mass transfer regime.

The catalytic wall for all the considered reactors are represented in Figure 50.

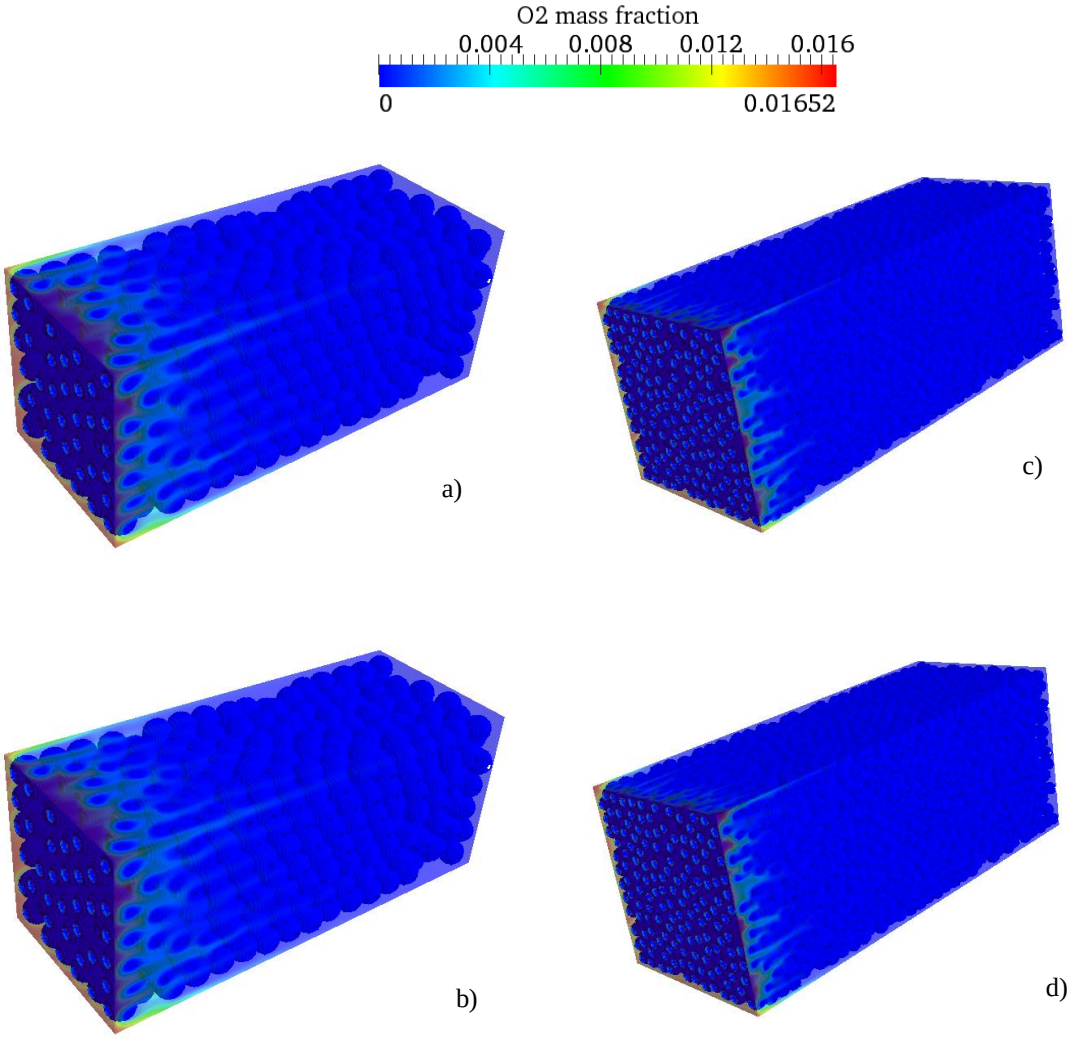

Figure 50: Oxygen mass fraction on the catalytic wall for all the considered reactors: a) 0.6 mm; b) 6 mm; c) 0.3 mm; d) 3 mm

The oxygen mass fraction on the catalytic wall is zero in all the reactors, thus they are controlled by the transport phenomena at these operating conditions. The mass transfer regime is described also in Figure 51, that shown the skip gradient near the catalytic wall

.

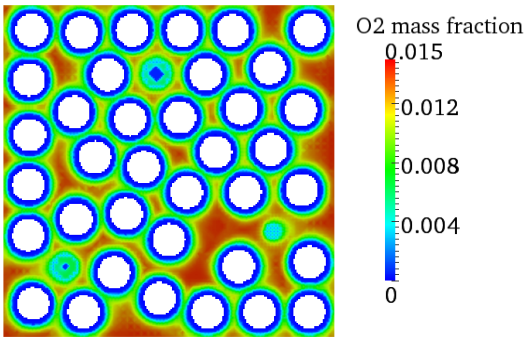

Figure 51: Cross-section for the 600 μm micro-channel

3.5.2 IMB method and entry region effect

The Inert Integral Mass Balance Method (IMB) will be used to study the mass transfer phenomena. As discussed in chapter 2, this method has the great advantage that can be applied to complex geometry, but the disadvantage depends on the entry region. For this reason this effect must be analyzed for micro-channel reactors.

Reactor length [m]	Asymptotic Sherwood number
0.0050	8.803
0.0075	7.728
0.0100	7.126
0.0125	6.686
0.0200	6.719

Table 18: Entry region effect for micro-channel reactors 0.0006 m spheres diameter

Table 18 shows that the entry region effect in micro-channel reactor can be ignored if the channel length is bigger than 0.0125 cm.

The entry region effect on the Sherwood number for micro-channel with different tube-to-particle diameter is shown in Figure 52.

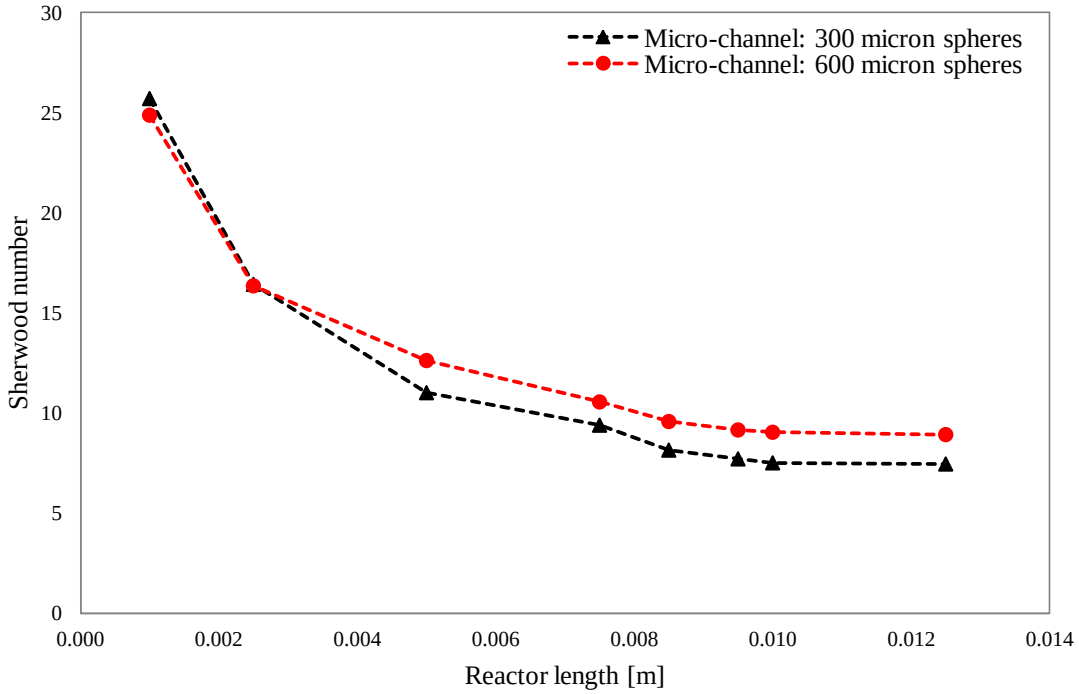

Figure 52: Entry region effect for micro-channel reactors (Re = 76.753)

Figure 52 does not describe an axial profile of the Sherwood number in the channel, because the IMB method cannot describe the local Sherwood number, as discussed in chapter 2, but it shows the presence of an entry region. The entry region depends on the mixing of the reactant at the begging of the reactor, when they impact with the catalytic spheres. This mixing for the micro-channel with 600 μm spheres is shown in Figure 53.

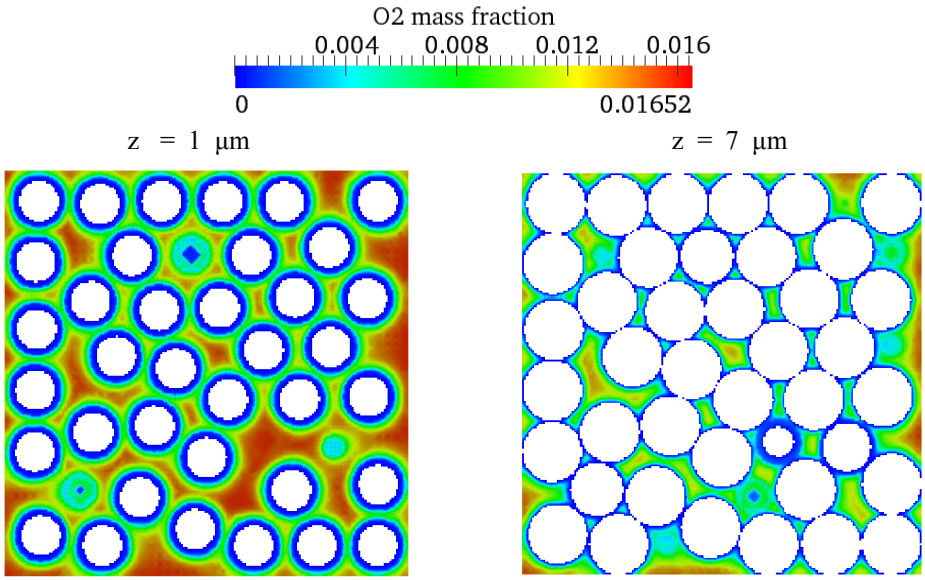

Figure 53: Entry region effect on the oxygen mass fraction for the micro-channel with 600 μm spheres diameter

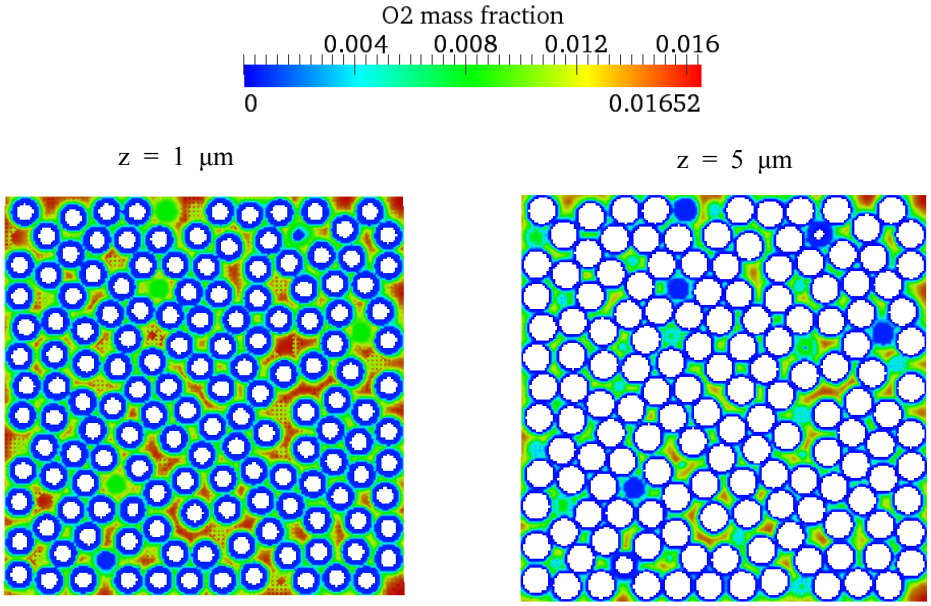

Figure 54: Entry region effect on the oxygen mass fraction for the micro-channel with 300 µm spheres diameter

Figure 54 and Figure 53 show the mixing of the oxygen in the entry region of the considered micro-channels packed bed reactors. At the begging of the reactor (z = 1 µm) the reactant are not already mixed and a skip mass fraction gradient is present near the catalytic wall. After few microns (z = 5/7 µm) the reactant are mixed and a less skip gradient is observed near the catalytic spheres. The blue points in Figure 54 are not related to an inhomogeneous mass fraction distribution, but they depend on the cutting plane. The reactor cross-section is represented by cutting the reactor at a fixed distance from the entrance. If the reacting sphere is cut far from its center, the mass fraction close to zero on the catalytic surface create the blue points. Therefore the blue points are only a problem of representation and not a inhomogeneous flow distribution.

The entry region effect was observed also by Tronconi and Forzatti [21] for monolith reactor, and their result is compared with the micro-channel in Table 19, considering the dimensionless reactor length (eq. [2.30]).

Table 19: Minimum reactor length to ignore the entry region effect for micro-channel and monolith (Re = 77)

	Micro-channel (600 µm)	Monolith
Reactor length [m]	0.0125	0.75
Dimensionless reactor length	0.56	0.93

This comparison shows that the minimum reactor length is smaller for micro-channel reactors. The minimum reactor length is related to the entry region, thus the entry region is smaller for micro-channel packed bed than for monolithic reactor because the presence of spheres helps the mixing of the inlet flow.

3.5.3 Comparisons with literature correlations

The Sherwood number is investigated in laminar flow conditions, and chosen velocity range is:

$$1 \le v_0 \le 6 \ \frac{m}{s} \Rightarrow 12 < \mathrm{Re} < 77 \qquad [3.31]$$

The comparison of the Sherwood number estimated for the micro-channel and the correlations of Yoshida et al. [2] and Wakao and Funazkri [1] is shown in Figure 55.

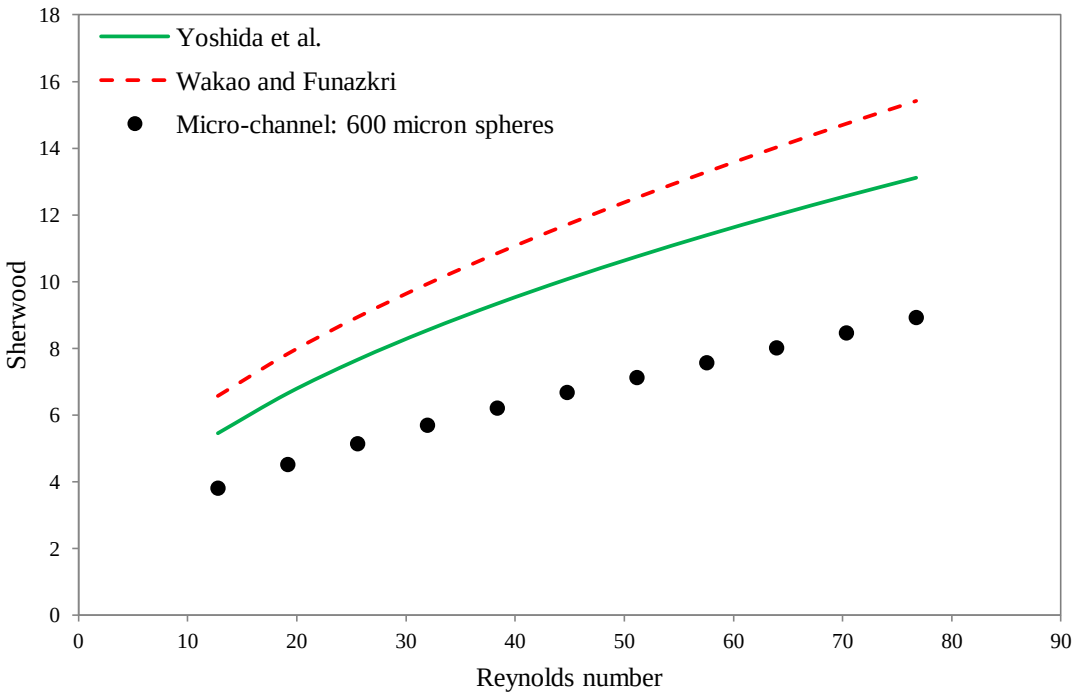

Figure 55: Comparisons of Sherwood number for micro-channel (600 μm) with experimental correlations

Figure 55 shows that the literature correlations overestimate the Sherwood number. However the trend, that describes the dependence of the Sherwood number on the Reynolds number, is similar.

3.5.4 One-dimensional model for micro-channel reactors

Ad described before the aim of this thesis is to verify if the experimental correlations for Sherwood number can be applied to micro-channel reactors. In the previous paragraphs was demonstrated that the Yoshida et al. [2] and Wakao and Funazkri [1] correlations overestimate the Sherwood number of micro-channel reactor. A one-dimensional model is used to verify if the difference between the Sherwood number estimated with CFD analysis and the Sherwood number predict by the literature correlations is acceptable or not. In this model the mass transfer phenomena are described by the mass transfer coefficient define as:

$$K_{MAT,i} = \frac{Sh\mathfrak{D}_i}{D_h}$$

The micro-channel considered is the micro-channel with 0.6 mm spheres, shown in Figure 35. The operating conditions are the same of the CFD simulation (Table 20):

Table 20: Operating conditions for the one-dimensional model

	Value	Unit dimension
Temperature	573	K
Pressure	101325	Pa
Velocity	6	m/s
Inlet mass fraction		
Nitrogen (AR)	0.95	
Oxygen (O_2)	0.014	
Hydrogen (H_2)	0.036	
Kinetic model		
Kinetic constant	100	m/s
Damkohler number	939	

The Sherwood numbers implemented in the one dimensional model are:

Table 21: Sherwood numbers implemented in the one-dimensional model (Re=77)

	This work	Yoshida et al. [2]	Wakao and Funazkri [1]
Sherwood number	8.926	13.121	15.418

The effect of the different Sherwood numbers is shown in Figure 56:

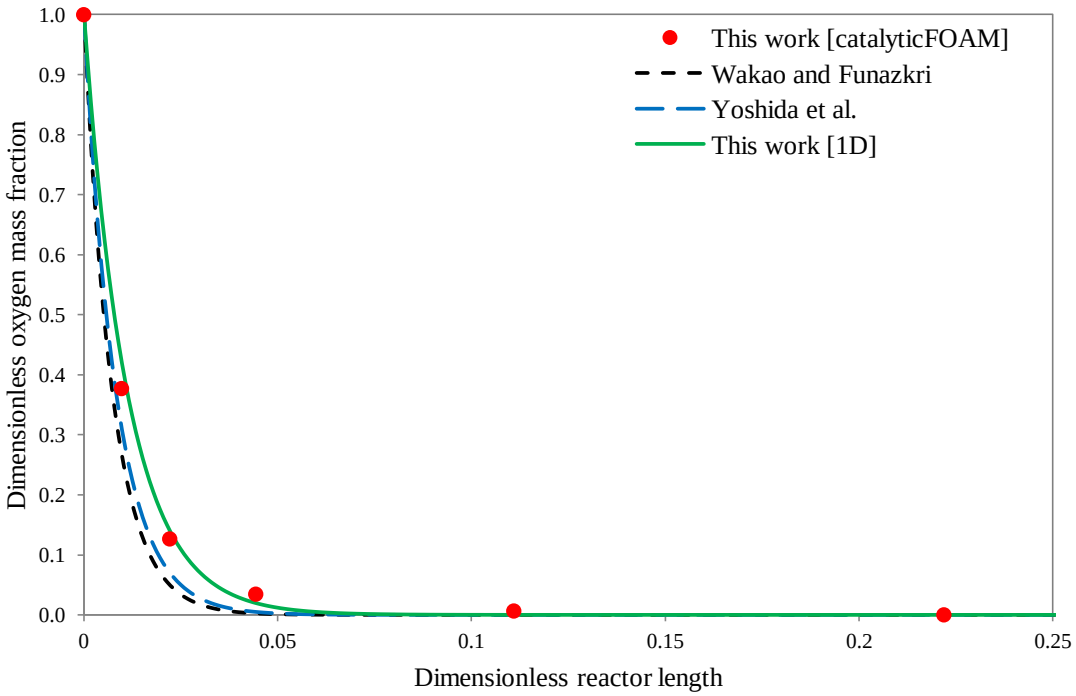

Figure 56: Axial profile of the oxygen mass fraction in a micro-channel reactor estimated with the one-dimensional model for different Sherwood numbers

The dimensionless mass fraction is defined as:

$$\omega_i^* = \frac{\omega_i}{\omega_i^{IN}} \qquad [3.32]$$

where ω_i^{IN} is the inlet mass fraction. The dimensionless reactor length is define in equation [2.30]. The one-dimensional model can describe the micro-channel reactor only when the Sherwood number estimated in this thesis is implemented. For this reason the different between the Sherwood number of micro-channel reactor and the experimental correlations cannot be ignored.

3.5.5 Tube-to-particle diameter ratio effect

The different trend and value of Sherwood number in micro-channel reactor can be related to its unusual properties. These properties are the tube-to-particle diameter ratio and the micro dimensions, which will be investigated in this paragraph.

A packed bed with a different geometry will be created with the methodology proposed by Freund et al. [24, 25] . The packed bed geometry is:

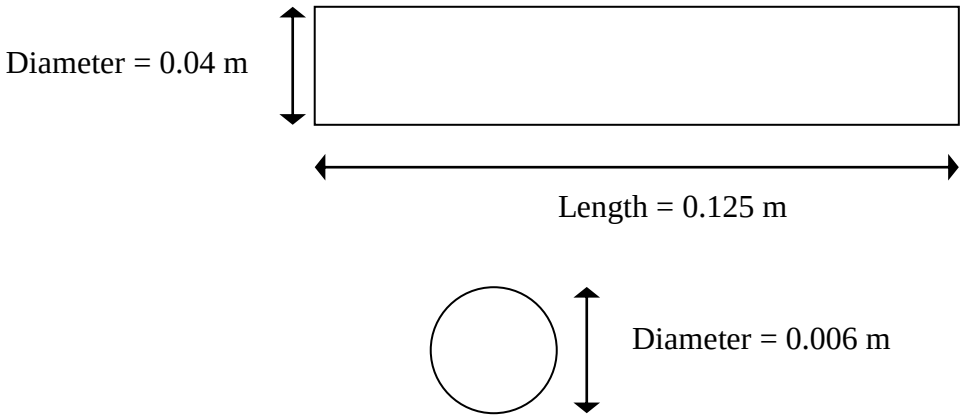

Figure 57: Packed bed geometry with spheres diameter of 0.006 m

This channel is developed with the purpose to create a packed bed with spheres diameter similar to industrial applications. The dependence of the Sherwood number on the micro-dimensions or on the tube-to-particle diameter ratio can be investigated with this packed bed because it has a tube-to-particle diameter ratio similar to micro-channel reactor. For this reason the main difference with a conventional reactor is the bigger tube diameter (Table 22).

Table 22: Tube-to-particle diameter ratio for micro-channel packed bed and conventional packed bed

	Micro-channel	Considered channel geometry	Conventional packed bed
Sphere diameter [m]	0.0006	0.006	0.006
Tube diameter [m]	0.004	0.04	0.032
Tube-to-particle diameter ratio	6.7	6.7	5.3

The Sherwood number of this packed bed can be compared with the Sherwood number of the micro-channel, with 600 μm spheres diameter, only if the first one works in external mass transfer regime and in the same range of Reynolds number. The external mass transfer regime is described by high Damkohler number and Table 16 shows that the packed bed performances are controlled by the external mass transfer phenomena with a kinetics constant of 100 m/s. Moreover the range of Reynolds number described in equation [3.31] is conserved if the inlet velocity is reduced:

$$0.1 \leq v_0 \leq 0.6 \frac{m}{s}$$

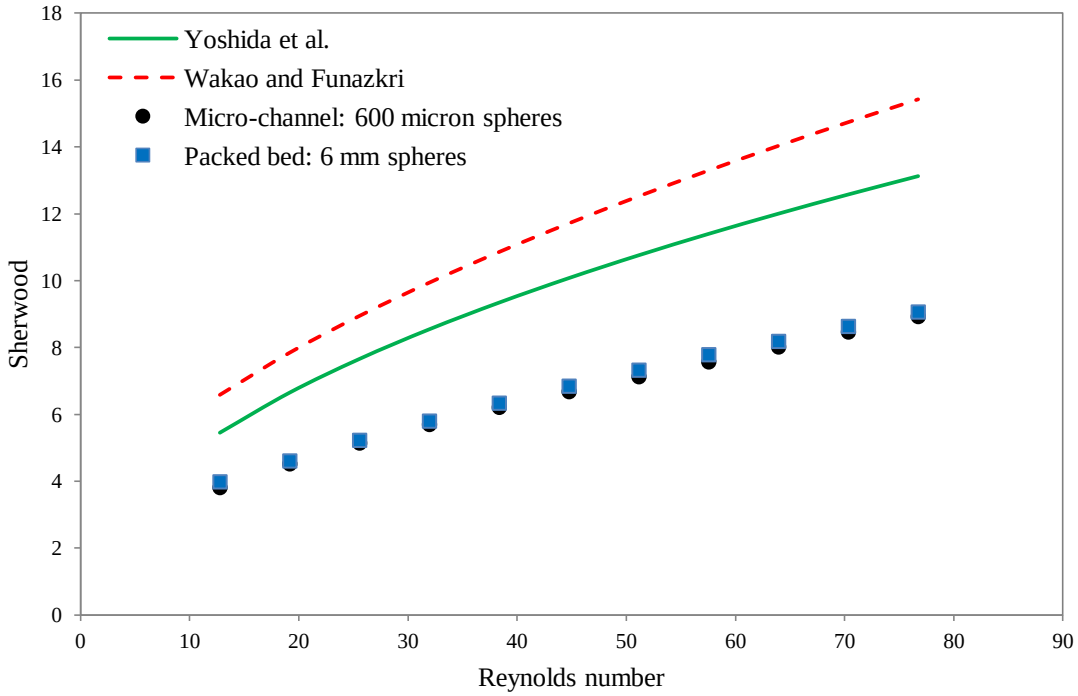

Figure 58: Micro-channel VS standard reactor with the same tube-to-particle diameter ratio (N = 6.7)

Figure 58 shows the comparisons between the Sherwood number of the micro-channel and the Sherwood number of packed bed with the same tube-to-particle diameter ratio. The Sherwood number of the channel with 6 mm sphere diameter is similar to the Sherwood number of the micro-channel and it is completely different from those predicted by the experimental correlations.

Investigating a micro-channel reactor with a different spheres diameter, can demonstrate the dependence of the Sherwood number on the tube-to-particle diameter ratio. The geometry of this micro-channel was described in Figure 45. The Sherwood numbers of the two different micro-channels are compared with the experimental correlations in Figure 59. Comparing those values is possible because also the micro-channel reactor with smaller spheres works in external mass transfer regime (Table 16). Moreover the inlet velocities are changed to consider the same range of Reynolds numbers. Thus the new inlet velocity range is:

$$2 \leq v_0 \leq 12 \ \frac{m}{s}$$

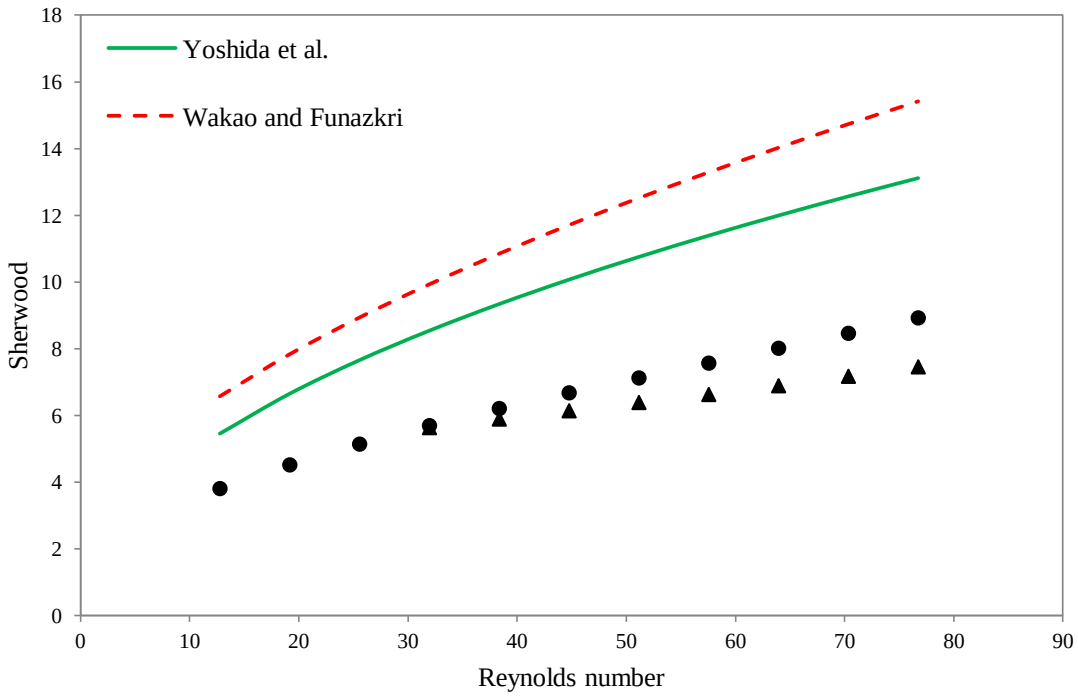

Figure 59: Comparisons of Sherwood number for micro-channel (600 µm and 300 µm) with experimental correlations

As observed for the micro-channel with 600 µm sphere diameter, the experimental correlations overestimate the Sherwood number for the micro-channel with 300 µm spheres diameter. Moreover in Figure 59 is shown that the difference between the Sherwood numbers estimated for the two micro-channel geometris increases with the Reynolds number. The Sherwood number of the micro-channel of 300 µm spheres is smaller than those estimated for the micro-channel with 600 µm spheres.Then the error to evaluate the mass transfer coefficient in a one-dimensional model with a literature correlation, shown in Figure 56, is bigger for the micro-reactor with smaller spheres.

The different trend of Sherwood number estimated for the micro-channel with 600 μm spheres diameter and those calculated for the reactor with 300 μm spheres can be related to the different tube-to-particle diameter ratio (Table 23).

Table 23: Tube-to-particle diameter ratio for the two micro-channels

	Micro-channel	
Sphere diameter [m]	0.0006	0.0003
Tube diameter [m]	0.004	0.004
Tube-to-particle diameter ratio	6.7	13.3

This effect of the tube-to-particle diameter ratio on the Sherwood number was observed by Tidona et al. [14]. In their work the Wakao and Funazkri correlation parameters where modified to describe different micro-channel with different tube-to-particle diameter ratio (Table 1). The effect of the tube-to-particle diameter ratio on the Sherwood number observed by Tidona et al. [14] is described in Figure 60.

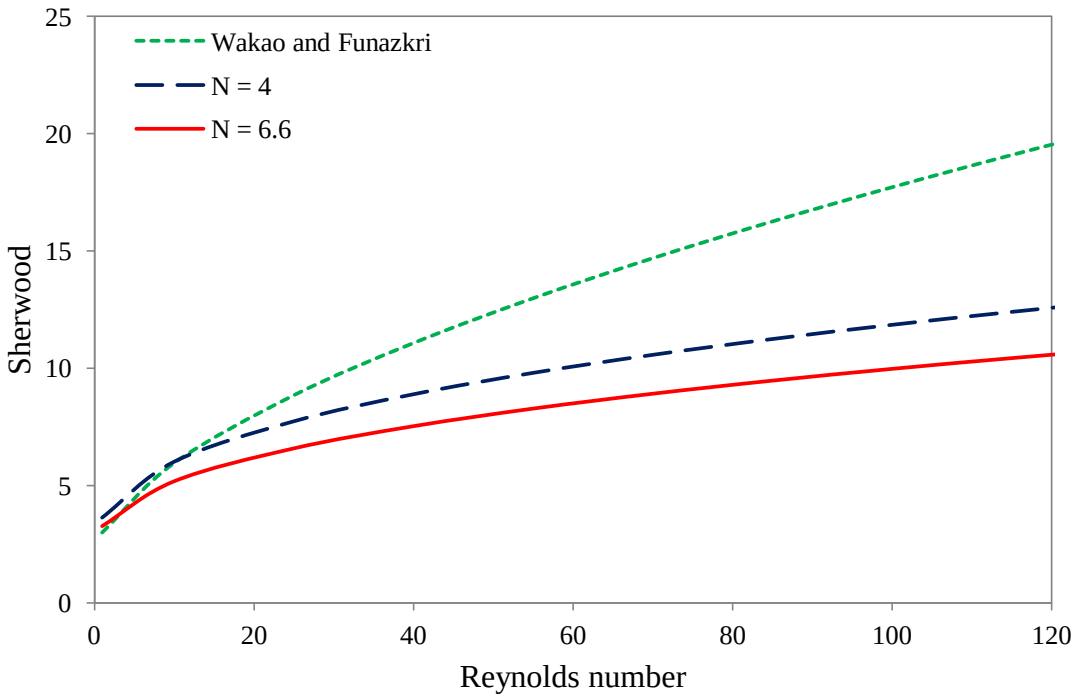

Figure 60: Effect of tube-to-particle diameter ratio (N) observed by Tidona et al. [14]

This property is induced by the wall effects that create an inhomogeneous flow distribution over the cross section. This leads to lower mass transfer properties for these unconventional devices, due to the large amount of fluid flowing close to the wall where the porosity is high and the contact area between fluid and particles per volume of packed bed is smaller.

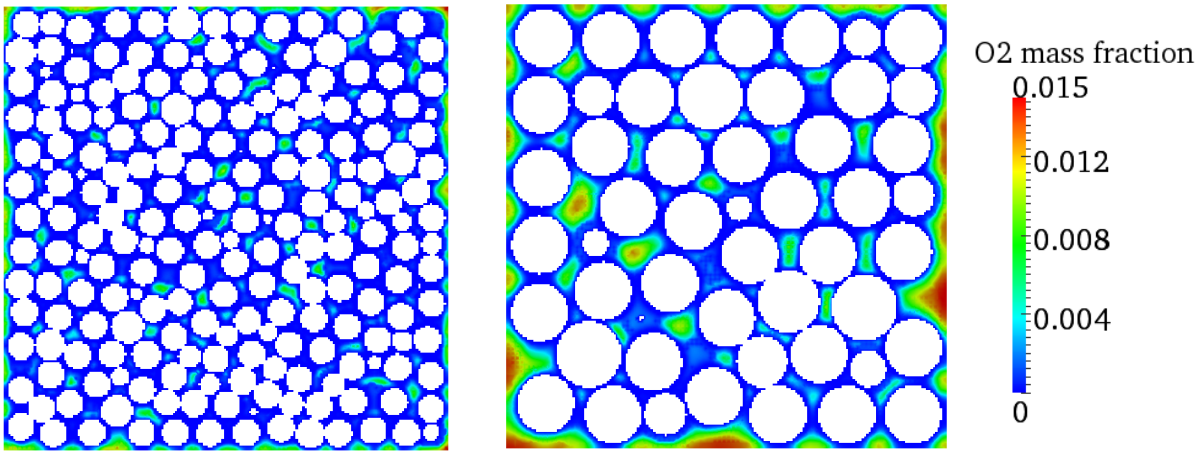

Figure 61: Wall effect on the mass transfer properties on micro-channel reactors

Figure 61 shows the presence of the wall effects on the mass fraction of the limiting reactant. The preferential paths have a negative effect on the mechanism thought which the reactants reach the center of the channel and the catalytic wall.

The results shown in Figure 61 are in disagreement with the results of the Figure 59, where a smaller Sherwood number is related to a smaller spheres diameter and a higher tube-to-particle diameter ratio, because the channel with bigger spheres is more affected by the wall effects. This different can be explain if the Sherwood number definition (eq. [2.9]) is considered. As discussed in chapter 1, the Sherwood number definition in packed bed reactors take into account the particle Reynolds number:

$$\mathrm{Re} = \frac{\rho v D_{Particle}}{\mu}$$

This expression does not considered the presence of confining walls, which influence the Sherwood number, as shown in Figure 59. Therefore, for a deeper understanding of the mass transfer properties of these devices, the mass transfer coefficients (K_{MAT}) for the two micro-channel geometries are compared.

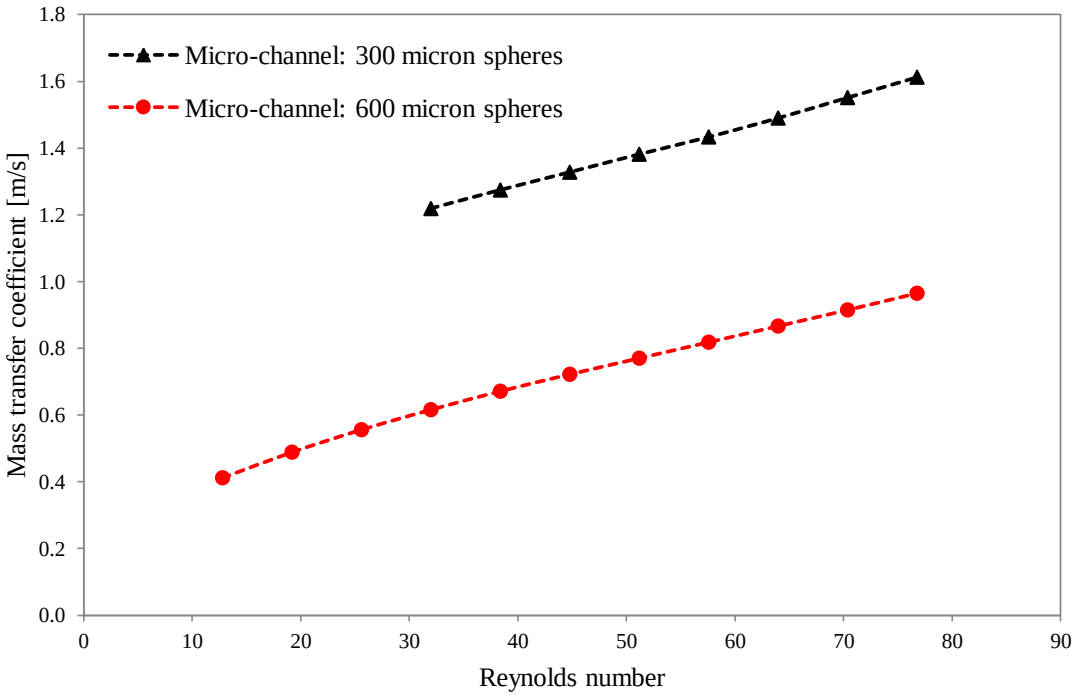

Figure 62: Comparisons of mass transfer coefficient for the two different considered micro-channel packed bed reactors

Figure 62 shows higher mass transfer coefficient for the micro-channel reactor with 300 µm spheres diameter. This effect agrees with the results shown in Figure 61 and demonstrates that decreasing the spheres diameter reduces the influence of the wall effects on the mass transfer properties.

3.6 Micro-channel mass transfer properties

In the previous paragraphs it was observed that the experimental correlations overestimate the value of Sherwood number for micro-channel reactors. This demonstrates that the excellent mass transfer properties, described in chapter 1, are not related to the mass transfer coefficient but to the interfacial surface area per reactor volume. The mass transfer coefficient, as explain in chapter 2, is applied in one-dimensional model to describe the flux from the bulk phase to the catalytic surface. This mass transfer coefficient is related with the catalytic surface area, define as:

$$a_V = \frac{catalyticArea}{reactorVolume} \qquad [3.33]$$

For a packed bed reactor this value depends on the void fraction and on the particle diameter:

$$catalyticArea = nA_{sphere} \qquad [3.34]$$

where n is the number of spheres in the reactor. Due to the void fraction definition (eq. [3.1]) the reactor volume can be written as:

$$reactorVolume = \frac{nV_{sphere}}{1-\varepsilon} \qquad [3.35]$$

For the equation [3.34] and [3.35] the specific catalytic area of a packed bed reactor is:

$$a_V = \frac{nA_{sphere}}{\frac{nV_{sphere}}{1-\varepsilon}} \qquad [3.36]$$

And if the volume and the area of sphere are considered the specific catalytic area can be written as:

$$a_V = \frac{\pi D_P^2}{\pi \frac{D_P^3}{6}}(1-\varepsilon) \qquad [3.37]$$

$$a_V = \frac{6}{D_P}(1-\varepsilon) \qquad [3.38]$$

Therefore a smaller particle diameter increases the specific catalytic area. This effect on the micro-channel reactor is shown in Table 24:

Table 24: Specific catalytic are for micro-channel reactors and conventional packed bed

	Micro-channel	Conventional packed bed
Sphere diameter [m]	0.0006	0.006
Void fraction	0.41	0.41
Specific catalytic surface [1/m]	5900	590

The increased specific catalytic area has effect also on the mass transfer properties.

Table 25: Mass transfer properties for micro-channel reactors and packed bed for different Reynolds numbers

	$K_{MAT}a_v$ [1/s]	
Reynolds number	Micro-channel	Conventional packed bed
13	2394	34
19	2840	42
26	3231	48
32	3580	54
38	3902	59
45	4197	63
51	4478	68
58	4757	72
64	5037	75
70	5319	79
77	5609	82

The comparisons of the mass transfer properties of a micro-channel reactor and a conventional packed bed reactor for the range of Reynolds number studied in this work are described in Table 25. The micro-channel reactor has a sphere diameter of 0.0006 m and the mass transfer coefficient (K_{MAT}) is estimated with the Sherwood number evaluated in this work. The conventional packed bed has a sphere diameter of 0.006 m and the mass transfer coefficient (K_{MAT}) is calculated with the correlation of Yoshida et al. [2]. The micro-dimensions have two different effects on this micro-channel reactor. The first one is a reduced Sherwood number and mass transfer coefficient.

This effect is related to the tube-to-particle diameter ratio, which is bigger than in conventional packed bed. The second one is the high specific catalytic area. Due to the micro-catalytic particle the catalytic surface per reactor volume is greater than in packed bed with standard dimensions. These effects are counteracting, but the high specific catalytic area is dominant and the estimated mass transfer coefficient ($K_{MAT}a_v$) is 60 times bigger for micro-reactors, ad discussed in chapter 1.

Conclusions

The CFD solver catalyticFOAM [4, 5] was successfully applied for detailed analysis of the gas-to-particle mass transfer in micro-channel packed bed.

State of the art literature correlations are found to overestimate Sherwood number in micro-channel reactor with the tube-to-particle diameter ratio investigated at the considered operating conditions ($10 < \mathrm{Re} < 90$). The CFD analysis of pressure drops shows that only literature correlations that account for the wall effects are able to predict the pressure drops in the investigated conditions.

Likewise, also the overestimation of the Sherwood number by the literature correlations can be related to wall effects, which turn to be relevant for the range of tube-to-particle diameter ratio investigated in this work. The preferential paths and the high void fraction close to the reactor walls reduce the contact area between the flow and the catalytic surface that is described by lower Sherwood number and mass transfer coefficient. For this dependence on the wall effects, the mass transfer coefficient is related to the tube-to-particle diameter ratio, and lower mass transfer coefficients are related to smaller tube-to-particle diameter ratio. This effect depends on the less importance of the channeling in micro-channels with smaller sphere diameter. The wall effects have a negative influence on the mass transport coefficient, thus reducing the channeling increases the mass transfer property.

Nevertheless, this effect cannot be properly described by the Sherwood number, defined with respect sphere diameter:

$$Sh = \frac{K_{MAT} D_{Particle}}{\mathfrak{D}_i}$$

In fact, the mass transfer phenomena in micro-channel reactors are controlled by the tube-to-particle diameter ratio, but the Sherwood number does not take into account the presence of the confining wall.

Finally, this work demonstrates that the literature correlations, developed for conventional packed bed, cannot describe mass transfer phenomena for the investigated tube-to-particle diameter ratio.

Future developments will deal with improving the understanding of the mechanism of mass and heat transfer for these micro-devices, specifically:

- ✓ The development new Sherwood number correlations that take into account the effect of the tube-to-particle diameter ratio on mass transfer phenomena.
- ✓ The understanding the mechanisms of heat transfer inside the micro-channel and compare the results of Nusselt number with the literature correlations, as done for Sherwood number.

Appendix

In this section the derivation of the mass balance for the one dimensional model used in the previous chapters is provided.

The simplified one dimensional model used to describe gas-solid catalytic reactors is based on mass balance at the continuum level:

$$IN - OUT + PROD = ACC$$

where:

- ✓ IN : this term is the amount of considered specie introduced per unit of time.
- ✓ OUT : this describes the amount of considered specie leaving per unit of time.
- ✓ $PROD$: this is the reacting term and represents the amount of considered specie converted per unit of time.
- ✓ ACC : this term is the amount of considered specie accumulated in the reactor per unit of time.

This balance is applied on a infinitesimal volume of the reactor and the considered fluxes are shown in Figure 63:

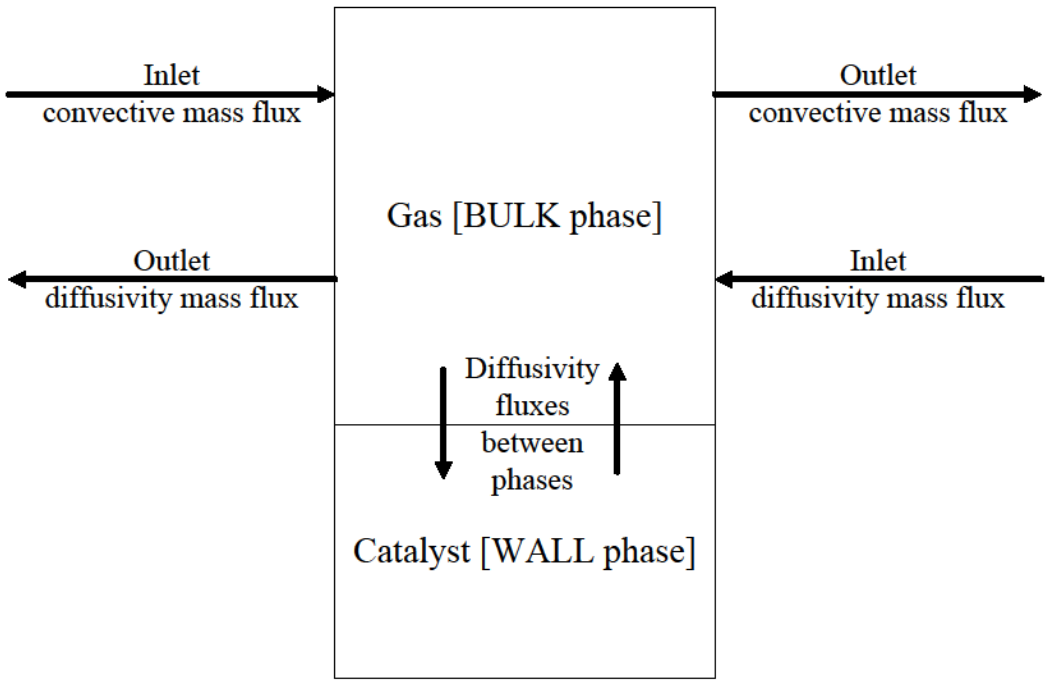

Figure 63: Fluxes for a gas-solid reactor

3.7 Bulk phase

Once the mass fluxes are identified the mass balance for the bulk phase can be written as:

$$IN = \left[\dot{m}_i^B \right]_V - \left[\mathfrak{D}_i A \frac{\partial \rho_i^B}{\partial z} \right]_V \quad [4.1]$$

$$OUT = \left[\dot{m}_i^B \right]_{V+dV} - \left[\mathfrak{D}_i A \frac{\partial \rho_i^B}{\partial z} \right]_{V+dV} \quad [4.2]$$

$$PROD = 0 \quad [4.3]$$

$$ACC = \frac{\partial m_i^B}{\partial t} \quad [4.4]$$

where $\dot{m}_i^B$ is the mass flux, $\mathfrak{D}_i$ is the diffusivity of the considered specie and A is the cross-section area. The reacting term is zero because the chemistry of the whole process happen in the catalyst. The diffusivity fluxes between the two phases are described with a linear term.

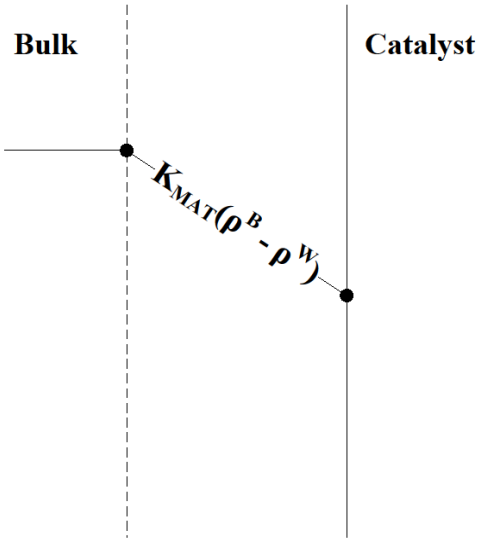

Figure 64: Linear expression for the diffusivity flux at the catalytic wall

This term is composed by the driving force and the mass transfer coefficient. The difference between the density in bulk phase and the density on the catalytic wall is chosen as driving force.

$$K_{MAT}(\rho_i^B - \rho_i^W) dS \quad [4.5]$$

The dS is introduced because these fluxes are defined per unit of catalytic surface.

The OUT term (eq. [4.2]) can be modified with the Taylor series:

$$OUT = \left[\dot{m}_i^B\right]_V + \left[\frac{\partial \dot{m}_i^B}{\partial V}\right]\partial V - \left[\mathfrak{D}_i A \frac{\partial \rho_i^B}{\partial z}\right]_V - \frac{\partial}{\partial z}\left[\mathfrak{D}_i A \frac{\partial \rho_i^B}{\partial z}\right]_V \partial z \qquad [4.6]$$

The cross-section area and the diffusivity are assumed constant in the whole reactor, thus:

$$OUT = \left[\dot{m}_i^B\right]_V + \left[\frac{\partial \dot{m}_i^B}{\partial V}\right]\partial V - \mathfrak{D}_i A\left[\frac{\partial \rho_i^B}{\partial z}\right]_V - \mathfrak{D}_i A\left[\frac{\partial^2 \rho_i^B}{\partial z^2}\right]_V \partial z \qquad [4.7]$$

Due to the equation [4.1],[4.2],[4.4],[4.5],[4.7] the global mass balance is:

$$\frac{\partial m_i^B}{\partial t} = -\partial \dot{m}_i^B + \mathfrak{D}_i A \frac{\partial^2 \rho_i^B}{\partial z^2}\partial z - K_{MAT}(\rho_i^B - \rho_i^W)dS \qquad [4.8]$$

The specific catalytic area is define as:

$$a_v = \frac{dS}{dV} \qquad [4.9]$$

and, due to the hypothesis of a constant cross-section area, the infinitesimal reactor volume is:

$$dV = d(Az) = Adz \qquad [4.10]$$

The global mass balance can be written as:

$$\frac{\partial m_i^B}{\partial t} = -\partial \dot{m}_i^B + \mathfrak{D}_i \frac{\partial^2 \rho_i^B}{\partial z^2} Adz - K_{MAT}(\rho_i^B - \rho_i^W)a_v Adz \qquad [4.11]$$

$$\varepsilon Adz \frac{\partial \rho_i^B}{\partial t} = -\partial \dot{m}_i^B + \mathfrak{D}_i \frac{\partial^2 \rho_i^B}{\partial z^2} Adz - K_{MAT}(\rho_i^B - \rho_i^W)a_v Adz \qquad [4.12]$$

where ε is the void fraction of the considered reactor. Now the mass balance can be simplified if a constant velocity profile is considered:

$$\dot{m}_i^B = vA\rho_i^B \qquad [4.13]$$

At the end the one-dimensional mass balance for the bulk phase is:

$$\frac{\partial \rho_i^B}{\partial t} = -\frac{v}{\varepsilon}\frac{\partial \rho_i^B}{\partial z} + \frac{\mathfrak{D}_i}{\varepsilon}\frac{\partial^2 \rho_i^B}{\partial z^2} - K_{MAT}(\rho_i^B - \rho_i^W)\frac{a_v}{\varepsilon} \qquad [4.14]$$

3.8 Wall phase

The mass balance terms for the wall phase are:

$$IN = 0 \qquad [4.15]$$

$$OUT = 0 \qquad [4.16]$$

$$PROD = \sum_{k=1}^{NR} \nu_{i,k} r_i \alpha_{CAT} \qquad [4.17]$$

$$ACC = 0 \qquad [4.18]$$

The IN and the OUT terms are zero because there are not convective fluxes in the catalyst. Moreover the ACC is zero because there are not accumulated specie in the catalyst. Due to these assumptions the mass balance for the wall phase is:

$$K_{MAT}(\rho_i^B - \rho_i^W)a_v + \sum_{k=1}^{NR} \nu_{i,k} r_i \alpha_{CAT} = 0 \qquad [4.19]$$

where NR is the number of considered reactions and α_{CAT} is an experimental parameter introduced to describe the active sites on the catalyst surface.

3.9 PDE problem

Due to the equations [4.19] and [4.14] the one-dimensional model obtained to describe gas-solid reactors is:

$$\begin{cases} \dfrac{\partial \rho_i^B}{\partial t} = -\dfrac{v}{\varepsilon}\dfrac{\partial \rho_i^B}{\partial z} + \dfrac{\mathfrak{D}_i}{\varepsilon}\dfrac{\partial^2 \rho_i^B}{\partial z^2} - K_{MAT}(\rho_i^B - \rho_i^W)\dfrac{a_v}{\varepsilon} \\ K_{MAT}(\rho_i^B - \rho_i^W)a_v + \sum_{k=1}^{NR} \nu_{i,k} r_i \alpha_{CAT} = 0 \end{cases} \qquad [4.20]$$

The first step in obtaining a numerical solution of this problem is to define a numerical grid. In finite different discretization method the grid for a one-dimensional domain is:

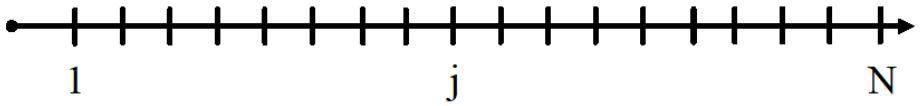

Figure 65: Discretization grid for a one-dimensional domain

In this case the descritzed domain is the reactor length and the first and the second order derivative at the *j* node can be written as:

$$\left(\frac{\partial \phi}{\partial z}\right)_j \approx \frac{\phi_j - \phi_{j-1}}{z_j - z_{j-1}} \qquad [4.21]$$

$$\left(\frac{\partial^2 \phi}{\partial z^2}\right)_j \approx \frac{\phi_{j+1}(z_j - z_{j-1}) + \phi_{j-1}(z_{j+1} - z_j) - \phi_j\left(z_{j+1} - z_{j-1}\right)}{\frac{1}{2}\left(z_{j+1} - z_{j-1}\right)(z_{j+1} - z_j)(z_j - z_{j-1})} \qquad [4.22]$$

Therefore the one-dimensional model shown in equation [4.20] is discretized and the equations solved at every j node of the grid are:

$$\begin{cases} \left(\dfrac{\partial \rho_i^B}{\partial t}\right)_j = -\dfrac{v}{\varepsilon}\dfrac{\rho_{i,j}^B - \rho_{i,j-1}^B}{z_j - z_{j-1}} + \dfrac{\mathfrak{D}_i}{\varepsilon}\dfrac{\rho_{i,j+1}^B(z_j - z_{j-1}) + \rho_{i,j-1}^B(z_{j+1} - z_j) - \rho_{i,j}^B\left(z_{j+1} - z_{j-1}\right)}{\frac{1}{2}\left(z_{j+1} - z_{j-1}\right)(z_{j+1} - z_j)(z_j - z_{j-1})} - K_{MAT}(\rho_{i,j}^B - \rho_{i,j}^W)\dfrac{a_v}{\varepsilon} \\ K_{MAT}(\rho_{i,j}^B - \rho_{i,j}^W)a_v + \sum_{k=1}^{NR} \nu_{i,k} r_i \alpha_{CAT} = 0 \end{cases}$$

Moreover boundary conditions for this problem must be introduced:

$$\begin{aligned} \rho_{i,1}^B &= \rho_i^{B,IN} \\ \rho_{i,(N-1)}^B &= \rho_{i,N}^B \end{aligned} \qquad [4.23]$$

Due to the discretization of the domain the PDE problem now is DAE problem and a numerical solution can be easily find out. The problem can be easily solved because the Jacobian matrix is sparse and tri-diagonal:

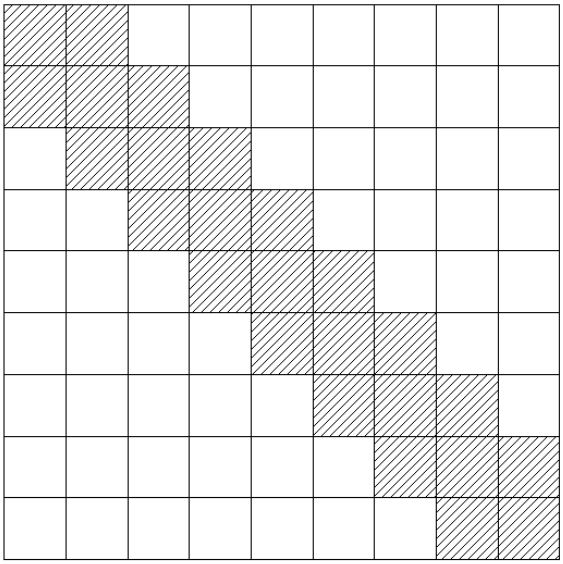

Figure 66: Jacobian matrix for the one-dimensional model

List of figures

List of tables

Bibliography

1. Wakao, N. and T. Funazkri, *Effect of fluid dispersion coefficients on particle-to-fluid mass transfer coefficients in packed beds: Correlation of sherwood numbers.* Chemical Engineering Science, 1978. **33**(10): p. 1375-1384.
2. Yoshida, F., D. Ramaswami, and O.A. Hougen, *Temperatures and partial pressures at the surfaces of catalyst particles.* Aiche Journal, 1962. **8**(1): p. 5-11.
3. Eisfeld, B. and K. Schnitzlein, *The influence of confining walls on the pressure drop in packed beds.* Chemical Engineering Science, 2001. **56**(14): p. 4321-4329.
4. Maestri, M. and A. Cuoci, *Coupling CFD with detailed microkinetic modeling in heterogeneous catalysis.* Chemical Engineering Science, 2013. **96**(0): p. 106-117.
5. Maestri, M. and A. Cuoci, *www.catalyticfoam.polimi.it*. 2011-2013.
6. Srinivasan, R., et al., *Micromachined reactors for catalytic partial oxidation reactions.* Aiche Journal, 1997. **43**(11): p. 3059-3069.
7. Morbidelli, M. and A. Varma, *A Generalized Criteria for Parametric Sensitivity: Application to Thermal Explosion Theory*. Chemical Engineering Science, 1988. **43**: p. 91.
8. Colburn, A.P., Trans. Am. Inst. Chem. Engrs., 1933. **29**: p. 174.
9. Tadepalli, S., R. Halder, and A. Lawal, *Catalytic hydrogenation of o-nitroanisole in a microreactor: Reactor performance and kinetic studies.* Chemical Engineering Science, 2007. **62**(10): p. 2663-2678.
10. Ouyang, X. and R.S. Besser, *Effect of reactor heat transfer limitations on CO preferential oxidation.* Journal of Power Sources, 2005. **141**(1): p. 39-46.
11. Kin Yeong, K., et al., *Experimental studies of nitrobenzene hydrogenation in a microstructured falling film reactor.* Chemical Engineering Science, 2004. **59**(16): p. 3491-3494.
12. Losey, M.W., M.A. Schmidt, and K.F. Jensen, *Microfabricated Multiphase Packed-Bed Reactors: Characterization of Mass Transfer and Reactions.* Industrial & Engineering Chemistry Research, 2001. **40**(12): p. 2555-2562.
13. Bird, R.B., W.E. Stewart, and E.N. Ligthfott, eds. *Transport Phenomena*. Second ed. 2002, John Wiley & Sons, Inc.: New York.
14. Tidona, B., et al., *Liquid-to-particle mass transfer in a micro packed bed reactor.* International Journal of Heat and Mass Transfer, 2012. **55**(4): p. 522-530.

15. Dixon, A.G., M. Nijemeisland, and E.H. Stitt, *Packed Tubular Reactor Modeling and Catalyst Design using Computational Fluid Dynamics*, in *Advances in Chemical Engineering*, B.M. Guy, Editor. 2006, Academic Press. p. 307-389.
16. Klöker, M., et al., *CFD-based Study on Hydrodynamics and Mass Transfer in Fixed Catalyst Beds.* Chemical Engineering & Technology, 2005. **28**(1): p. 31-36.
17. Romkes, S.J.P., et al., *CFD modelling and experimental validation of particle-to-fluid mass and heat transfer in a packed bed at very low channel to particle diameter ratio.* Chemical Engineering Journal, 2003. **96**(1–3): p. 3-13.
18. Atmakidis, T. and E.Y. Kenig, *Numerical analysis of mass transfer in packed-bed reactors with irregular particle arrangements.* Chemical Engineering Science, 2012. **81**(0): p. 77-83.
19. OpenFoam, *www.openfoam.com*. 2001. p. OpenFoam: the open source CFD.
20. Foumeny, E.A., et al., *Correlations of pressure drop in packed beds taking into account the effect of confining wall.* International Journal of Heat and Mass Transfer, 1993. **36**(2): p. 536-540.
21. Tronconi, E. and P. Forzatti, *Adequacy of Lumped Parameter Models for Scr Reactors with Monolith Structure.* Aiche Journal, 1992. **38**(2): p. 201-210.
22. Grigull, U. and H. Tratz, *Thermischer einlauf in ausgebildeter laminarer rohrströmung.* International Journal of Heat and Mass Transfer, 1965. **8**(5): p. 669-678.
23. Shan, R.K. and A.L. London, eds. *Laminar Flow Froced Convection in Ducts*. 1978, Academic Prees: New York.
24. Freund, H., et al., *Detailed Simulation of Transport Processes in Fixed-Beds.* Industrial Engineering Chemical Resource, 2005. **44**: p. 6423-6434.
25. Freund, H., et al., *Numerical simulations of single phase reacting flows in randomly packed fixed-bed reactors and experimental validation.* Chemical Engineering Science, 2003. **58**(3–6): p. 903-910.
26. Dixon, A.G., Can. J. Chem. Eng., 1988. **66**: p. 705.
27. Foumeny, E.A. and F. Benyahia, *Predictive characterization of mean voidage in packed beds.* Heat Recovery Systems and CHP, 1991. **11**(2–3): p. 127-130.
28. Haughey, D.P. and G.S.G. Beveridge, Can. J. Chem. Eng., 1969. **47**: p. 130.
29. Soppe, W., *Computer simulation of random packing of hard spheres.* Powerd Techol., 1990. **62**: p. 189-196.

30. Wildenschild, D., et al., *Using X-ray computed tomography in hydrology: Systems,resolution, and limitations.* J. Hydrol., 2002. **267** (3): p. 285-297.
31. Gladden, L.F., *Magnetic resonance: Ongoing and future role in chemical engineering research.* Aiche Journal, 2003. **49**(1): p. 2-9.
32. Eisfeld, B., *Pseudokontinuierliche Modellierung der Strömung in Schüttschichtreaktoren.* Dissertation, Brandenburgische Technische, 1999.